Identification of a novel subset of alveolar type 2 cells expanding following pneumonectomy, responding differently to *Fgfr2b* deletion and enriched in PD-L1

Inaugural Dissertation
submitted to the
Faculty of Medicine
in partial fulfillment of the requirements
for the PhD-Degree
of the Faculties of Veterinary Medicine and Medicine
of the Justus Liebig University Giessen

by
Negah Ahmadvand
of
Toyserkan, Iran

Giessen 2020

From the Department of Internal Medicine
and Excellence Cluster Cardio-Pulmonary System (ECCPS)
Director: Prof. Dr. Werner Seeger
Faculty of Medicine of the Justus Liebig University Giessen

First Supervisor: Prof. Dr. Saverio Bellusci

Co-Supervisor: Dr. Mohammad Hajihosseini

Committee Member (chairperson): Prof. Dr. Norbert Weißmann
Co-Supervisor and Committee Member: Prof. Dr. Stefan Arnhold

Date of Doctoral Defense

07.12.2020

This dissertation is dedicated to my husband

Farhad

for his unconditional love and support

Declaration

"I declare that I have completed this dissertation single-handedly without the unauthorized help of a second party and only with the assistance acknowledged therein. I have appropriately acknowledged and referenced all text passages that are derived literally from or are based on the content of published or unpublished work of others, and all information that relates to verbal communications. I have abided by the principles of good scientific conduct laid down in the charter of the Justus Liebig University of Giessen in carrying out the investigations described in the dissertation."

_____

Negah Ahmadvand

Table of contents

List of Figures

List of Tables

Abbreviations and Acronyms

ABCA3	ATP-binding cassette A3
AEPs	Alveolar epithelial progenitor
APC	Allophycocyanin
AT1	Alveolar epithelial type 1
AT2	Alveolar epithelial type 2
ASMCs	Airway smooth muscle cells
AXIN2	Axis inhibition protein 2
BADJ	Bronchoalveolar duct junction
BASCs	Bronchoalveolar stem cells
BPD	Bronchopulmonary dysplasia
BSA	Bovine Serum Albumin
BSCs	Basal stem cells
cDNA	complementary DNA
COPD	Chronic obstructive pulmonary disease
Cre-ERT2	fusion protein between Cyclization recombinase and triple mutated human estrogen receptor ligand binding domain
DAPI	4′,6-diamidino-2-phenylindole
DNA	Deoxyribonucleic acid
DMEM	Dulbecco's Modified Eagle's Medium
dpi	Days post-infection
DT	Diphtheria toxin
ER	Endoplasmic reticulum
FACS	Fluorescent Activated Cell Sorting
FGF10	Fibroblast Growth Factor 10
FGFR	Fibroblast Growth Factor receptor
FITC	Fluorescein isothiocyanate
Fox	Forkhead box family
LIF	Lipofibroblast
EDTA	Ethylenediaminetetraacetic acid
ER	Endoplasmic reticulum
EpiSPC	Epithelial stem/progenitor cells
FACS	Fluorescence-activated cell sorting

FBS	Fetal bovine serum
H&E	Hematoxylin and Eosin stain
HBSS	Hank's balanced salt solution
Hopx	Homeobox only protein x
HPRT	Hypoxanthine-guanine phosphoribosyltransferase
IF	Immunofluorescence
IPF	Idiopathic pulmonary fibrosis
KRT5	Cytokeratin 5
KEGG	Kyoto Encyclopedia of Genes and Genomes
LB	Laminar body
LNEP	Lineage negative epithelial stem/progenitor
min	Minute
NO2	Nitrogen dioxide
PBS	Phosphate buffered saline
P63	Transformation-related protein 63
PCLS	Precision-cut lung slices
PCR	Polymerase chain reaction
Pdpn	Podoplanin
PN	Postnatal day
PNECs	Pulmonary neuroendocrine cells
PNX	Pneumonectomy
Pro-SPC	Pro-surfactant protein C
PFA	Paraformaldehyde
qPCR	quantitative polymerase chain reaction
RA	Retinoic acid
RBC	Red blood cells
RFP	Red fluorescent protein
RNA	Ribonucleic acid
RT	Room temperature
S	Supplementary
Scgb1a1	Secretoglobin1A
SEM	Standard error of the mean
SFTPA	Surfactant protein A

SFTPB	Surfactant protein B
SFTPC	Surfactant protein C
SFTPD	Surfactant protein D
SPF	Specific Pathogen-Free
Tam	Tamoxifen
TBS	Tris-buffered saline
tdTom	tdTomato
Tom^{High}	tdTomato High
Tom^{Low}	tdTomato Low
TUNEL	Terminal deoxynucleotidyl transferase dUTP nick end labelling
WT	wild type

1. INTRODUCTION

1.1 Epithelial stem cells in the adult lung

Distinct epithelial stem cells maintain different regions of the adult lung. In mice, pseudostratified epithelium covers the trachea, main stem bronchi and most proximal regions of intralobar airways, while the remaining airway is lined with simple columnar epithelium. In humans, distal airways and small airways are also covered with pseudostratified epithelium. Pseudostratified epithelium in both mice and humans contain basal cells, club (secretory), ciliated, and neuroendocrine cells. These cells display remarkable plasticity in response to injury and transdifferentiate one to another [1].

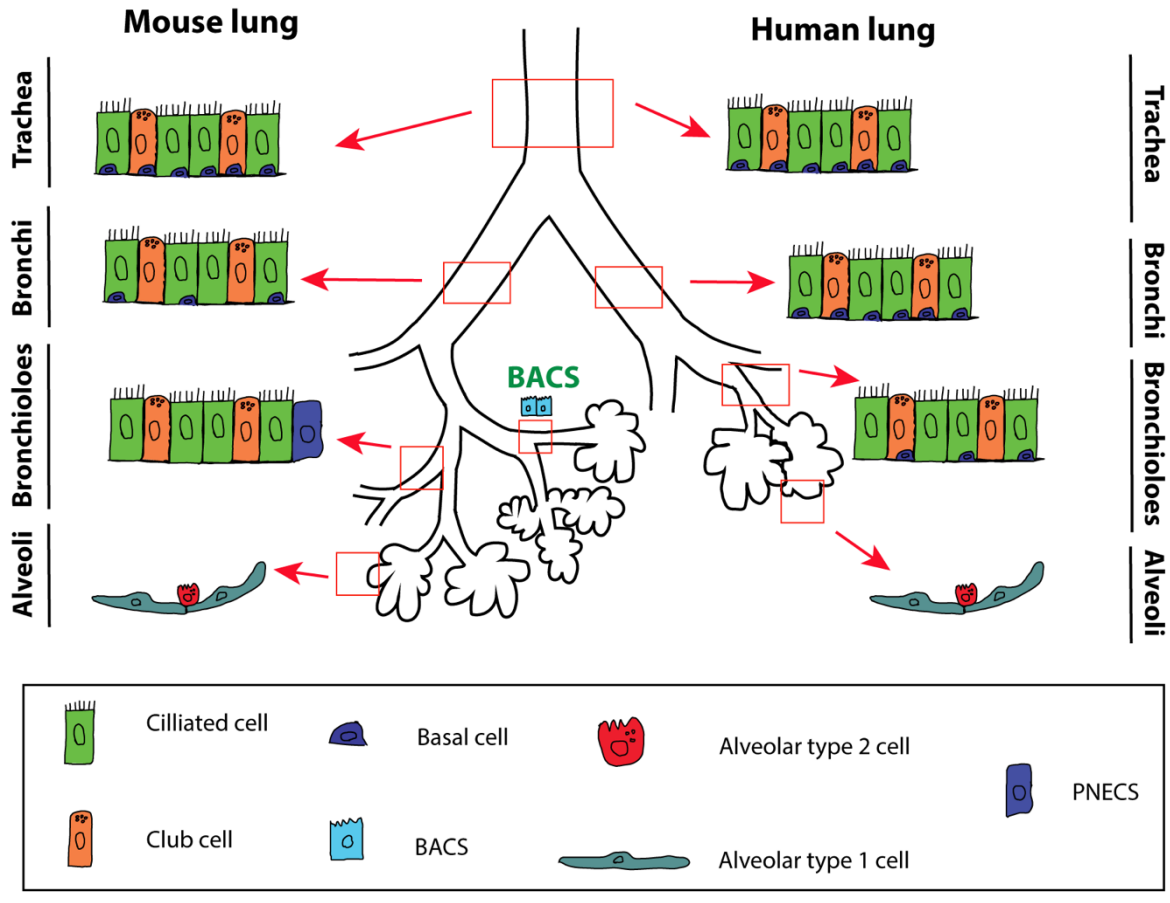

Figure 1: Mice and human lung epithelium. Airway epithelium contains different cell populations that vary along the proximodistal axis. In human airways, basal cells extend throughout the small airways, whereas in mouse, basal cells extend only up to the mainstem bronchi. Most of the small airway in mouse is composed of a cuboidal epithelium consisting mainly of ciliated and club cells, while in the human such epithelium is restricted to only the very most distal cells of the bronchioalveolar duct junction.

Basal cells are present in the murine trachea and main stem bronchi, while in humans are present throughout human airways expanding small bronchioles. These cells are characterized by the expression of *Trp63* and *cytokeratin 5 (KRT5)* [2][3]. Basal cells are considered a heterogeneous population as subsets of these cells have been described based on the expression of different markers like KRT8, Notch21CD and c-myb [4][5]. Basal cells function as epithelial stem cells, being able to self-renew and replenish lost club, ciliated and neuroendocrine cells. Their transdifferentiation into ciliated and club cells during homeostasis and in response to epithelial injury was demonstrated with lineage tracing using Krt5-CreER driver line [6]. In addition, subsets of basal cells expressing Krt14, locating in mice trachea and bronchi, also proliferate and generate ciliated and club cells after epithelial injury [7][8][9]. Furthermore, isolated basal cells from both mice and humans appears to be multipotent *in vitro* since they display self-renew capability and differentiation to ciliated and club cells [2][10][11].

Club cells or secretory cells are described with a cytoplasm filled with secretory granules. These cells in mice are present in the trachea, bronchi and bronchioles, however in humans, with lower numbers, are scattered in most regions of airway epithelium. They are characterized by the high expression of the secretoglobin *Scgb1a1*. Identification of subsets of club cells represents their heterogeneity. They are categorized into mature and less mature subpopulations based on the expression of *SSEA1* and *Atp6v1b1* [12]. Furthermore, subpopulations of club cells at the branch points of small airways called ‘variant club cells’ which are more resistant to naphthalene- induced injury [13]. Variant club cells might be related to subsets of club cells expressing a low level of Scgb1a1 which are Upk3a positive (a family member of uroplakin proteins) locating proximity to pulmonary neuroendocrine cells (PNECs) [14][13]. Additionally, more subsets of club cells are described based on the differential expression of secretoglobin family proteins like Scgb3a1 and Scgb3a2 [15]. Since different studies have been shown the contribution of Scgb1a1 positive cells to the airway epithelium during homeostasis and in response to the epithelium injury, club cells are considered as intralobar airway stem cells. Lineage tracing of these cell using *Scg1a1* promoter-driven CreER has shown their self- renewal capability and their transdifferentiating into ciliated cells *in vivo* and *in vitro*. There is also evidence of deriving rare basal cells from Scg1a1+ club cells after lung epithelial injury [16].

Ciliated cells do not contribute to the airway epithelium maintenance during homeostasis and in response to injury, however, these cells might convert to other cell types like goblet cells under pathological condition [17][18].

Pulmonary neuroendocrine cells (PNECs) are located individually in proximal airways and as clusters named as neuroepithelial bodies (NEBs) in intralobar airways. In mice, these cells reside in both large and small airways with more density at the branch points of airways. PNECs self-renew during homeostasis, but there is no evidence of their transdifferentiation into other cell types [15][14][19]. PNECs in the bronchiolar epithelium are considered to function as niche cells for naphthalene-resistant variant club cells [13][14].

Bronchioloalveolar stem cells (BASCs) are located in the bronchioalveolar duct junction (BADJ), which is the transition zone from bronchiloles to the alveolar region. These cells initially were identified based on their proliferation following bleomycin-induced injury and they express markers of both club cells (Scgb1a1) and AT2 cells (Sftpc) [20]. BASCs are proposed to function as stem cells for the airways and alveoli, since they give rise to airway and alveolar epithelial lineage *in vitro*, however, their progenitor activity during homeostasis is very low [20][21]. Recently a new lineage tracing approach with the expression of a fluorescent marker in these double positive cells was developed which facilitate studying the behaviour of BASCs in the context of different injury models [22]. These cells have not been identified in humans so far [23][24][25].

Alveolar epithelial type 2 cells are known as adult lung alveoli progenitor cells. The alveolar epithelium is composed of squamous alveolar epithelial type 1 (AT1) cells, which cover more than 90% of the alveolar surface area, and cuboidal alveolar epithelial type 2 (AT2) cells, which are the most abundant alveolar epithelial cells, located in the corners of alveoli and account for 5% of the alveolar surface [26][27]. AT2 cells maintain the homeostatic turnover of both AT1 and AT2 cells and thereby contribute to alveolar repair following injury [28][29][30].

1.2 Alveolar epithelial type 2 cells

AT2 cells composed 10-15% of lung cells and 60% of cells within the alveolus. AT2 cells have the characteristics of a secretory cell with distinct apical microvilli, large nucleus, abundant cytoplasm with mitochondria, extensive endoplasmic reticulum (ER)

and Golgi apparatus. The most distinct morphological feature of AT2 cells is the presence of laminar bodies (LBs) in the cytoplasm. LBs are the organelle responsible for assembly, storage and secretion of pulmonary surfactants. These cells are equipped with membrane-bound water channels and ion pumps that are effective in keeping the alveolar space free of excess fluid and ions by transporting sodium and fluid from the apical surface of the alveolus into the interstitium of the lung [31][26][32].

1.2.1 Function of AT2 cells

AT2 cells are known as multifunctional cells. Three main functions of AT2 cells are as follows:

1. Production and secretion of pulmonary surfactants
2. Interaction with alveolar macrophages to defend alveolus
3. Function as alveolar stem cells

1.2.1.1 Production and secretion of pulmonary surfactants

AT2 cells produce and secret pulmonary surfactants with two critical roles in respiratory system. First, they reduce surface tension at the air-liquid interface, thereby preventing alveolar collapse, facilitating gas exchange and alveolar stability during breathing. Second, surfactants function as an innate component of the lung's immune system in order to control inflammation and prevent microbial infections of the distal lung [33].

1.2.1.1.1 Pulmonary surfactant

Pulmonary surfactant consists of 90% lipids and 10% protein. The principal lipid components of surfactant are phospholipids (80-85%), mainly including phosphatidylcholine, and cholesterol (8-10%) [34]. These Lipids are synthesized either de novo from precursors, such as palmitate and choline, or via an acylation or reacylation pathway that reuses lipid recycled from the distal airspace [35].

Protein components of pulmonary surfactants consist of four unique proteins namely SP-A, SP-B, SP-C, and SP-D. These four proteins are expressed at relatively high levels in AT2 cells and possess distinct structures and functions. SP-A with 50-70% is the most abundant surfactant protein. Notably, SP-B comprises 10% of surfactant

proteins and is considered as the most critical surfactant protein, since its absence or dysfunction due to mutations results in respiratory failure and death shortly after birth [36].

Furthermore, specific characteristics of surfactant proteins impact on their roles in the respiratory system. SP-B and SP-C as hydrophobic proteins are involved in lamellar body formation, secretion, and formation of the surfactant monolayer that is critical in reducing the surface tension at the air-liquid interface [37]. These two surfactant proteins are also play role in immunomodulation that is essential for the stability and host defense of the airways [38]. SP-A and SP-D are hydrophilic proteins and mainly function as antimicrobial. These proteins belong to the collectin family of antimicrobial peptides and provide an innate defense mechanism against pathogen challenge. Their hydrophilic nature enables them to bind to the surface of pathogens via their carbohydrate parts and act as opsonins. In addition, they play role in macrophage activation, facilitation of chemotaxis, and inflammatory cytokine expression. Surfactant proteins also facilitate the removal of apoptotic cell from lower airways that is particularly important for the resolution of pulmonary inflammation [39].

Pulmonary surfactants are recycled by AT2 cells or catabolized by alveolar macrophages in a highly regulated system that maintains precise levels of pulmonary surfactant throughout life [33].

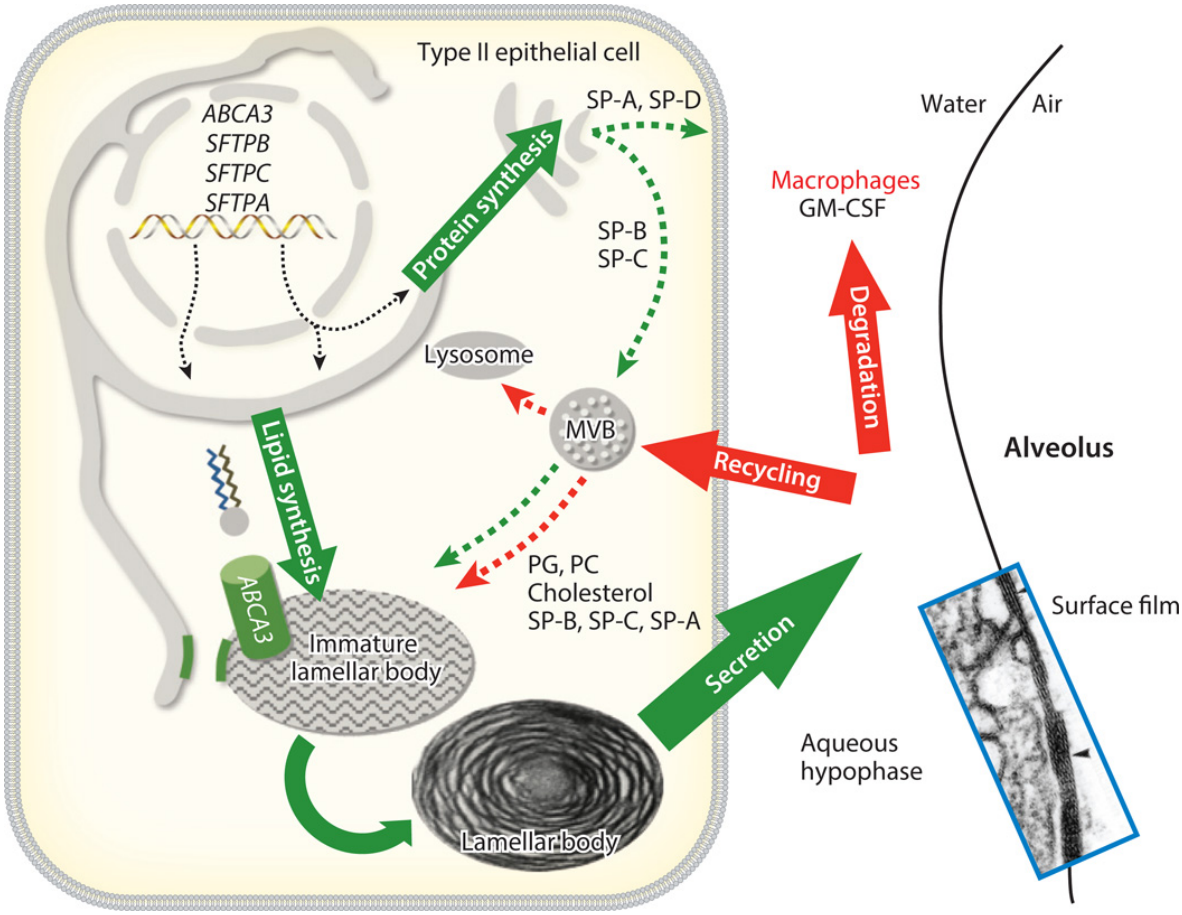

Figure 2: Biosynthesis of pulmonary surfactant. Proteins and lipids components of pulmonary surfactant are likely produced from distinct pathways. SP-B and SP-C are trafficked from the endoplasmic reticulum to lamellar bodies via the Golgi apparatus and MVB; whereas surfactant phospholipids are directly transported from the endoplasmic reticulum to specific lipid importers (ABCA3) in the lamellar body–limiting membrane. Surfactant proteins and lipids are assembled into bilayer membranes that are secreted into the alveolar airspace, where they form a surface film at the air–liquid interface. Surfactant components removed from the film are degraded in alveolar macrophages or are taken up by AT2 cells for recycling or degradation in the lysosome. The MVB plays a key role in the integration of pathways for surfactant synthesis, recycling, and degradation. (ABCA3: ATP-binding cassette transporter A3, GM-CSF: granulocyte macrophage colony–stimulating factor, MVB: multivesicular body, PC: phosphatidylcholine, PG: phosphatidylglycerol, SP/SFTP: surfactant protein. (Adopted from Jeffrey A. Whitsett 2015, Diseases of Pulmonary Surfactant Homeostasis).

1.2.1.2 Interaction with alveolar macrophages to defend alveolus

AT2 cells interact with macrophages through the secretion of various cytokines in response to pathogens and alveolar damage in order to activate macrophages and defend the alveolus [26][40]. AT2 cells also play critical role in activation and deactivation of inflammatory responses by alveolar macrophages through production

of pulmonary collectins, SP-A and SP-D, which bind to the surface of pathogens and regulate microbial phagocytosis [41]. Moreover, AT2 cells with the expression of high levels of xenobiotic-metabolizing enzymes detoxify inspired compounds which cause alveolar damage [33].

1.2.1.3 Function as alveolar stem cells

AT2 cells function as alveolar stem cells, renewing both AT1 cells and AT2 cells during homeostasis and repair after alveolar injury. These cells are known as long-term alveolar stem cells as they self-renew and differentiate over a year [26] [28][29]. During renewal process, AT2 cells form clonal foci, which enlarge slowly and clusters of AT2 cells and AT1 cells derives from AT2 cells in renewal foci over time. It has been shown that, during steady state, the rate of AT2 cells to AT1 cells turnover is less than 1% after 1 month, 3.9% after 4 months and 7.5% after 16 months. Each renewal focus derives from a single self-renewing AT2 cells that generate multiple AT1 and/or AT2 cells and their progenitor activity is widely activated by AT1 injury [29]. AT2 cells also display stem cell features *in vitro* as Individual lineage traced AT2 cells self-renew in culture and differentiate into alveolar-like structure consisting of AT2 cells and differentiated AT1 cells [28]. However, it is still debatable whether all AT2 cells possess progenitor cell capabilities or whether these capacities are present only in specific AT2 cell subpopulations.

1.2.2 AT2 cell stemness and niche

Long-term maintenance of the potency of stem cells depends on their communication with their microenvironment or niche [42][43][44][44]. The niche keeps stem cells quiescence, directs their self-renewal, regulates their differentiation into appropriate cell types, govern their migration decisions during homeostasis and in regenerative response after lung injury [14][45][46][47]. The niche consists of different cell types, extracellular matrix and diffusible factors such as cytokines and growth factors [43][48]. Stem cell niches are located at different regions of the lung and play crucial roles in protecting stem cells from depletion [43][49].

Lipofibroblasts (LIFs) are known as niche in the alveoli and are located proximity to AT2 cells and contribute to maintaining their stemness [28]. LIFs are lipid droplet-

containing interstitial fibroblasts, which assist in the production of pulmonary surfactant by assimilating neutral lipids and transferring triglycerides to AT2 cells for the final processing of the pulmonary surfactant [50][51][52]. LIFs express Fibroblast growth factor 10 (Fgf10) [49][53], which act directly on AT2 cells via Fgfr2b receptor [47][54] [55][56]. The significance of the presence of LIF to support AT2 cells stem cells activity was demonstrated with co-culture of isolated AT2 cells with PDGFRa+ mesenchymal cells including LipidTOX^{+} lipofibroblasts which promote AT2 cells growth and differentiation of alveolospheres in 3D culture [28]. Similarly, clonal expansion of alveolar stem cells enriched for α6β4 integrins relies on co-culture of these cells with Sca1+ mesenchymal cells, which can be substituted by exogenous Fgf0 [23]. Dysfunctional epithelial stem cell-niche unit may lead to chronic lung diseases such as chronic obstructive pulmonary disease (COPD), chronic asthma and idiopathic pulmonary fibrosis (IPF) [57][58][59].

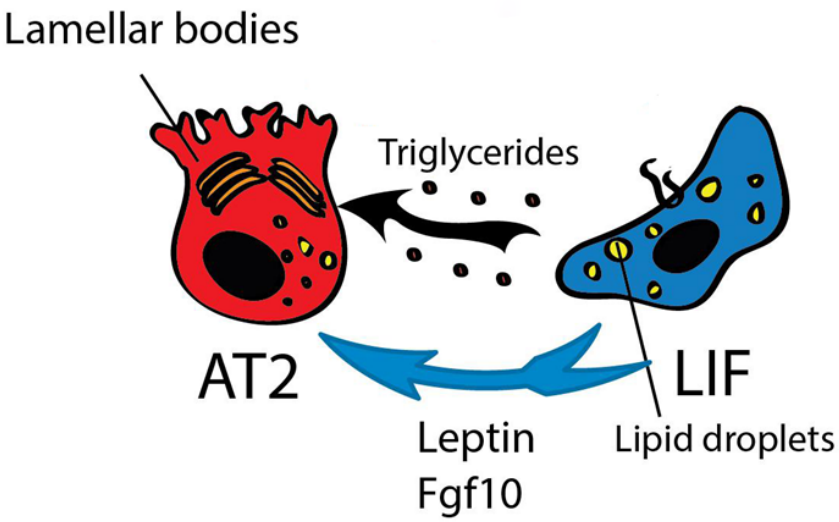

Figure 3: Interaction between AT2 cells and lipofibroblasts (LIFs) for surfactant production. LIF secrete triglycerides and leptin that are essential for surfactant production. (Adopted and modified from Chao CM 2015, A breath of fresh air on the mesenchyme: impact of impaired mesenchymal development on the pathogenesis of bronchopulmonary dysplasia.)

1.2.3 AT2 cells heterogeneity

AT2 cells are heterogeneous population. Different subpopulations within this lineage, with different stem cell properties, have been identified based on various markers such as E-cadherin, Axin2, integrin α6β4 and the dual expression of Surfactant protein C (Sftpc)/ Secretoglobin family 1A member a (Scgb1a1) [60][61][62][63][16].

In rodents, AT2 cells are divided equally into E-cadherin negative and E-cadherin positive subpopulations, which respond differently to the hyperoxia injury. E-cadherin negative population are more resistance to the hyperoxia and exhibit more proliferation rate with higher level of telomerase activity, while E-cadherin positive population are more sensitive to the damage [60].

In the adult mouse lung, Axin2-positive cells are another identified subset of AT2 cells which make up 1% of the mature AT2 (Sftpc-high) cells and are distributed throughout the lung [62]. This ratio of Axin2-positive cells is stable over time. *In vivo* lineage tracing of Axin2-positive cells revealed their ability to form clones of 2 to 5 cells accompanied by their expansion and differentiation into AT1 expressing Podoplanin (Pdpn). These cells are located close to *Pdgfrα*-expressing fibroblasts which keep their stemness with the secretion of Wnts. In addition, these cells display enhanced self-renewal capabilities in alveolosphere assays compared to the Axin2-negative AT2 cells suggesting that these Axin2-positive cells represent a subpopulation of mature AT2 cells with enhanced stem cell capacities [62].

In a similar and independent study, Zacharias et al. characterized a Wnt-responsive alveolar epithelial progenitor (AEP) lineage within the mature AT2 cell population as an evolutionarily conserved alveolar progenitors. These cells compromise around 20% of adult AT2 cells and are enriched for Wnt targets genes. Lineage tracing of these cells using $Axin2^{creERT2:TdT}:R26R^{EYF}$ mice showed converting of few non-Axin2^{+} AT2 to AEPs after nine months, which shows that these population are relatively stable.

These cells also showed enriched gene expression profile of lung developmental genes like *Fgfr2*, *Nkx2.1*, *Id2*, *Etv4*, *Etv5*, and *Foxa1*. Moreover, ATAC-seq analysis revealed different open chromatin regions between AEPs and AT2 cells genomes. The common open chromatin is located close to housekeeping genes, but regions of AEP-enriched open chromatin are found near lung development genes. AEPs express specifically *Tm4sf1*, which is an epithelial cancer stem cell membrane protein.

Equivalent of AEPs was identified in human (hAEPs) by the expression of the *TM4SF1* and comprise approximately 29% of the human AT2 SFTPC positive cells. Human AT2 cells generate alveolosphere in 3D culture, which respond to Wnt activation by increasing AT2 cell differentiation, and to Wnt inhibition by increasing AT1 cell differentiation. Isolated and cultured hAEPs form a greater and larger number of organoids that respond more robustly to Wnt modulation. Depletion of TM4SF1 positive cells from the human AT2 population leads to a dramatic loss of organoid formation. Suggesting hAEPs are the subpopulation of AT2 cells capable of organoid formation. hAPEs is also enriched for Wnt signalling targets and FGFR2 and showed specific responsiveness to Wnt and Fgf signalling as treatment of both mouse and human AEPs with Fgf7 or Fgf10 results in substantial increases in colony size and colony-forming efficiency, while mouse and human AEPs-depleted AT2 cells exhibit a diminished response [63].

Chapman et.al introduced a subset laminin receptor integrin α6β4 positive cells of Sftpc negative or low, which are able to regenerate AT2 Sftpc+ cells in the alveoli after severe injury. These cells are located in both bronchoalveolar junction and within alveoli. Some β4+ cells in junctional regions show low Scgb1a1 expression and β4+ cells in alveolar wall display low level of Sftpc. These cells show progenitor potential as they expand clonally ex vivo (mixed with E14.5 lung single cells and implanted under a kidney capsules), and differentiate to mature cell types. Cultured β4+ cells on Matrigel form large colonies while small cluster of single cells was observed 7 days after culture of β4 negative cells. This indicates that β4 negative cells as mature AT2 cells are not capable to form colonies without having the niche. In addition, β4+ cells are more proliferative in culture compared to β4 negative cells The colonies arising from β4+ positive cells are heterogenous with the mixture of $Sftpc^{Pos}$ $Scgb1a1^{Neg}$, $Sftpc^{Pos}$ $Scgb1a1^{Pos}$ and $Sftpc^{Neg}$ $Scgb1a1^{Neg}$ cells, indicating cultured β4 positive cells are able to differentiate into either airway or alveolar lineage [61]. Further characterization of these cells showed that they are not traceable using lineage labelling with Scgb1a1- and Sftp-CreERT2 derivers. These cells are amplified after bleomycin or influenza injury and activate ΔNp63 and cytokeratin 5 program which is depending on Notch signalling [61][64].

AT2 cells heterogeneity is equally shown in the context of diphtheria toxin injury as a subpopulation of lineage-labelled AT2 cells displaying relatively more resistance to DT

toxicity was capable to repopulate the AT2 pool following injury. The identity of these survivor cells, however, is not clear. Furthermore, AT2 cells displayed different self-renewal capability *in vitro* since around %1-%2 of co-cultured AT2 cells with primary PDGFRα+ lung stromal cells capable of giving rise to self-renewing alveolospheres [28].

Interestingly, AT2 cells heterogeneity is not limited to the adult lung. During the alveologenesis phase of lung development, Axin2-positive AT2 cells exhibit enhanced cell growth compared to total AT2 cells during alveolus generation [65].

1.2.4 AT2 cells replacement after lung injury

Alveolar epithelium is maintained by AT2 stem cells which self-renew and give rise to AT1 cells during homeostasis and repair after lung injury. AT2 cells progenitor behavior and their replacement in different lung injury models like bleomycin, influenza virus, diphtheria toxin and compensatory lung growth following pneumonectomy have been studied.

1.2.4.1 Bleomycin injury model

Bleomycin is a chemotherapeutic agent that damages multiple cell types in the alveoli and induces transient inflammation and fibrosis [66]. Decreased number of AT1 cells and AT2 cells has been reported during the injury phase of bleomycin-induced lung fibrosis [28][30][61]. Several studies have been performed to find out which type of progenitor cells are activated and contribute to the repair of alveolar epithelium. BASCs which are resistant to bronchiolar and alveolar injury, are one of the proposed cells. The number of these cells is elevated 14 days after bleomycin-induced injury, suggesting BACS may behave as alveolar progenitors in the case of losing AT1 cells and AT2 cells. However, it is still unclear whether these cells directly differentiate to AT1 cells or they first give rise to AT2 cells and then AT1 cells [20]. Aso et.al, showed that depleted AT1 cells following bleomycin injury are repopulated with different mechanisms depending on the region of injury. For instance, in the area close to bronchiole, undifferentiated bronchiolar progenitors activated and give rise to AT2 cells, and these cells subsequently transdifferentiate into AT1 cells, whereas in the alveoli AT2 cells proliferate and replenish the lost AT1 population [67]. Club cells are

also known as a population involving in the alveolar repair process, which has been demonstrated using the lineage tracing of Scgb1a1-expressing cells. According to a study by Zheng et.al, most (around 78%) of newly formed AT2 cells, and many AT1 cells in the same region originate from Scgb1a1 positive cells. In addition, small number of proliferating AT2 cells also were reported throughout the 21 days of the repair process [68].

In Barkauskas et.al study, to confirm whether Scgb1a1+ cells contributing to restoring AT2 cells, *Sftpc-CreER;Scgb1a-CreER;Rosa-Tm* triple-heterozygous mouse line was used and Cre recombines was induced with a high dose of tamoxifen to label AT2 cells, double-positive Sftpc+ Scgb1a1+, located in bronchoalveolar duct junction, and Scgb1a1+ throughout the bronchioles. AT2 cell ablation was observed 21 days after intratracheal bleomycin treatment and the number of AT2 cells reduction was much lower compared to what already was observed in *Sftpc-CreER;Rosa-Tm* bleomycin treated mice. This suggests part of restored AT2 cells originates from Scgb1a1+ cells, but it is not still clear what is the other source of AT2 cells replacement during the repair process. Moreover, to identify the clonal origin of Scgb1a1 lineage-labeled AT1 cells and AT2 cells, *Scgb1a1-CreER; Rosa-Confetti* mice was induced by a single dose of tamoxifen. Analysis of lung sections revealed the existence of clones of lineage-labeled bronchiolar epithelial cells in some BADJ regions, which extended into the alveolar compartment in some areas. Suggesting some Scgb1a1+ cells deriving from bronchiolar epithelium can give rise to AT1 cells and AT2 cells in a clonal manner. However, some damaged AT2 cells are replaced by $Sftpc^{neg}$ or $Sftpc^{Low}$, $Scgb1a1^{neg}$ cells. These cells could be integrin $\alpha_6\beta_4$ positive cells or other cells with unknown identity [28].

Altogether, AT1 and AT2 lineages are replenished with cells originate from BACS, Scgb1a1-positive cells, and subpopulations of AT2 cells in response to bleomycin-induced lung injury. Moreover, AT2 to AT1 conversion is elevated in the context of pulmonary fibrosis.

1.2.4.2 Influenza virus-induced infection

Influenza virus infection induces damage to bronchiolar and alveolar epithelium. After murine-adapted H1N1 (PR8) influenza A infection, the loss of AT1 cells and AT2 cells is evident 5 days post-infection (dpi) which begin to be replaced with newly generated

AT2 cells at 11 dpi that are largely increased by 17 dpi and ultimately leads to complete lung recovery after several months [68][69][70]. Different progenitor cells have been introduced as the origin of newly formed AT1 cells and AT2 cells. In a study by Zheng et al., lineage tracing of Scgb1a1- expressing cells showed the appearance of labelled AT2 cells throughout the alveolar region, which compose around 48% of AT2 cells in the damaged parenchyma. Also, labelled AT1 cells were detected among labelled AT2 cells. In the Scgb1a1-CreER lineage tracing system, club cells are the majority of labelled cells, although BASCs and some AT2s are also labelled. In this study club cells, are reported as the source of the majority of regenerated AT2s following severe pulmonary injury induced by influenza virus infection [68].

It is proposed that club cells convert to intermediate cells with the club cells morphology expressing Scgb1a1 and Sftpc and then these cells differentiate to AT2 cells. These cells are named pro-SPC$^+$ bronchiolar epithelial cells (SBECs) which slowly lose club cell markers and give rise to pro-SPC$^+$ cells in the ring structures in response to severe lung damage induced by either influenza virus infection or bleomycin. The formation of bronchiole-like structures in alveoli resembles alveolar bronchiolization which has been observed in severe lung damage [71][72]. Alveolar bronchiolization is characterized by the presence of cuboidal or often columnar cells lining the alveoli. Alveolar bronchiolization may originate either from bronchiolar epithelial cells scattering to the alveoli or from the expansion of terminal bronchioles into the alveoli [71][73][74]. It seems that SBECs are induced following severe alveolar damage as these cells have not observed after naphthalene treatment which damages bronchiolar epithelium [68][75].

In contrast, in another study using the same approach, club cells found to be involved in the repair of terminal bronchiolar epithelium but not the alveolar epithelium [16].

Transformation-related protein 63 (p63)- expressing cells are another population appearing following extensive epithelial damage after influenza virus infection and expand to the sites of injured lung parenchyma. These p63 positive cells are also positive for Krt5 and Krt14 and generate discrete clusters that resemble foci of alveoli and express genes related to alveolar function. These cells undergo rapid proliferation after infection and disperse to alveolar regions with ablated cells and form discrete, Krt5+ pods and express Pdpn gene which is a specific AT1 cell marker. Interestingly, Krt5+ pods exclusively found in the regenerative areas of the lung and were not

observed in the normal lung tissue. Furthermore, the involvement of $p63^+$ cells in the repair process after bleomycin treatment is controversial as one study reported patches of $p63^+$ cells in the damaged parenchyma 21 days after bleomycin treatment and another not. It seems $p63^+$ cells are activated in the damaged parenchyma in response to severe alveolar epithelial damage after influenza virus infection or bleomycin treatment [70][76]. Moreover, cloned $p63^+$ cells from the infected lung were able to differentiate *in vitro* into AT1 expressing aquaporin 5 cells, raising the possibility that $p63^+$ cells may contribute to the repair of the damaged alveolar epithelium. However, because of the lack of Sftpc+ cells in the regenerated epithelia by $p63^+$ cells, it does not appear that these cells contribute to the regeneration of AT2 cells [70][76].

Using Scgb1a1-CreER transgenic system it revealed that $p63^+$ patches in the damaged parenchyma are likely derived from $Scgb1a1^+$ cells and not originate from the pre-existing $p63^+$ basal cells in the trachea. Moreover, Lineage tracing of the $p63^+$ cells using the Krt14 promoter did not show their differentiation into AT1 and AT2 cells. Therefore, their contribution to the repair of the alveolar epithelium is not still clear [70][76].

Another progenitor population contributing to alveolar epithelial repair after influenza-induced injury is Wnt-responsive alveolar epithelial progenitor (AEP) lineage which is traceable using $Axin2^{CreERT2}$ driver line. Interestingly, Zacharias et.al identified heterogeneous lung injury consisting of 4 distinct zones based on the injury severity. These zones are characterized as Zone 1 with no morphological changes, Zone 2 with a minor injury and mild interstitial thickening, Zone 3 with a significant injury, and Zone 4 with total alveolar destruction. Analysis of AEPs in different zones one month after induction of influenza infection showed the presence of AEPs and their progeny at the homeostatic level in zone 1. However, the percentage of lineage labelled AT1 and AT2 cells in zone 2 and 3 was increased with the elevated proliferation of AEP lineage. In Zone 4, Krt5+ cells were observed, which are not derived from AEPs.

During the repair process, AEPs self-renew to maintain the AEP lineage and generate a large number of new lineage-traced alveolar epithelial cells. However, few non-AEP AT2 cells acquire the AEP phenotype [63].

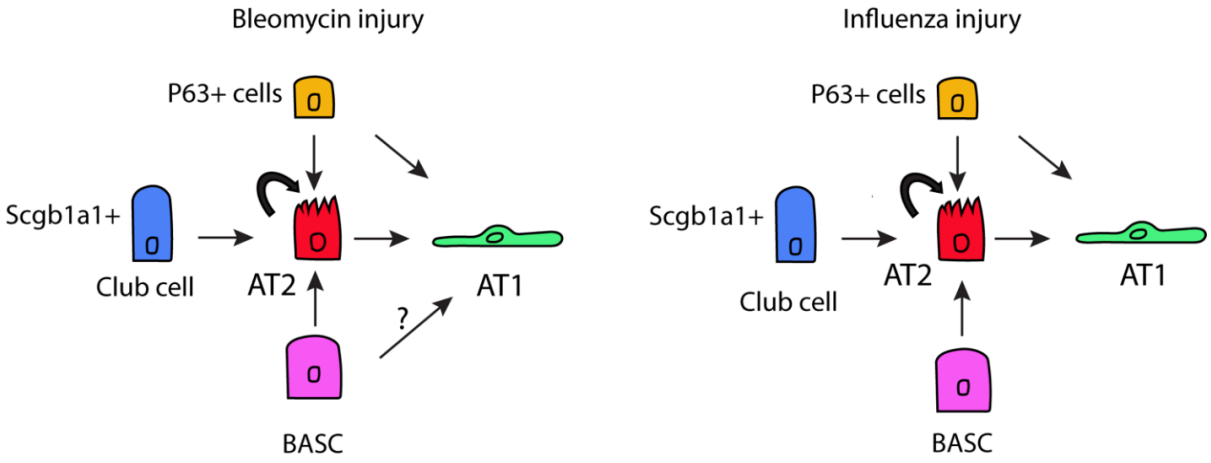

Figure 4: AT2 cell replacement following bleomycin- and influenza - induced lung injury. AT2 lineages are replenished with cells originate from P63-positive cells, Scgb1a1-positive cells, BACS and subpopulations of AT2 cells in response to bleomycin- and influenza - induced lung injury.

1.2.4.3 Hyperoxia injury model

Hyperoxia is a lung injury model inducing AT2 cells damage and ablation after exposure to high O_2 concentration [77][78]. In the adult mice the rate of AT2 cells proliferation is low in steady-state and during hyperoxia exposure no change in proliferation has been observed. However, AT2 cell proliferation rate increase during the recovery period in room air and return to the normal levels after 7 days. After repair completion, around eight weeks later, the number of AT2 cells and lung structure is similar to healthy lung [79][80].

To study the origin of newly generated AT2 cells, lineage tracing of Scgb1a1$^+$ positive cells using *Scgb1a1-CreER™; Rosa26R-eYFP* mice, which were induced with different amount of tamoxifen dosage, was performed. In this approach with 2 tamoxifen injection club cells, BASCs and few AT2 cells are labelled, whereas with doubling the number of injections more AT2 cells are labelled. This approach provides no evidence of the contribution of Scgb1a1$^+$ club cells and putative BASCs to the alveoli repair after exposure to O_2. It appears that newly produced AT2 cells and AT1 cells after O_2 injury originate from AT2 cells [81][16].

Since Hyperoxia resembles Bronchopulmonary dysplasia (BPD) in premature infants, several studies have been performed in neonatal mice [82]. In newborn mice, AT2 cells

highly proliferate. Exposing pups to hyperoxia inhibits AT2 cell proliferation, which is resumed during the recovery period. Lineage tracing of Scgb1a1$^+$ cells showed that Scgb1a1$^+$ cells also do not contribute to alveolar repair during postnatal development after hyperoxia injury [16][79][83].

Fgf10 plays a critical role in the differentiation of AT2 cells in neonatal mice. The ratio of AT2 cells is decreased in the lungs of *Fgf10*$^{+/-}$ (heterozygous) compared to *Fg10*$^{+/+}$ (WT) mice. Interestingly, this ratio is not substantially different after hyperoxia injury between *Fgf10*$^{+/-}$ and *Fg10*$^{+/+}$ lungs at postnatal day 3 (PN3). This normalization of the ratio in *Fgf10*$^{+/-}$ lungs in hyperoxia was associated with increased cell proliferation in lungs from *Fgf10*$^{+/-}$ pups following hyperoxia injury, suggesting the existence of cells attempting to replenish the AT2 cells pool. However, the identity of these cells is still unknown [84].

Altogether, depleted AT2 cells following exposure to hyperoxia are replenished with AT2 cells in both adult and neonatal lungs, but it is not still clear whether all AT2 cells or subsets of these cells contributing to alveolar repair. Moreover, activation AT2 cells after hyperoxia injury led to a significantly increased number of renewed AT1 cells.

1.2.4.4 Diphtheria toxin-mediated depletion

AT2 cell specific injury model was developed by the generation of *Sftpc-CreER; Rosa-DTA*/*Rosa-Tm* triple heterozygous mice. Following tamoxifen treatment, the expression of the catalytic subunit of diphtheria toxin is induced in Sftpc$^+$ AT2 cells triggering AT2 cell death [85][86]. Interestingly, AT2 subpopulations respond differently to diphtheria toxin. Although the majority of AT2 cells undergo apoptosis, subpopulations of these cells showed resistance to the damage and survived. These cells proliferate and repopulate lost AT2 cells and make the normal distribution of Sftpc$^+$ AT2 cells in the alveoli after 21 days post toxin injection (dpi), revealing the completion of the repair. Despite the massive loss of AT2 cells, the overall histology of the lung remained remarkably intact at 2, 4, 7, and 21 days dpi, and no evidence of alveolar collapse was observed. Lineage tracing with high-resolution imaging demonstrated the clonal expansion of survivor cells. Therefore, a subset of AT2 cells with progenitor behaviour involved in replenishing of AT2 cells after diphtheria toxin mediated depletion. At the beginning of repair phase, single AT2 cells form clones and subsequently small clusters that separate from each other. No evidence of involvement

Scgb1a1^{+} cells located in BADJ was observed after targeted AT2 cell injury. In addition, imaging of lungs revealed remarkably more clones in the alveolar region rather than close to BADJ. Suggesting Sftpc^{+} AT2 are capable of clonal proliferation and differentiation after DTA-induced injury [28].

1.2.4.5 Pneumonectomy

Pneumonectomy (PNX) is a known model to study lung regeneration as it promotes the formation of new alveoli in the remaining lobes. In response to the removal of one lung lobe, the compensatory growth occurs in the remaining lung [87][88]. Lung regeneration during compensatory lung growth is associated with significant AT2 cells proliferation, their increased size and metabolic activity [89][90][91][92][93].

The proliferation of BASCs and club cells also has been reported in the first 7 days after PNX, which contributes to around 25% of newly generated AT1 and AT2 cells. During lung regrowth, BASCs move to peribronchiolar regions and alveolar spaces near BADJs. Therefore, BASCs perhaps differentiate to club cells and involve in the development of local bronchiolar during the expansion of the alveolar compartment rather than distal AT2 cells. AT2 and club cells may be replenished from a subset of these cells which are activated during lung regeneration [94].

AT2 cells as major proliferative epithelial cells in neo alveolarization contribute to restoring lung surface area through differentiation into AT1 cells. Interestingly, AT1 cells proliferation and their differentiation to AT2 cells following pneumonectomy has been demonstrated using lineage tracing of Hopx (Homeobox only protein x) positive cells [95].

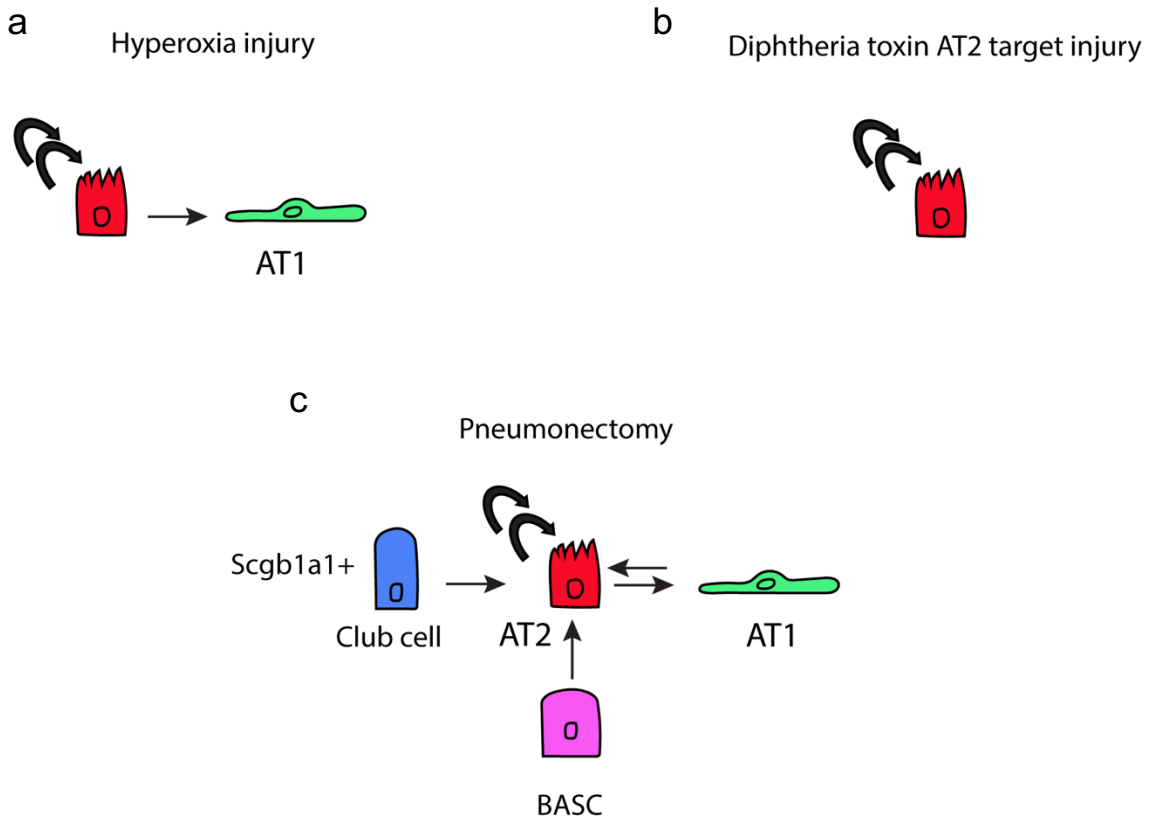

Figure 5: AT2 cell replacement following hyperoxia injury, diphtheria toxin AT2 target injury and pneumonectomy. a) AT2 cells proliferate to repopulate lost AT1 and AT2 cells after hyperoxia injury. **b)** Survivors AT2 cells are the source of AT2 replenishment after diphtheria toxin AT2 target injury. **c)** AT2 lineages are replenished with cells originate from Scgb1a1-positive cells, BACS and proliferation of subpopulations of AT2 cells during compensatory lung growth after pneumonectomy.

1.2.5 Diseases related to AT2 cells deficiency

Different pulmonary diseases are associated with deficient pulmonary surfactant and disrupted AT2 cell homeostasis [96]. Abnormal surfactant levels and deficiencies in their protein components causes different diseases in human such as respiratory dysfunction, inflammation in ARDS [97][98], pulmonary fibrosis [99], emphysema [100][101], cystic fibrosis [102], COPD [103] , RDS in new-borns [104]. Mutations in essential surfactant related genes result in the number of acute and chronic lung diseases. For instance, the mutation in genes encoding SP-C and SP-A leading to the production of misfolded protein which normally is degraded by proteasome. The lack of clearness of misfolded protein causes cytotoxicity and, ultimately, interstitial lung disease (ILD).

Altered lamellar body structure and the loss of surfactant function are the consequences of mutations in genes encoding SP-B and ATP-binding cassette A3 (ABCA3), a required gene for surfactant packaging in AT2 cells. All these mutated genes disrupt AT2 cell function are the cause of acute respiratory distress syndrome and chronic interstitial lung disease in neonates and adults [105].

Moreover, the lack of an adequate number of differentiated AT2 cells in premature human newborns leads to insufficient production of the amount of pulmonary surfactant, which results in neonatal respiratory distress syndrome (RDS) and death [34]. Alveoli structure is disrupted in several pathological conditions such as the reduced number of AT2 cells in chronic obstructive pulmonary fibrosis (COPD) which is contributed to increased apoptosis and senescence [106][107]. AT2 cells obliteration, ER stress and mutations associated with abnormal surfactant protein processing are reported in idiopathic pulmonary fibrosis and hereditary fibrotic lung diseases [108].

1.3 Fgf10-Fgfr2b signalling in lung homeostasis and repair

Fibroblast growth factors (Fgfs) are essential for normal lung development, homeostasis, and repair after injury. Fgfs mediate their biological functions by binding and activating tyrosine kinase Fgf receptors (Fgfrs), namely Fgfr1-4. Fgfr2 with two alternative splice isoforms, which are Fgfr2b and Fgfr2c, found mainly in epithelial and

bind to four ligands: Fgf1, Fgf7, Fgf10 and Fgf20, which are mostly expressed in mesenchymal cells [109][110][111].

Fgf10 play a critical role in the differentiation of AT2 cells in the neonatal mice. It is reported that the ratio of AT2 cells is decreased in the lungs of *Fgf10*$^{+/-}$ (heterozygous) compared to *Fg10*$^{+/+}$ (WT), demonstrating that Fgf10 is indeed important for the formation of the AT2 lineage during alveologenesis [84].

During adult lung homeostasis, Fgf10 is expressed in mesenchymal stromal niches in the lipofibroblast adjacent to AT2 cells and in upper conducting airways in intercartilage rings proximity to basal cells. Fgf10-Fgfr2b signalling is required in stemness maintenance and epithelial amplification after injury [112][53]. For instance, deletion of one copy of *Fgfr2b* in basal stem cells (BSCs) results in the reduction of their self-renewal and turning them to senescent cells [113].

Fgf10-Fgfr2b signaling is activated in differentiated epithelial cells following airway epithelial injury. For example, after naphthalene mediated injury, Fgf10 expression is induced in airway smooth muscle cells (ASMCs), thereby activating Fgfr2b signaling in a subpopulation of club cells resulting in their expansion and differentiation [49]. In addition, the inhibition of Fgf10-Fgfr2b signaling in bronchial epithelial cells in the context of bleomycin injury led to impairment of neo-basal cells and alveolar epithelial cells regeneration. On the other side, the overexpression of Fgf10 in bronchial epithelial cells after injury promoted their differentiation into AT2 rather than into basal cells, indicating the significance of Fgfr2b signaling to promote AT2 cells differentiation [114]. Moreover, activated Fgfr2b signaling in epithelial stem cells is instrumental in the repair of damaged epithelium after Influenza virus infection and in the restoration of alveolar barrier function. In addition, Fgfr2b signaling attenuation leads to the loss of epithelial stem cell proliferation, while the overexpression of Fgf10 results in enhanced proliferation of these cells [115].

The significance of Fgf10 in the adult lung has been revealed from different lung diseases which appear as a result of Fgf10 dysregulation like idiopathic pulmonary fibrosis (IPF), bronchopulmonary dysplasia (BPD), and chronic obstructive disease (COPD) [57][116][117].

It has been shown that conditionally Fgf signalling inhibition in respiratory epithelium impair lung recovery after hyperoxia [118]. Moreover, Fgf10 treatment resulting in

recovering Lipopolysaccharide (LPS)-induced acute lung injury restoration of Sftpc and SftpA synthesis [119][120].

Induced Fgf10 expression in alveolar epithelium in bleomycin induced lung injury leads to fibrosis attenuation and it seems that Fgf10 protects alveolar epithelium through increasing AT2 cells survival. This suggests the existence of AT2 progenitor cells which are capable of responding to FGF10 in the fibrotic lung, however their identity is unknown [47].

Aims of study:

AT2 cells are heterogeneous population; where specialized AT2 subpopulations within this lineage exhibit stem cell properties. However, it is still debatable whether quiescent and immature AT2 progenitor cells exist in mouse and human lungs and if surface markers can be used to isolate these cells. Furthermore, AT2 cells reside adjacent to Fgf10 expressing lipofibroblasts which keep Fgf10-Fgfr2b active in these cells. However, it is not clear that, whether Fgf10-Fgfr2b signaling is essential for the maintenance of different AT2 subpopulations.

Aims of this study are summarized as following:

1. Studying AT2 cells heterogeneity and the existence of immature and quiescent AT2 cells in the adult lung
2. Examine AT2 subpopulations responses during lung regeneration
3. Investigation of AT2 cells behavior *in vitro* upon injury
4. Identification of surface markers allowing better characterization of AT2 cell subpopulations
5. Response of AT2 cell subpopulations to *Fgfr2b* deletion

2 Material and Methods

2.1 Animal experiments

All animals were housed under specific pathogen-free (SPF) conditions with free access to food and water. Genetically modified mice including Sftpc$^{tm1(cre/ERT2,rtTA)Hap}$ (stock number 007905) [61] , and the Cre reporter line B6;129S6-Gt(ROSA)26Sor$^{tm9(CAG-tdTomato)Hze}$/J (stock number 007909) [121] were purchased from Jackson laboratory (Bar Harbor/ME, USA). Fgfr2^{tm1Dsn} (Fgfr2-IIIb^{flox}) was a gift from C. Dickson. All animal studies were performed according to protocols approved by the Animal Ethics Committee of the Regierungspraesidium Giessen (permit numbers: G7/2017–No.844-GP and G11/2019–No. 931-GP).

2.2 Mice Genotyping

Tissues from the distal tip of the tails were digested in 200 µl Viagen including 1 µl proteinase K in 55°C on a shaker overnight, then reaction was stopped in 85°C for 40 min. Genotyping were done by PCR using specific primers (Table 1) and according to the protocol (Table 2). PCR products were analyzed using a 1,5 % agarose gel containing TAE buffer with Sybrsafe (50 µl Sybrsafe + 500 ml 1x TAE buffer). PCR samples (10 µl) were loaded with 2 µl loading dye (Nucleic Acid Sample loading buffer, 5x, Bio-Rad, Berkeley, California), and then gel was run with 120V for 30-45 min. A molecular ladder (QX Size Marker, 100bp-2.5kb, Qiagen, Hilden, Germany) was used to detect the expected band sizes (Table 1).

2.3 Tamoxifen administration

8-16-weeks-old mice were treated with tamoxifen-containing water (1 mg/ml) (T5648, Sigma-Aldrich, Darmstadt/Germany) for 7 or 14 days to induce Cre recombinase activity.

Table 1: Primer sequences for genotyping

Mouse line	Primer sequences	Expected band size for WT	Expected band size for mutant
Sftpc^{CreERT2}	1) CCC AGT CCC TCT CTG AAT TTG 2) GTT TCT ACC GAC CCT GTG AAG 3) CAT CGC TCG ACC AGT TTA GTT A	500 bp	1000 bp
tdTomato^{flox}	1) CTG TTC CTG TAC GGC ATG G 2) GGC ATT AAA GCA GCG TAT CC 3) CCG AAA ATC TGT GGG AAG TC 4) AAG GGA GCT GCA GTG GAG TA	297 bp	196 bp
Fgfr2b^{flox}	1) CTG CCT GGC TCA CTG TCC 2) CTC AAC AGG CAT GCA AAT GCA AGG TC	380 bp	480 bp

Table 2: PCR protocols for genotyping

Mouse line	PCR protocol		
	Step	Temperature (°C)	Time
Sftpc^{CreERT2}	1	95	3 min
	2	95	30 sec
	3	50	30 sec
	4	72	72 sec (repeat 2-4 34 times, in total 35)
	5	72	3 min
tdTomato^{flox}	1	94	20 sec
	2	94	30 sec
	3	61	30 sec
	4	72	72 sec (repeat 2-4 34 times, in total 35)

	5	72	2 min
Fgfr2b^{flox}	1	94	2 min
	2	94	30 sec
	3	55	30 sec
	4	72	72 sec (repeat 2-4 34 times, in total 35)
	5	72	2 min

2.4 Human specimens

Human lung tissues from idiopathic pulmonary fibrosis (IPF) patients undergoing lung transplantation and non-IPF donors were provided from the Giessen biobank. The study protocol (AZ31/93) was approved by the ethics committee of University of Giessen that conforms to the principles outlined in the declaration of Helsinki. Tissues were subjected to flow cytometry followed by, cell isolation, RNA extraction and gene expression analysis by qPCR.

2.5 Lung dissociation and Flow Cytometry

Adult mice were sacrificed and lungs were perfused with 5 ml PBS through the right ventricle. Lungs were inflated via the trachea with dispase and kept in dispase (Coning, NY, USA) and Collagenase Type IV at 37°C for 40 min with frequent agitation. To achieve single cell suspensions, digested tissue was passed serially through 100-, 70- and 40-µm cell strainers (BD Biosciences, Heidelberg, Germany). Red blood cells (RBC) were eliminated using RBC lysis buffer (Sigma-Aldrich, Schnelldorf, Germany) according to manufacturer's protocol. Cells were pelleted, resuspended in FACS buffer (0.1% sodium azide, 5% fetal calf serum (FCS), 0,05% in PBS) and stained with antibodies: anti-EpCAM (APC-Cy7-conjugated, 1:50, Biolegend, Fell, Germany), CD49F (APC-conjugated, Biolegend,1:50), anti-PDPN (FITC-conjugated, Biolegend, 1:20) ,and anti-PD-L1 (unconjugated, , 1:100,Thermo Fisher Scientific, Langenselbold) antibodies for 20 minutes on ice in the dark, followed by washing. Then, the cells were stained for goat anti rabbit secondary antibody Alexa flour 488 (1:500 Invitrogen, Darmstadt, Germany) for 20 minutes on ice in the dark. Next, cells were washed and

stained with SYTOX (Invitrogen) a live/dead cell stain according to the manufacturer's instructions. Cells were sorted into collection medium (RPMI 10%FBS), spun down, resuspended in RLT plus buffer mRNA lysis buffer (Qiagen plus Micro), and kept at -80°C for further analysis. Flow cytometry data acquisition and cell sorting were carried out using FACSAria III cell sorter (BD Biosciences, San Jose/CA). Data were analyzed using FlowJo software version X (FlowJo, LLC).

To stain intracellular Sftpc, cells were pelleted, resuspended in FACS buffer and stained firstly for the surface markers: anti-EpCAM (APC-Cy7-conjugated, Biolegend,1:50), CD49F (APC-conjugated, Biolegend,1:50, PD-L1 (unconjugated antibody, Thermo Fisher 1:50) for 20 minutes on ice in the dark. After washing, cells were fixed and permeabilized using FoxP2 Transcription Factor Buffer Set according to the manufacturer's instructions (Invitrogen). Pro-SPC antibody (Santa Cruz, 1:1000) was added and incubated overnight in 4°C. After washing, the cells were stained with donkey anti rabbit Alexa flour 488 (Invitrogen,1:500) and donkey anti goat Alexa flour 647 (Invitrogen,1:200) secondary antibodies for 20 minutes on ice in the dark, followed by washing. Flow cytometry data acquisition and cell sorting were carried out using FACSAria III cell sorter (BD Biosciences, San Jose/CA). Data were analyzed using FlowJo software version X (FlowJo, LLC).

2.6 Human Lung Dissociation and Flow Cytometry

Human IPF or donor tissue were weighed, chopped and minced into small pieces of approximately 1mm^3, washed 3 times with RPMI and then resuspended in a solution of 10 % Dispase (Cornig) 30 μg/ml DNAse I (Sigma-Aldrich) in RPMI (Thermo Fischer Scientific) and incubated for 2h at 37^{o}C. At the end of incubation, cells were strained through 100 μm, 70 μm and 40 μm cell strainers to obtain a single cell suspension. Cells were cryopreserved in 20% FBS (PAA) 5% DMSO (Sigma-Aldrich) RPMI in the UGMLC Biobank until the time of the flow cytometry analysis.

Cryo-preserved vials were thawed rapidly and resuspended in 10mls RPMI 10% FBS, washed and maintained on ice throughout the staining, acquisition and sorting procedure. After thawing, 10^6 cells were resuspended in a master mix of cells surface antibodies in FACS buffer (HBSS 2%FBS 30 μg/ml DNase 0.1mM HEPES) and incubated on ice for 30 minutes. The following antibodies were used: anti-human EpCAM APC-Cy7 (1:100, Clone 9C4, Biolegend), anti-human CD45 Pe-Cy7 (1:100,

Clone 2D1, Biolegend), anti-human CD31 Pe-Cy7 (1:100, Clone WM59, Biolegend), HTII-280 (1:100, Terrace Biotech), anti-human PD-L1 APC (2.5:100, Clone B7-H1, Biolegend). For indirect detection of HTII-280, cells were incubated again on ice for 30 min in the secondary antibody anti-mouse IgM Alexa Fluor 488 (1:2000, Life Technologies A-21042) resuspended in FACS buffer. Cells were washed one time in FACS buffer, resuspended in FACS buffer with DAPI (1:3000, Sigma Aldrich) and immediately used for acquisition of flow cytometry data (BDCanto II, BD Biosciences) or Sorting (BD FACSAria III, BD Bioscicences, Allschwil, Schweiz). Cells were sorted into collection medium (RPMI 10%FBS), spun down, resuspended in RLT buffer mRNA lysis buffer (Qiagen Mini), and kept at -80 °C for further analysis. Flow cytometry data analysis was performed using FlowJo Version X (FlowJo LLC).

2.7 RNA extraction and quantitative real-time PCR

Following lysis of FACS-isolated cells from mouse or human lungs in RLT buffer, RNA was extracted using a RNeasy plus Micro kit (Qiagen) and cDNA synthesis was carried out using QuantiTect reverse transcription kit (Qiagen) according to the instructions provided by supplier. Thereafter, selected primers were designed via NCBI's primer-BLAST option (https://www.ncbi.nlm.nih.gov/tools/primer-blast/) (Table 3 and Table 4). Quantitative real-time polymerase chain reaction (qPCR) was performed using PowerUp SYBR Green Master Mix kit according to the manufacturer's protocol (Applied Biosystems, Foster City, California) and LightCycler 480 II machine (Roche Applied Science). hypoxantine-guanine phosphoribosyltransferase (Hprt) and glyceraldehyde 3-phosphate dehydrogenase (GAPDH) were used as reference genes for mice and human, respectively. Data were presented as mean expression relative to Hprt and GAPDH. Data were assembled using GraphPad Prism software (GraphPad Software, La Jolla/CA). Statistical analyses were performed utilizing two tailed-paired Student t-test. Results were regarded significant when $p < 0.05$.

Table 3: **Mouse primer sequences for qPCR**

Gene (Mouse)	**Forward primer (5'->3')**	**Reverse primer (5'->3')**
HPRT	CCTAAGATGAGCGCAAGTTGAA	CCACAGGACTAGAACACCTGCTAA
Fgfr2IIIb	TAAATACGGGCCTGATGGGC	CAGCATCCATCTCCGTCACA
Etv5	CAGCCCGCCACGGAG	CCGCTATCACTTTGAAGGGC
Sftpc	GGTCCTGATGGAGAGTCCAC	GATGAGAAGGCGTTTGAGG
Sftpb	GGCTAGACAGGCAAAAGTGTG	GACCGCGTTCTCAGAGGTG
Sftpa1	CAGTGTGATTGGGAGAAACCA	ATGCCAGCAACAACAGTCAA
CD33	TCTGTCTCGTGTTTCTCATTGTG	GCAGTTGGAGATAGGCAGTGA
PD-L1	AAGTCAATGCCCCATACCGC	TTCTGGATAACCCTCGGCCT
Ki67	CTGCGAGCTTCACCGAGAG	CAATACTCCTTCCAAACAGGCAG
CCNd1	TCAAGTGTGACCCGGACTG	CCACATCTCGCACGTCGG
CCNd2	TACCTGGACCGTTTCTTGGC	TACCAGTTCCCACTCCAGCA
Scgb1a1	GCCTCCAACCTCTACCATGA	TCAGGGATGCCACATAACCA

Table 4: Human primer sequences for qPCR

Gene (Human)	**Forward primer (5'->3')**	**Reverse primer (5'->3')**
GAPDH	ACCCAGAAGACTGTGGATGG	GTGTCGCTGTTGAAGTCAGAG
SCGB1A1	CCCTCCTCCACCATGAAACTC	AGGGTTTCGATGACACGCTG
ETV5	AGGGGCAGAAAACCACCAAA	GTCCCGTTTTGCGGGTACTA
SFTPC	CACTGAAGCGGGGTCATCCA	TGCAAAAGCTGCAAAAGACCC

2.8 Immunofluorescent Staining

After lung perfusion with PBS through the right ventricle, isolated lungs were fixed with 4% paraformaldehyde. Afterward, tissues were embedded in paraffin and sectioned at 5 µm thickness. For deparaffinization process slides were placed in the jars with specified reagents in the following orders:

- Xylol (6 min)
- Xylol (6 min)
- 100% Ethanol (2 min)
- 100% Ethanol (2 min)
- 95% Ethanol (2 min)
- 70 % Ethanol (2 min)
- 50% Ethanol (2 min)
- 30% Ethanol (2 min)
- Deionized water (2 min)

Following deparaffinization, slides were blocked with 3% bovine serum albumin (BSA) (Jackson Immunoresearch Laboratories) in PBS for 1 hour at RT. Immunofluorescent (IF) staining was performed using overnight incubation with polyclonal anti-Prosurfactant Protein C (ProSP-C) (Merck/Millipore/Sigma-Aldrich, 1:500). This was followed by staining with polyclonal secondary antibody Goat anti rabbit Alexa flour 488 (Invitrogen,1:500). Slides were finally mounted with ProLong Gold Antifade Reagent containing DAPI (Molecular Probes). For quantification, cells were counted in 10 independent 63x fields per sample. For each experiment, sections from at least four independent lungs were analyzed.

2.9 Hematoxylin and eosin staining

Mouse lung tissues were fixed using 4% PFA followed by embedding in paraffin. Paraffin blocks were sectioned into 5-µm-thick slices and placed on glass slides. Following deparaffinization, lung sections were stained with hematoxylin (Roth) for 2 min, washed with running tap water for 10 min and then stained with eosin (Thermo Fisher Scientific) for 2 min.

2.10 Alveosphere assay

Sorted epithelial cells (Tom^{Low} and Tom^{High}) from [$Sftpc^{CreERT2/+}$; $tdTom^{flox/flox}$] and *$Sftpc^{CreERT2/+}$; $Fgfr2b^{flox/flox}$; $tdTom^{flox/flox}$*] mice mice and resident mesenchymal cells from C57BL/6J mice ($Epcam^{neg}$, $CD31^{neg}$, $CD45^{neg}$, $Sca1^{pos}$) were centrifuged and resuspended separately in cell culture medium (Dulbecco's Modified Eagle Medium, Life Technologies). To adjust the optimal concentrations, $1x10^3$ epithelial cells in 25 µL media and $2x10^4$ mesenchymal cells in 25 µL media per insert (12 mm cell culture inserts with 0.4 µm membrane Millipore) were used. Mesenchymal and epithelial cell suspensions were mixed, followed by an addition of cold Matrigel® growth factor-reduced (Corning) at a 1:1 dilution resulting in 100 µL final volume per insert. Matrigel cell suspensions were placed on the top of the filter membrane of the insert and incubated at 37°C for 5 min. Next, 350 µL of medium was transferred to each well. Cells were incubated under air-liquid conditions at 37°C with 5% CO2 for two weeks. Media were changed 3 times per week.

Immunofluorescent (IF) staining was performed using overnight incubation with polyclonal anti-Prosurfactant Protein C (ProSP-C) (Merck/Millipore/Sigma-Aldrich, 1:500) ant anti Rage (R&D Systems,1:100). This was followed by staining with polyclonal secondary antibody Goat anti rabbit Alexa flour 647 (Invitrogen,1:500) and Goat anti mouse Alexa flour 488 (Invitrogen,1:500). Slides were finally mounted with ProLong Gold Antifade Reagent containing DAPI (Molecular Probes).

2.11 Pneumonectomy

Prior to surgery, adult mice (8–12 weeks old) were weighed, given Buprenorphine (0.1 mg/kg, and shaved at the surgical site on the left lateral side. Mice were anesthetized with 2.5% isofluorane and intubated for ventilation using a Harvard mini-vent ventilator. Mice were anesthetized and ventilated throughout the pneumonectomy procedure with 200 µL of stroke volume at 170 strokes per minute. The surgical site was sterilized with beta-iodine and then a 2 cm long incision was made on the left lateral side of the skin. Left-sided thoracotomy was performed with a 1 cm long incision at the 5^{th} intercostal space to expose the left lung lobe underneath. The ribs were spread by retraction and the left pulmonary vasculature and mainstem bronchus were ligated with a titanium clip. The left lobe was resected, and the ribs and skin closed. An angiocath port was

inserted to evacuate the void space and re-establish negative intrathoracic pressure. Sham control surgeries were performed as thoracotomy procedure without lung removal. Mice were disconnected from the ventilator when autonomous breathing recovered. Mice were placed on a warming pad and monitored until awake. A second Buprenorphine dose was given 24 hours later and monitored to ensure that a full recovery was made. Metamizole was added to the drinking water one day before surgery and continue to 4 days post operation.

2.12 Microarray

Purified total RNA was amplified using the Ovation PicoSL WTA System V2 kit (NuGEN Technologies). Per sample, 2 µg amplified cDNA was Cy5-labeled using the SureTag DNA labeling kit (Agilent). Hybridization to 8x60K 60mer oligonucleotide spotted microarray slides (Human Mouse Genome, Agilent Technologies, design ID 074809) and subsequent washing and drying of the slides was performed following the Agilent hybridization protocol in Agilent hybridization chambers, with following modifications: 3 µg of the labeled cDNA were hybridized for 22 hours at 65°C. The cDNA was not fragmented before hybridization.

The dried slides were scanned at 2 µm/pixel resolution using the InnoScan is900 (Innopsys). Image analysis was performed with Mapix 6.5.0 software, and calculated values for all spots were saved as GenePix results files. Stored data were evaluated using the R software [122] and the limma package [123] from BioConductor [124]. Log2 mean spot signals were taken for further analysis. Data was background corrected using the NormExp procedure on the negative control spots and quantile-normalized [123][125] before averaging. Log2 signals of replicate spots were averaged, and from several different probes addressing the same gene only the probe with the highest average signal was used. Genes were ranked for differential expression using a moderated t-statistic [123]. Pathway analyses were done using gene set tests on the ranks of the t-values [123][126]. Pathways were taken from the KEGG database (http://www.genome.jp/kegg/pathway.html).

2.13 ATAC-seq

25.000 FACS-sorted cells were collected and used for ATAC Library preparation using Tn5 Transposase from Nextera DNA Sample Preparation Kit (Illumina). Cell pellet was resuspended in 50 µl Lysis/Transposition reaction (12.5 µl THS-TD-Buffer, 2.5 µl Tn5, 5 µl 0.1% Digitonin and 30 µl water) and incubated at 37°C for 30 min with occasional snap mixing. Following purification of the DNA, fragments was done by Min Elute PCR Purification Kit (Qiagen). Amplification of Library together with Indexing Primers was performed as described [127]. Libraries were mixed in equimolar ratios and sequenced on NextSeq500 platform using V2 chemistry. Trimmomatic version 0.38 was employed to trim reads after a quality drop below a mean of Q15 in a window of 5 nucleotides [128]. Only reads longer than 15 nucleotides were cleared for further analyses. Trimmed and filtered reads were aligned versus the mouse genome version mm10 (GRCm38) using STAR 2.6.1d with the parameters "--outFilterMismatchNoverLmax 0.1 --outFilterMatchNmin 20 --alignIntronMax 1 --alignSJDBoverhangMin 999 --outFilterMultimapNmax 1 --alignEndsProtrude 10 ConcordantPair"[129] and retaining only unique alignments to exclude reads of uncertain origin. Reads were further deduplicated using Picard 2.18.16 (Picard: A set of tools (in Java) for working with next generation sequencing data in the BAM format) to mitigate PCR artefacts leading to multiple copies of the same original fragment. Reads aligning to the mitochondrial chromosome were removed. The Macs2 peak caller version 2.1.2 was employed to accommodate for the range of peak widths typically expected for ATAC-seq [130]. Minimum q-value was set to -4 and FDR was changed to 0.0001. Peaks overlapping ENCODE blacklisted regions (known misassemblies, satellite repeats) were excluded. In order to be able to compare peaks in different samples to assess reproducibility, the resulting lists of significant peaks were overlapped and unified to represent identical regions. Sample counts for union peaks were produced using bigWigAverageOverBed (UCSC Toolkit) and normalized with DESeq2 1.18.1 to compensate for differences in sequencing depth, library composition, and ATAC-seq efficiency [131]. Peaks were annotated with the promoter of the nearest gene in range (TSS ± 5000 nt) based on reference data of GENCODE vM15.

2.14 Statistical analysis

Statistical analysis and graph assembly were carried out using GraphPad Prism 6 (GraphPad Prism Software). Significance was determined by unpaired two-tailed Student's t-tests. Data are presented as mean ± standard error of mean (SEM). Values of $p < 0.05$ were considered significant. The number of biological samples (n) for each group are stated in the corresponding figure legends.

3 Results

This section will be divided into two parts:

Part 3.1 Identification a novel subset of alveolar type 2 cells expanding following pneumonectomy and enriched in PD-L1

Part 3.2 Evidence that *Fgfr2b* deletion in AT2 cells elicits a differential response in AT2 subpopulations

3.1 Identification a novel subset of alveolar type 2 cells expanding following pneumonectomy and enriched in PD-L1

3.1.1 Identification of two AT2 subpopulations with different Sftpc and Fgfr2b levels

Sftpc$^{CreERT2/+}$*; tdTomato*$^{flox/flox}$ mice were used to lineage label AT2 cells in the adult lung. Tamoxifen was delivered in the water for one week to trigger the translocation of Cre-ERT2 to the nucleus, thereby inducing in the *Rosa26* reporter locus and the removal of the STOP codon (Figure 6a). Two distinct subpopulations of tdTomato^{Pos} cells, were identified using flow cytometry analysis namely, tdTomato^{Low} (Tom^{Low}) and tdTomato^{High} (Tom^{High}) (Figure 6a). In average, Tom^{Low} represented 9.93% of the overall Epcam^{Pos} cells (9.93% ± 1.73%, n=4) and Tom^{High} represented 42.75% of the overall Epcam^{Pos} cells (42.75% ± 1.22%, n=4) (Figure 6b).

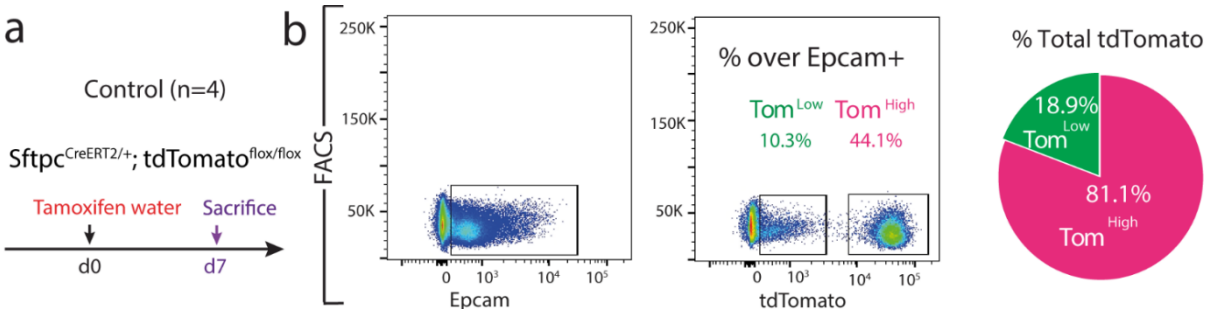

Figure 6: Identification of two subpopulations of AT2-lineage labeled cells, namely tdTomato^{Low} (Tom^{Low}) and tdTomato^{High} (Tom^{High}). a) Timeline of tamoxifen treatment of Sftpc$^{CreERT2/+}$, *tdTomato*$^{flox/flox}$ mice (n=4). **b)** Representative flow cytometry of EpCAM positive

population selection and identification of Tom^{Low} (10.3%) and Tom^{High} (44.1%) populations based on the tdTomato level. The pie chart shows the percentage of Tom^{Low} (18.9%) and Tom^{High} (81.1%) in total tdTomato positive cells.

It also was confirmed that in this mouse line, epithelial cells were specifically labeled and that it mostly targeted AT2 $Sftpc^{Pos}$ cells (Figure 7a,b). Very few BACS cells, identified through their localization at the BADJ, are labeled (0.1% of the total Tom^{Pos} cells), consistent with the literature [61]. The labeling efficiency of AT2 cells was 77% (77% ± 5.40%, n=4) (Figure 7b).

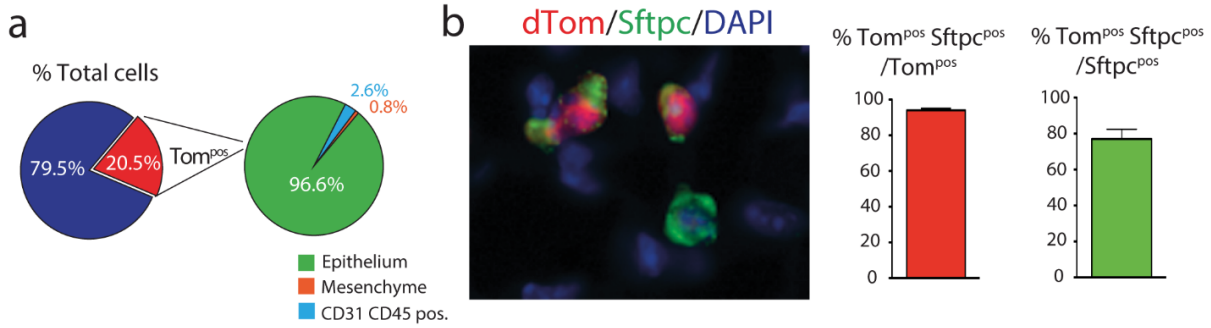

Figure 7: Validation of *$Sftpc^{CreERT2/+}$; $tdTomato^{flox/flox}$* mice. a) The pie chart represents the percentage of $tdTomato^{Pos}$ cells in total cells (20.5%) and the percentage of epithelial (96.6%), mesenchymal cells (2.6%), and CD31, CD45 positive cells (0.8%) of the labeled cells. **b)** Representative Sftpc immunofluorescence staining and quantification of $tdTomato^{Pos}$ $Sftpc^{Pos}$ of total $tdTomato^{Pos}$ as well as quantification of $tdTomato^{Pos}$ $Sftpc^{Pos}$ of total $Sftpc^{Pos}$ (n=4). Data are presented as mean values ± SEM.

In this mouse line, 4.5% of Tom^{pos}/total cells were labeled in mice exposed to normal water, indicating leakiness. This percentage is increased to 20.5% of Tom^{pos}/total cells in mice exposed to tamoxifen water for one week (Figure 8a-d) indicating robust induction of labelling.

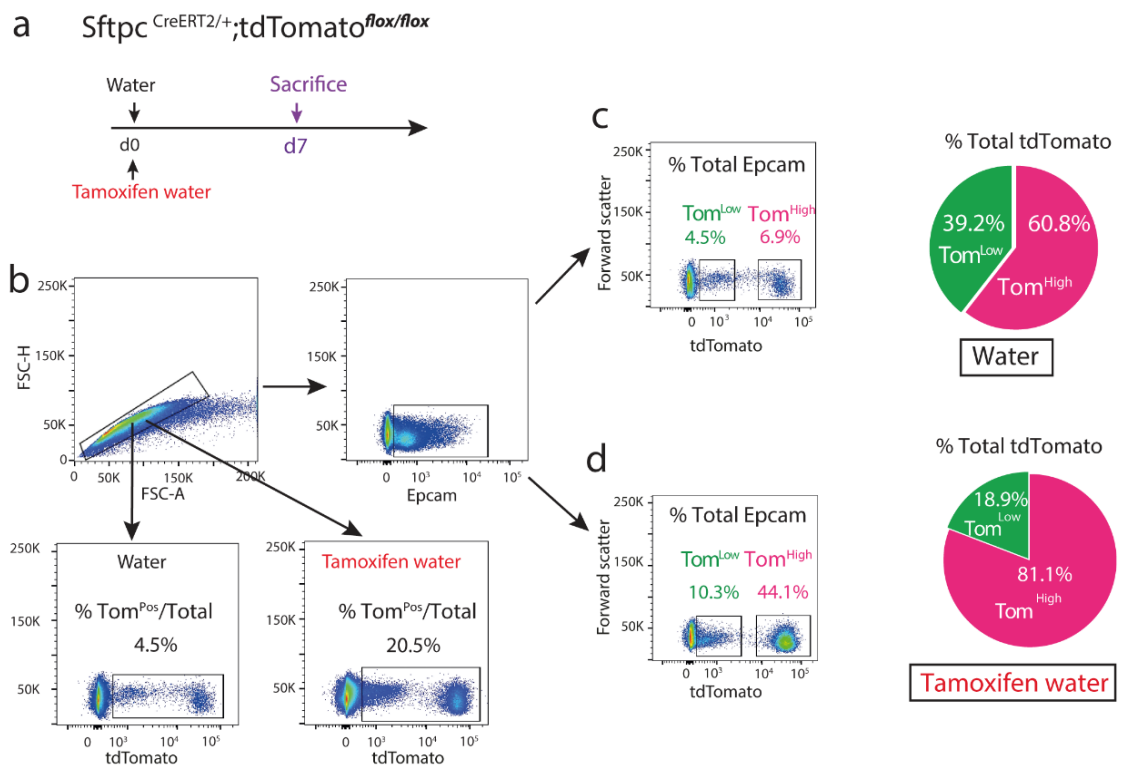

Figure 8: AT2 cells labeling in the absence and the presence of tamoxifen treatment. a) Timeline of tamoxifen treatment. One group of Sftpc$^{CreERT2/+}$, *tdTomato*$^{flox/flox}$ mice were treated with tamoxifen in drinking water for 7 days and another group no tamoxifen added to the water. **b)** Representative flow cytometry analysis of single-cell selection and further analysis of Epcam positive population in both groups. **c)** Representative flow cytometry analysis of Tom^{Low} (4.5%) and Tom^{High} (6.9%) in untreated mice with tamoxifen. The pie chart shows the percentage of Tom^{Low} (39.2%) and Tom^{High} (60.8%) in total tdTomato positive cells. **d)** Representative flow cytometry analysis of Tom^{Low} (10.3%) and Tom^{High} (44.1%) in treated mice with tamoxifen. The pie chart shows the percentage of Tom^{Low} (18.9%) and Tom^{High} (81.1%) in total tdTomato positive cells.

Next, the distribution of fluorescence intensity of the tdTomato^{Pos} cells was analyzed on lung sections. The threshold was set at 22% based on the flow cytometry data and then the intensity of Sftpc immunofluorescence staining was quantified in each cell located on the left side (Tom^{Low}) and the right side (Tom^{High}) of the threshold. Both populations contain Sftpc^{Low} and Sftpc^{High} cells, thereby suggesting heterogeneity of both Tom^{Low} and Tom^{high} subpopulations in terms of Sftpc level (Figure 9a-c). Interestingly, PCR from the genomic DNA for the presence of the STOP codon in the *Rosa26* locus (which is normally removed upon induction of Cre activity) indicated that the LoxP-STOP-LoxP site was partially recombined in Tom^{Low} cells versus Tom^{High}

cells (Figure 9d). This incomplete deletion could explain the presence of these two subpopulations of tdTomato cells.

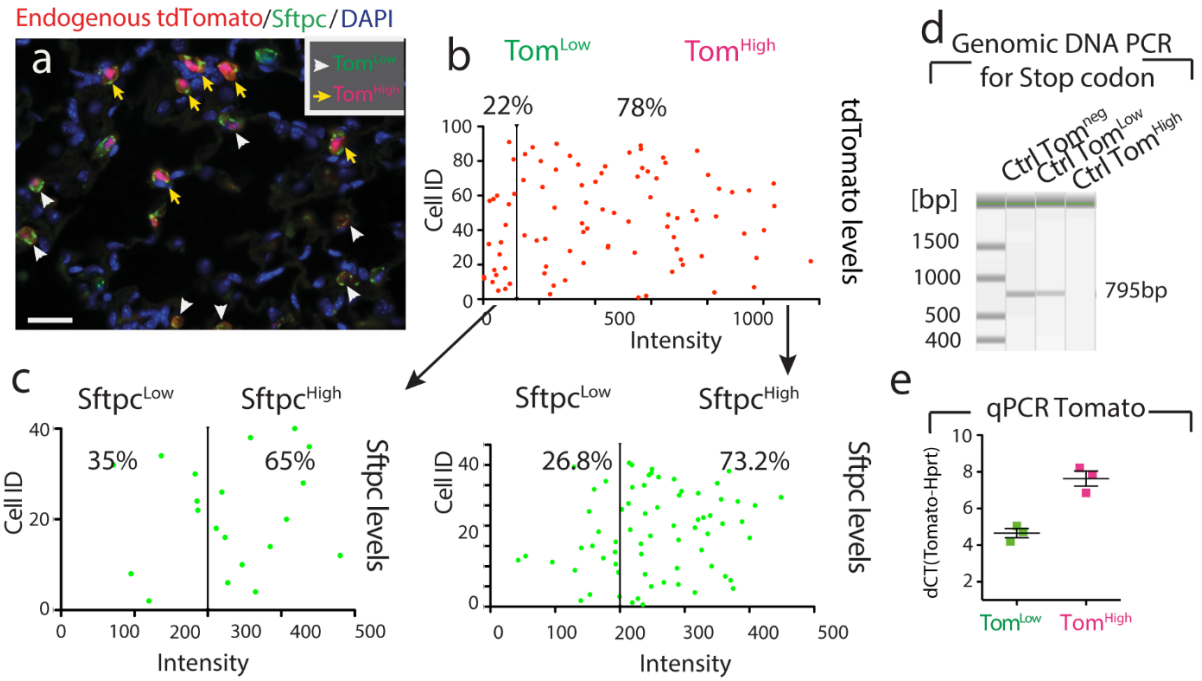

Figure 9: Heterogeneity of both Tom^{Low} and Tom^{high} subpopulations in Sftpc level and differential recombination in Tom^{Low} and Tom^{high} a) Representative Sftpc immunofluorescence staining and localization of Tom^{Low} and Tom^{High} in the alveoli (Scale bar: 50µm). **b)** Plots display quantification of tdTomato fluorescent intensity of tdTomato positive cells **c)** Plots show further quantification of Sftpc level in Tom^{Low} and Tom^{High} populations separately. **d)** PCR on genomic DNA isolated from FACS-based sorted Tom^{Low} and Tom^{High} cells. **e)** qPCR analysis of FACS-based sorted Tom^{Low} and Tom^{High} cells for the expression of *Tomato*.

Next, it was investigated whether incomplete deletion of the STOP codon in the [*Sftpc$^{CreERT2/+}$; tdTomato$^{flox/flox}$*], allowing in the Tom^{Low} population only one Tomato copy to be expressed against two copies for the Tom^{High} cells, was the sole reason for the difference in the expression of *Tomato*. To test this possibility, [*Sftpc$^{CreERT2/+}$; tdTomato$^{flox/+}$*] mice were used, with only one copy of Tomato. In case of insufficient recombination, only one population of Tomato positive cells should be observed. Upon treatment with tamoxifen, the flow cytometry results indicate the presence of Tom^{Low} and Tom^{High} subpopulations in these mice as well (Figure 10) supporting the conclusion that the existence of two subpopulations in [*Sftpc$^{CreERT2/+}$; tdTomato$^{flox/flox}$*] lungs, based on different levels of *Tomato* expression, results from the differential expression of

Tomato from the *Rosa26* promoter as well as from the incomplete recombination of the STOP codon in the *Rosa26* allele in Tom^{High} vs. Tom^{Low} cells.

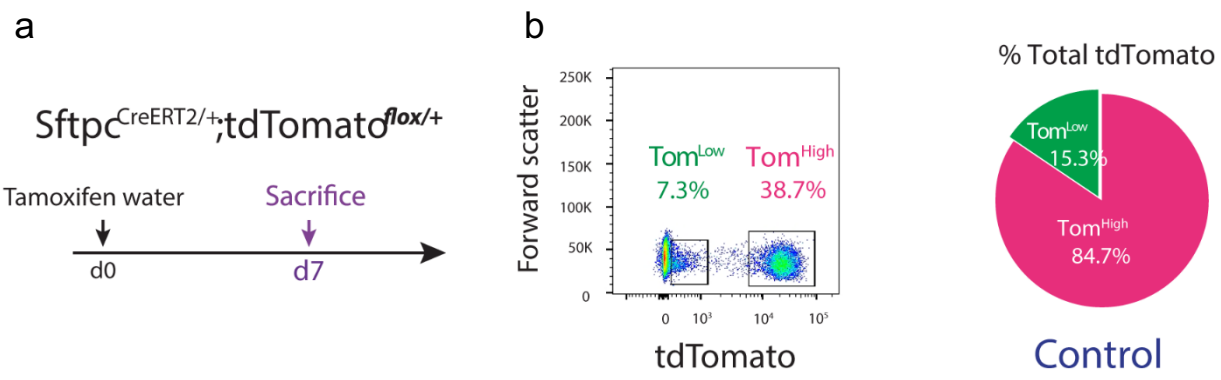

Figure 10: Identification of Tom^{Low} and Tom^{High} in *Sftpc$^{CreERT2/+}$, Tom$^{flox/+}$* mice. a) Timeline of tamoxifen treatment of *Sftpc$^{CreERT2/+}$, Tom$^{flox/+}$* mice. **b)** Representative flow cytometry analysis of Tom^{Low} (6.97%) and Tom^{High} (38.7%) of Sftpc$^{CreERT2/+}$, tdTomato$^{flox/+}$ mice. The pie chart shows the percentage of Tom^{Low} (15.3%) and Tom^{High} (84.7%) in total tdTomato positive cells.

Next, qPCR was performed on FACS-isolated Tom^{Low} and Tom^{High} cells. The results show that *Fgfr2b* and its associated downstream target *Etv5*, as well as the differentiation markers *Sftpc, Sftpb*, and *Sftpa1,* were significantly enriched in Tom^{High} vs. Tom^{Low} cells (Figure 11). Thus, it can be concluded that Tom^{High} represents the *bona fide* mature AT2 cells and promoted us to hypothesize that the lineage-related Tom^{Low} cells represent immature AT2 cells.

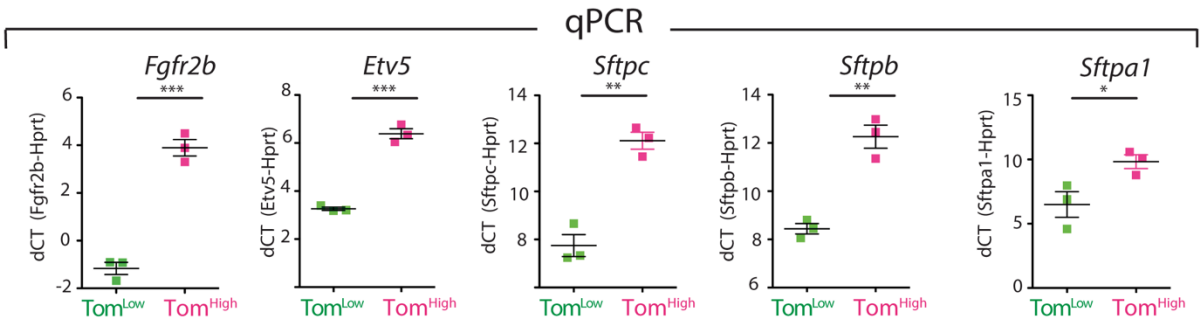

Figure 11: qPCR analysis of FACS-based sorted Tom^{Low} and Tom^{High} cells. qPCR analysis of FACS-based sorted Tom^{Low} and Tom^{High} cells for the expression of *Fgfr2b*, *Etv5*, *Sftpc*, *Sftpb,* and *Sftpa1*. Data are presented as mean values ± SEM. ∗p < 0.05, ∗∗p < 0.01, ∗∗∗p < 0.001.

3.1.2 ATAC-seq analysis indicates that Tom^{Low} cells and Tom^{High} cells are distinct cell populations

To analyse the genome-wide profiling of the epigenomic landscape, an assay for transposase-accessible chromatin using sequencing (ATAC-seq) was performed on Tom^{Low} and Tom^{High} subpopulations. Common and distinct peaks were identified for Tom^{Low} and Tom^{High} cells (Figure 13b). Further analysis of the ATAC-seq data using the Reactome database indicated that genes belonging to metabolism, cholesterol metabolism, surfactant metabolism, and triglyceride biosynthesis were enriched in Tom^{High} cells. These data agree with the known role of mature AT2 cells in surfactant production. On the other hand, Tom^{Low} cells were enriched in genes belonging to the immune system, both adaptive and innate as well as extracellular matrix organization, extracellular matrix proteoglycans, and degradation of the extracellular matrix. These results suggest a new and important function for the Tom^{Low} in interacting with the immune system, potentially displaying also migratory capabilities through ECM degradation (Figure 12).

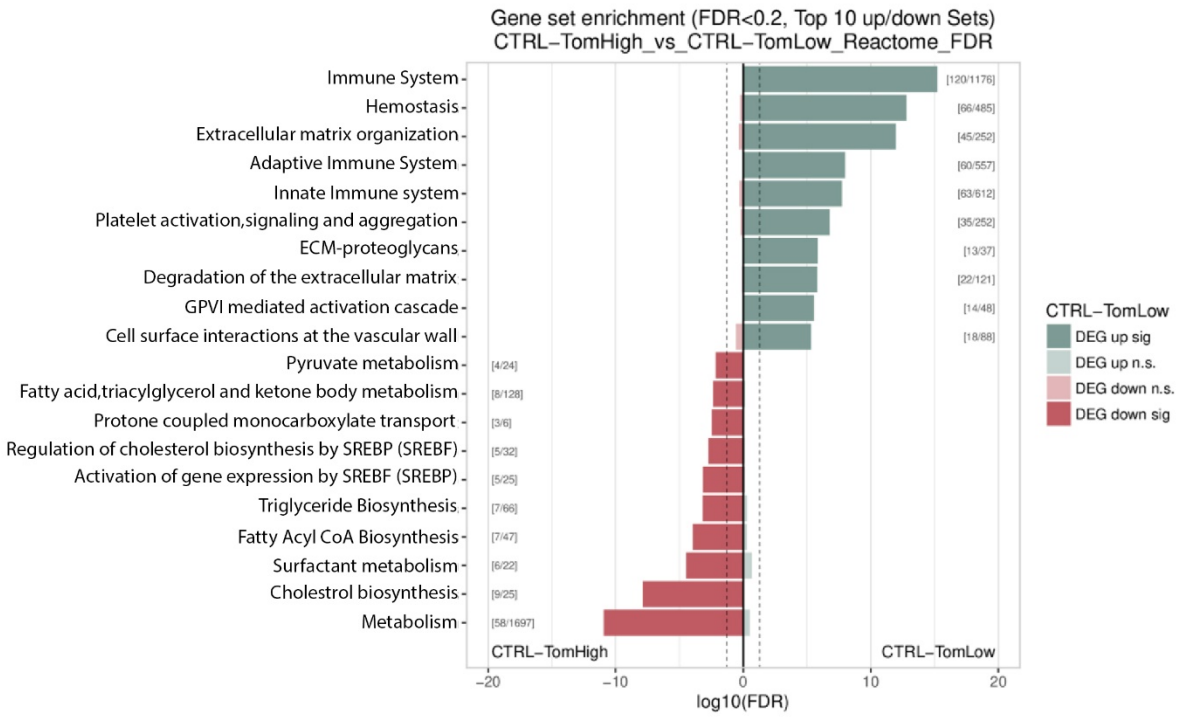

Figure 12: Gene set enrichment for accessible regions in Tom^{High} vs. Tom^{Low}. Analysis of peaks obtained in the ATAC-seq experiment for Tom^{High} and Tom^{Low} cells using Kobas for the Reactome database. Peaks overlapping the gene body or close to the transcription starting site of genes were annotated to the corresponding genes. All annotated peaks were split into lists of genes that display more open chromatin in Tom^{High} or Tom^{Low} cells using DESeq2 on unified peak regions. Observed significance was adjusted by Benjamini-Hochberg correction for multiple tests (FDR). The resulting lists were used as input for Kobas to search for enriched terms in different databases. Top 10 terms were chosen by significance (FDR < 0.2). Results indicate that the term immune system is highly enriched in Tom^{Low} cells, indicating that the chromatin of Tom^{Low} cells is more accessible in loci of genes (gene body or promoter) associated with the immune system. Higher accessibility is associated with more transcriptional activity. Numbers in brackets display the number of identified genes / total number of genes for the term in the database. DEG: Differentially expressed genes.

The ATAC-seq data also agree with the decrease in *Tomato* (expressed from the *Rosa26* promoter) and *Sftpc* expression at the mRNA level in Tom^{Low} vs. Tom^{High}. In the *Rosa26* and *Sftpc* loci (Figure 13c), the peaks corresponding to the open chromatin configuration were detected at a much higher level in Tom^{High} vs. Tom^{Low} and this difference was confirmed to be statistically significant upon quantification (Figure 13c). Interestingly, the analysis of ATAC-seq data also suggests that Tom^{Low} cells display reduced expression of cell cycle genes compared to Tom^{High} cells (Figure 13d). This decrease in cell cycle genes was confirmed by the analysis of the gene array data between Tom^{Low} and Tom^{High} (Figure S3). Overall, these data indicate that in homeostatic conditions the Tom^{Low} cells fit the profile of a quiescent population.

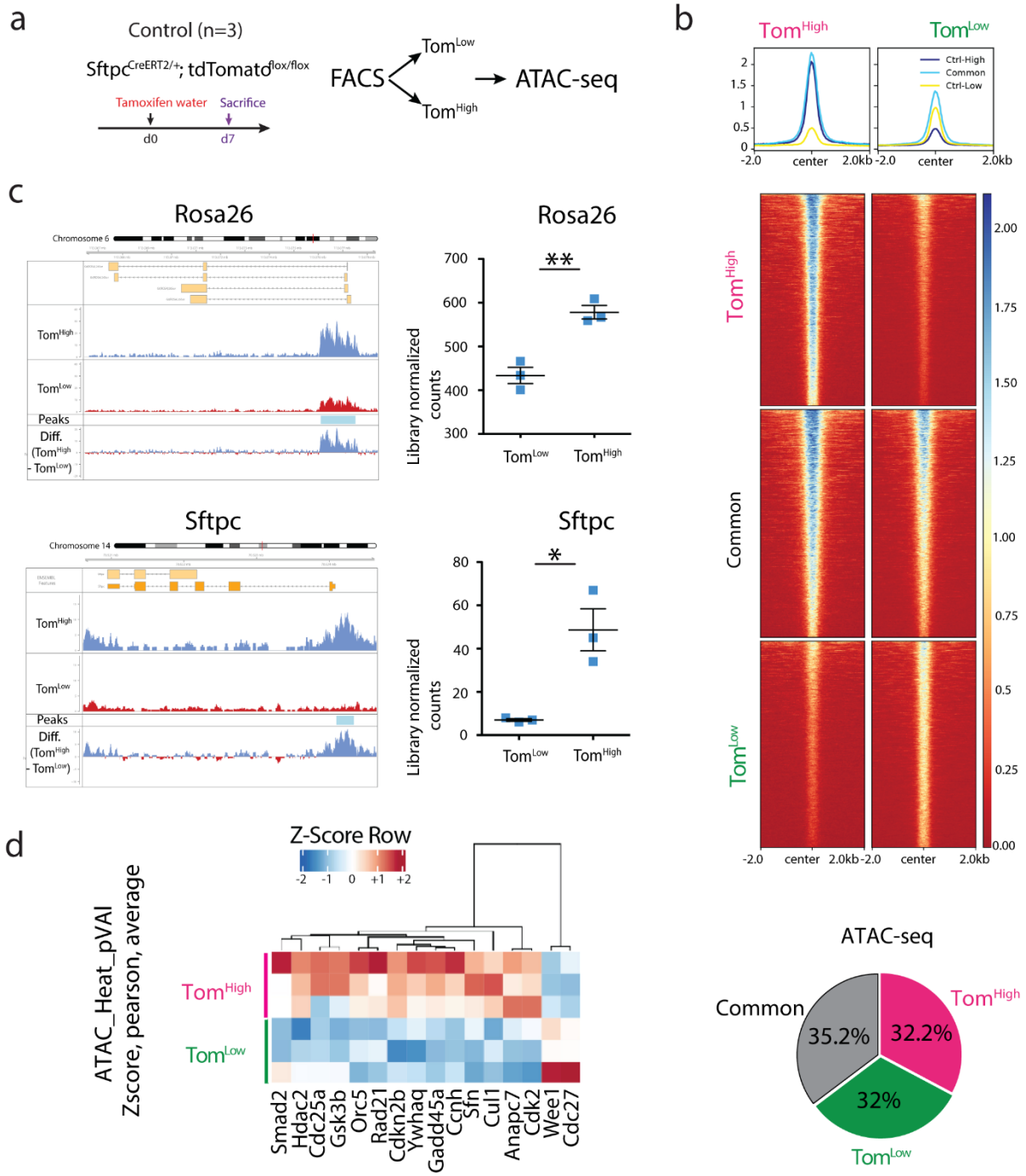

Figure 13: ATAC-seq analysis of FACS-based sorted Tom^{Low} and Tom^{High} populations. a) Timeline of tamoxifen treatment of Sftpc$^{CreERT2/+}$, *tdTomato$^{flox/flox}$* mice (n=3). ATAC-seq was carried on FACS-based sorted Tom^{Low} and Tom^{High} populations. **b)** Coverage heat maps of Tom^{Low} and Tom^{High}, displaying genome-wide regions of differential open chromatin peaks in Tom^{Low} versus Tom^{High}. Tom^{Low} chromatin is less open and transcriptionally less active compared to Tom^{High}. ATAC-seq analysis of peaks based on the cutoffs shows 3605 up-regulated in Tom^{High} (FDR < 0.05, log2FC > 0.585, baseMean > 20) , 3512 up-regulated in Tom^{Low} (FDR < 0.05, $\log_2$(FC) > 0.585, baseMean > 20) and 3878 non-regulated (baseMean > 20, FDR > 0.5, $\log_2$(FC) between -0.15 and 0.15) which means 32% and 32.8% of the genome is differently accessible in Tom^{Low} and Tom^{High}, respectively. **c)** ATAC-seq histogram of

average read coverage at *Rosa26* locus shows distinct ATAC-seq peaks at the promoter and denser chromatin in Tom^{Low} compared to Tom^{High} in this locus. Reprehensive peaks of Tom^{Low} and Tom^{High} are the average of three independent samples and the graph shows the quantification of peaks at *Rosa26* locus. ATAC-seq profile at *Sftpc* locus shows distinct ATAC-seq peaks at the promoter and denser chromatin in Tom^{Low} compared to Tom^{High}. Reprehensive peaks of Tom^{Low} and Tom^{High} are averages of three independent samples and the graph displays the quantification of peak regions of Sftpc locus. The ATAC-seq data have been normalized for sequencing depth and the scale on the y-axis was chosen for optimal visualization of peaks. **d)** Heatmap based on the ATAC seq data of top cell cycle-related genes differentially regulated in Tom^{Low} and Tom^{High}. FDR: the significance of results by Benjamini-Hochberg correction of multiple tests (n=3).

3.1.3 AT2-Tom^{Low} and Tom^{High} display different colony-forming capabilities

To compare the self-renewal capacity of Tom^{Low} and Tom^{High}, FACS-based sorted cells were co-cultured with CD31^{Neg}CD45^{Neg}Epcam^{Neg}Sca1^{Pos} resident lung mesenchymal cells according to a previously published protocol (Figure 14a). Tom^{High} behaved as *bona fide* AT2 cells as they formed alveolospheres with the expected colony-forming efficiency (Figure 14b-d), whereas Tom^{Low} displayed very weak organoid forming capabilities, which is in line with their proposed quiescent status. Both populations transdifferentiated into RAGE-positive AT1 cells after 14 days in culture (Figure 14c).

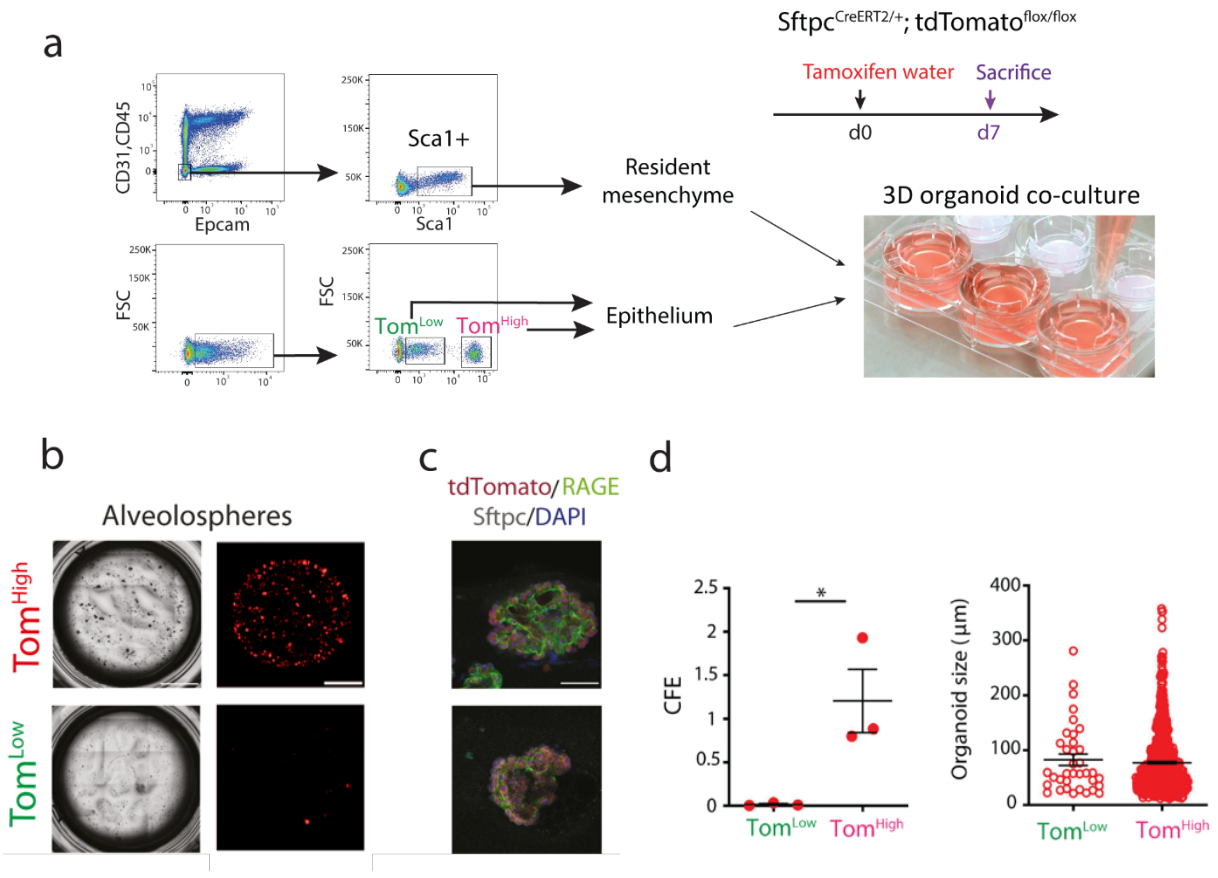

Figure 14: Different colony-forming capabilities of Tom^{Low} and Tom^{High}. a) Representative flow cytometry shows the gating strategy of CD31^{Neg}CD45^{Neg}Epcam^{Neg}population and further selection of Sca1+ resident mesenchymal cells, as well as the selection of Tom^{Low} and Tom^{High} from Epcam^{pos} population. Mesenchymal cells were co-cultured with Tom^{Low} and Tom^{High} separately (n=3). **b)** Representative alveolospheres from Tom^{Low} and Tom^{High} (n=3) (Scale bar: 100µm). **c)** Representative Sftpc and Rage Immunofluorescent staining of alveolospheres after 14 days in culture (Scale bar: 50µm). **d)** Quantification of Colony-forming efficiency (CFE) and alveolospheres size in Tom^{High} and Tom^{Low} (n=3).

3.1.4 Expansion of Tom^{Low} population following pneumonectomy

A critical question regarding these two populations of AT2 cells is whether they are differentially engaged in the context of lung regeneration. Therefore, the mouse pneumonectomy model was used to trigger lung regeneration, a process that is tightly associated with the proliferation of AT2 cells [93][132]. [*Sftpc$^{CreERT2/+}$; tdTomato$^{flox/flox}$*] mice (n= 4) were treated with tamoxifen water for one week to label the AT2 lineage. The mice were then put for 2 weeks on normal water to ensure enough time for tamoxifen clearance. Unilateral left lung pneumonectomy (PNX) was then performed to induce the process of compensatory growth in the remaining right lobes. Control mice (Sham) underwent the same process but without removal of the left lobe (Figure 15a). The animals were euthanized at day 7 post-surgery and the lungs were processed for FACS. The quantification of the abundance of the Tom^{Low} and Tom^{High} over the total number of Epcam^{Pos} cells in Sham and PNX indicates that the ratio of Tom^{High} cells/total number of Epcam^{Pos} cells remained unchanged between the two conditions, while the ratio of Tom^{Low} cells was significantly increased in the context of PNX versus Sham (Figure 15b). This suggests that Tom^{Low} cells rather than the previously thought Tom^{High} cells are the ones contributing to the process of lung regeneration.

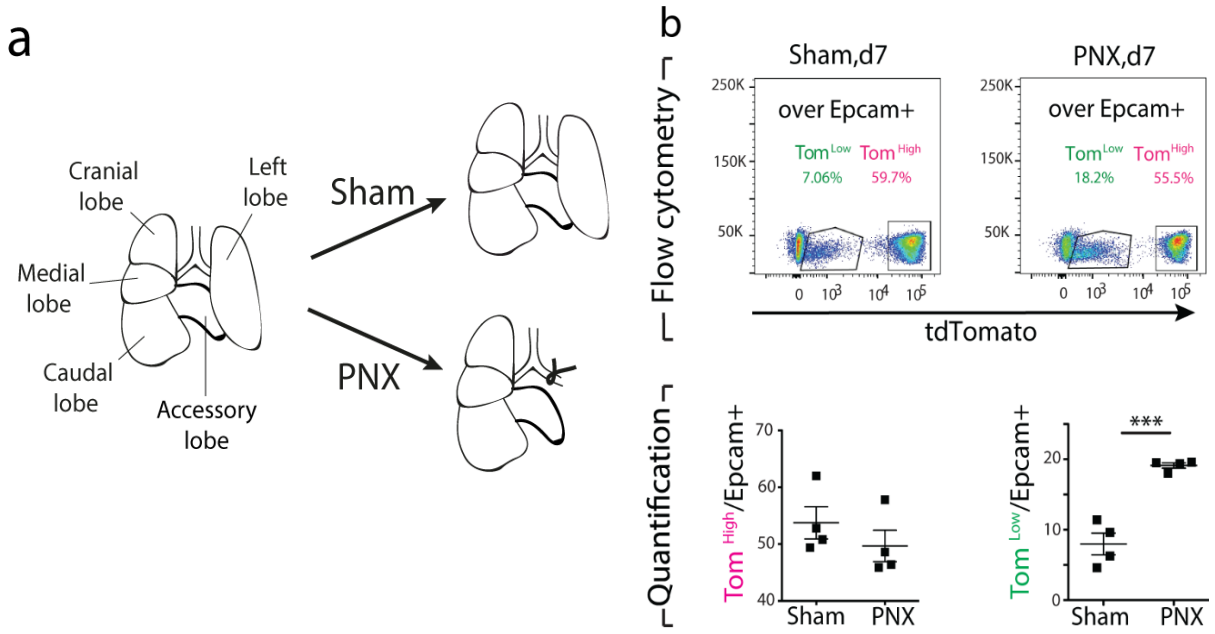

Figure 15: Expansion of Tom^{Low} but not Tom^{High} following pneumonectomy. a) Schematic representation of PNX and sham models. **b)** Representative flow cytometry analysis of Tom^{Low} and Tom^{High} populations 7 days after PNX and sham and the quantification of Tom^{Low} and Tom^{High} percentages in Epcam^{Pos} population between sham and PNX groups (n=4).

These two AT2 populations were isolated by FACS for further analysis by qPCR. Upon PNX, the expression of *Fgfr2b*, *Etv5*, *Sftpc*, as well as *Cyclin D1* (*Ccnd1*) and *Cyclin D2* (*Ccnd2*) was significantly upregulated in Tom^{Low}. A trend towards an increase was also observed in *Ki67* expression (Figure 16a). These results are consistent with Fgfr2b signaling activation and proliferation in Tom^{Low} cells in the context of lung regeneration. By contrast, Tom^{High} cells showed no difference in *Fgfr2b*, *Etv5* and *Sftpc* between PNX and Sham conditions. Surprisingly, an increase in *Ki67*, *Ccnd1* and *Ccnd2* (Figure 16b) was observed, but as the number of Tom^{High} cells is not increased in PNX vs. Sham, the significance of these results is not clear.

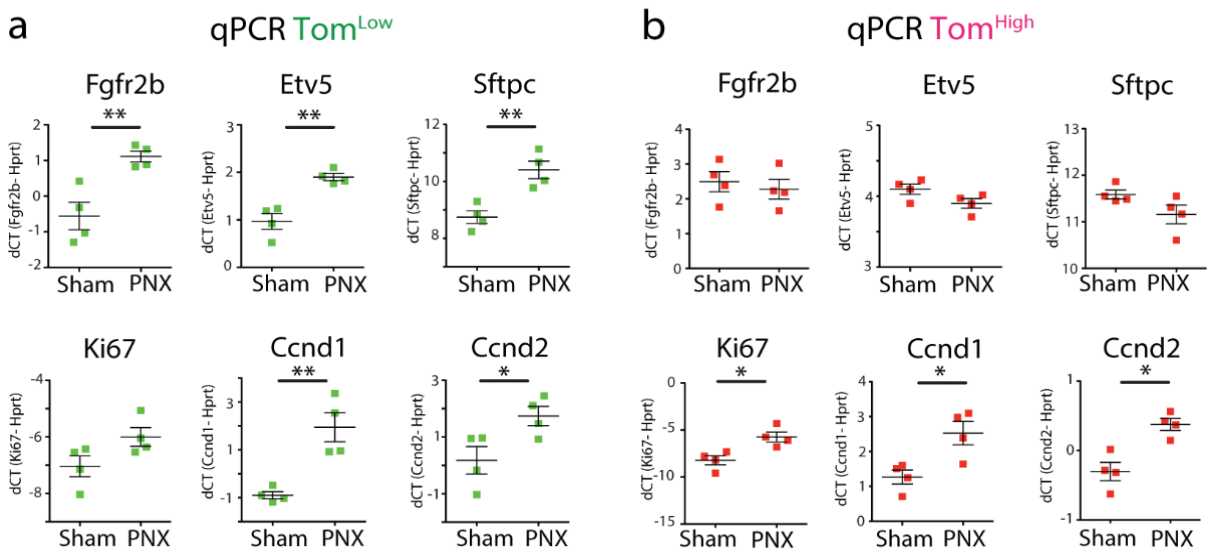

Figure 16: Fgfr2b signaling activation in Tom^{Low} cells and increase in cell cycle-related genes in Tom^{Low} and Tom^{High} a) qPCR analysis of FACS-based sorted Tom^{Low} population for *Fgfr2b*, *Etv5*, *Sftpc, Ki67 Ccnd1,* and *Ccnd2* expressions. **b)** qPCR analysis of FACS-based sorted Tom^{High} population for *Fgfr2b*, *Etv5*, *Sftpc, Ki67, Ccnd1,* and *Ccnd2* expressions (Scale bar: 250µm and 50µm). Data are presented as mean values ± SEM. ∗ $p < 0.05$, ∗∗ $p < 0.01$, ∗∗∗ $p < 0.001$.

3.1.5 Loss of Tom^{High} cells leads to expansion of Tom^{Low} cells

The precision-cut lung slices (PCLS) was applied to follow the fate of tdTomato^{Pos} cells over time *in vitro*. The flow cytometry results indicate that this approach leads to the drastic loss of the Tom^{High} cells (Figure 17a). Therefore, this system was used to monitor the fate of Tom^{Low} cells overtime after a massive loss of Tom^{High}. Over a culture period of 4 days, the formation of cell clusters and a significant increase in tdTomato intensity was observed (Figure 17 b,c), suggesting the differentiation of the Tom^{Low} cells towards mature (Tom^{High}) AT2 cells. The presence of clusters of tdTomato^{Pos} cells at day 10 was evident (Figure 17 d,e). Therefore, these results agree with the previous observation that Tom^{Low} cells are capable to proliferate in the context of PNX. In the future, innovative strategies to carry out the lineage tracing of Tom^{Low} cells will have to be developed to characterize their contribution to the Tom^{High} pool.

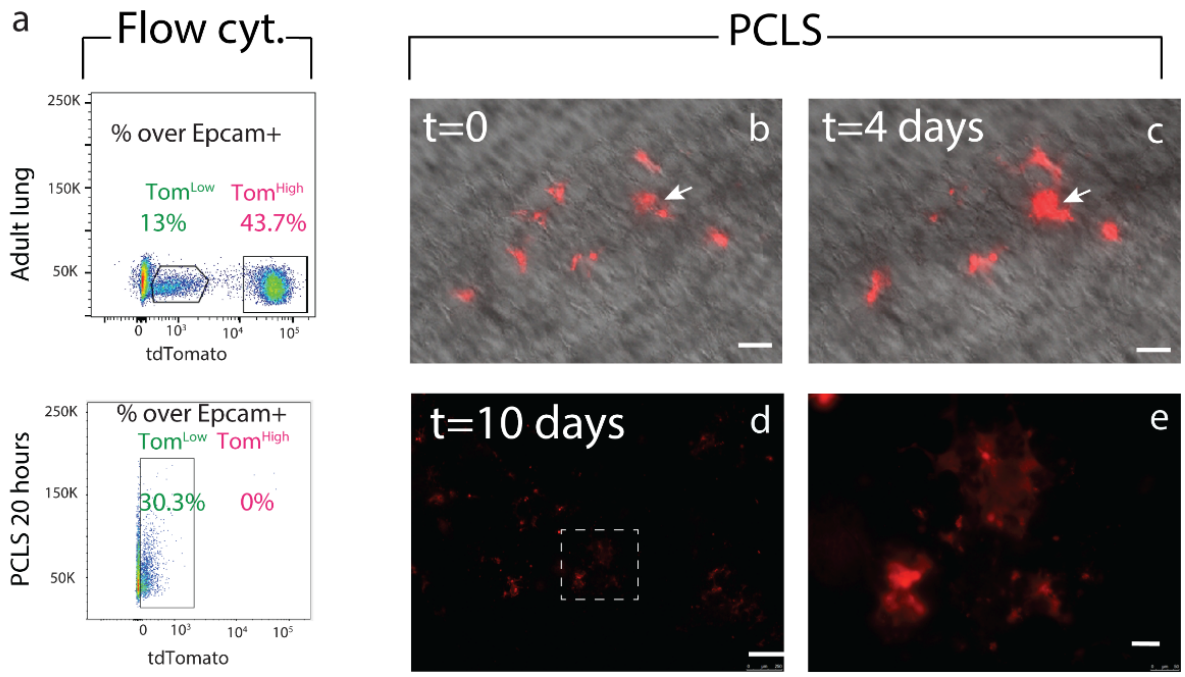

Figure 17: Characterization of the fate of Tom^{Low} cells in precision-cut lung slices (PCLS). a) Representative flow cytometry analysis of Tom^{Low} and Tom^{High} before processing the lungs for PCLS and in freshly generated PCLS. **b)** Visualization of the Tom^{Low} in PCLS at t=0. **c)** Visualization of the Tom^{Low} in PCLS at t=4 days. **d-e)** Visualization of the Tom^{Low} in PCLS at t=10 days. Low and high magnification. Scale bar 250 µm (low magnification) and 50 µm (high magnification).

3.1.6 PD-L1 is a specific surface marker enriched in Tom^{Low}

To identify markers differentially expressed between Tom^{Low} and Tom^{High}, a gene array was performed on FACS-isolated Tom^{Low} and Tom^{High} cells (Figure S1). Among the 100 top genes differentially expressed in Tom^{Low} vs. Tom^{High} cells three cell surface markers namely, *Cd33*, *Cd300lf*, and *PD-L1 (Cd274), all of* which were enriched in Tom^{Low} compared to Tom^{High}, were identified. qPCR analysis confirmed the significantly higher expression of *Cd33* and *PD-L1* expressions in Tom^{Low} compared to Tom^{High} (Figure 18). PD-L1 seems to be an interesting marker as it is an immune inhibitory receptor ligand and its expression is highly increased in adenocarcinoma [133][134]. The use of this marker is also relevant as the ATAC-seq analysis revealed that Tom^{Low} cells are enriched in genes belonging to the immune system (Figure 12).

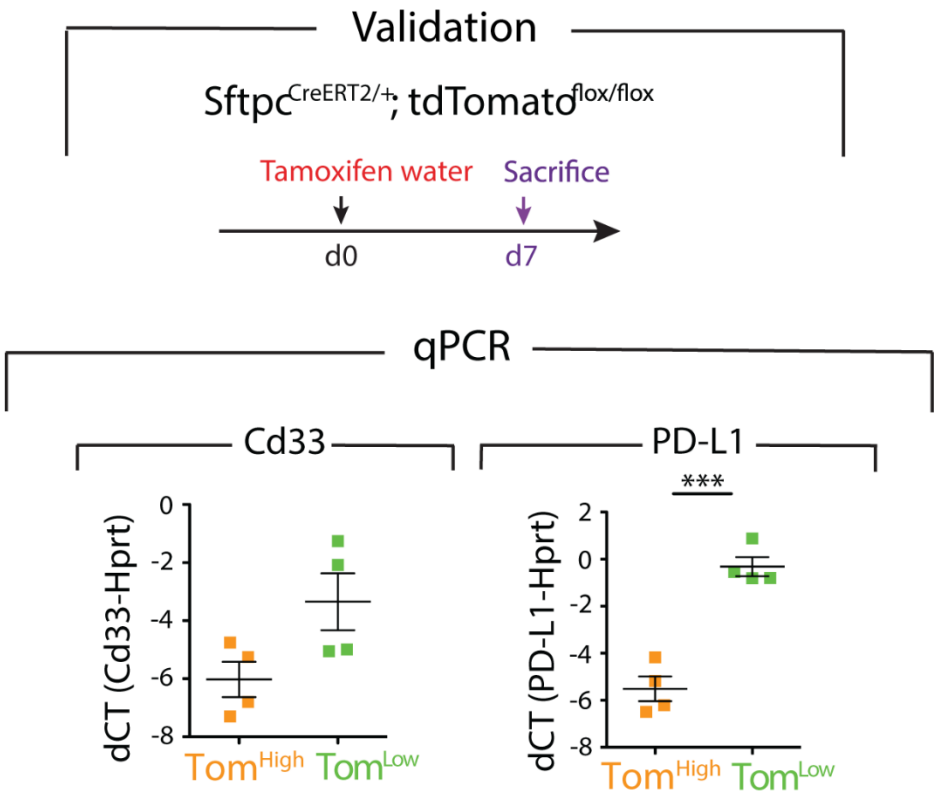

Figure 18: PD-L1 is a specific surface marker that is enriched in Tom^{Low}. Validation of acquired gene array data with qPCR for the expression level of *Cd33* and *PD-L1* in Tom^{Low} compared to Tom^{High}. Data are presented as mean values ± SEM. ∗p < 0.05, ∗∗p < 0.01, ∗∗∗p < 0.001.

The use of *PD-L1*, as a surface marker enriched in Tom^{Low} cells, was further validated using PD-L1 immunofluorescence staining and flow cytometry. To this end, PD-L1 immunofluorescence staining on cytospins confirms a higher level of protein at the plasma membrane in Tom^{Low} compared to Tom^{High} (Figure 19a). Moreover, flow cytometry analysis of Tom^{Low} and Tom^{High} populations separately showed that 46.9% of Tom^{Low} cells were PD-L1^{Pos} while only 0.77% of Tom^{High} cells were PD-L1^{Pos} (Figure 19b). In addition, PD-L1 immunofluorescence staining on lung sections localizes tdTomato^{Pos} PD-L1^{Pos} cells in the alveoli (Figure 19c). In conclusion, these results suggest that PD-L1 antibodies could be instrumental in differentially isolating the equivalent of Tom^{Low} vs. Tom^{High} in wild type lungs.

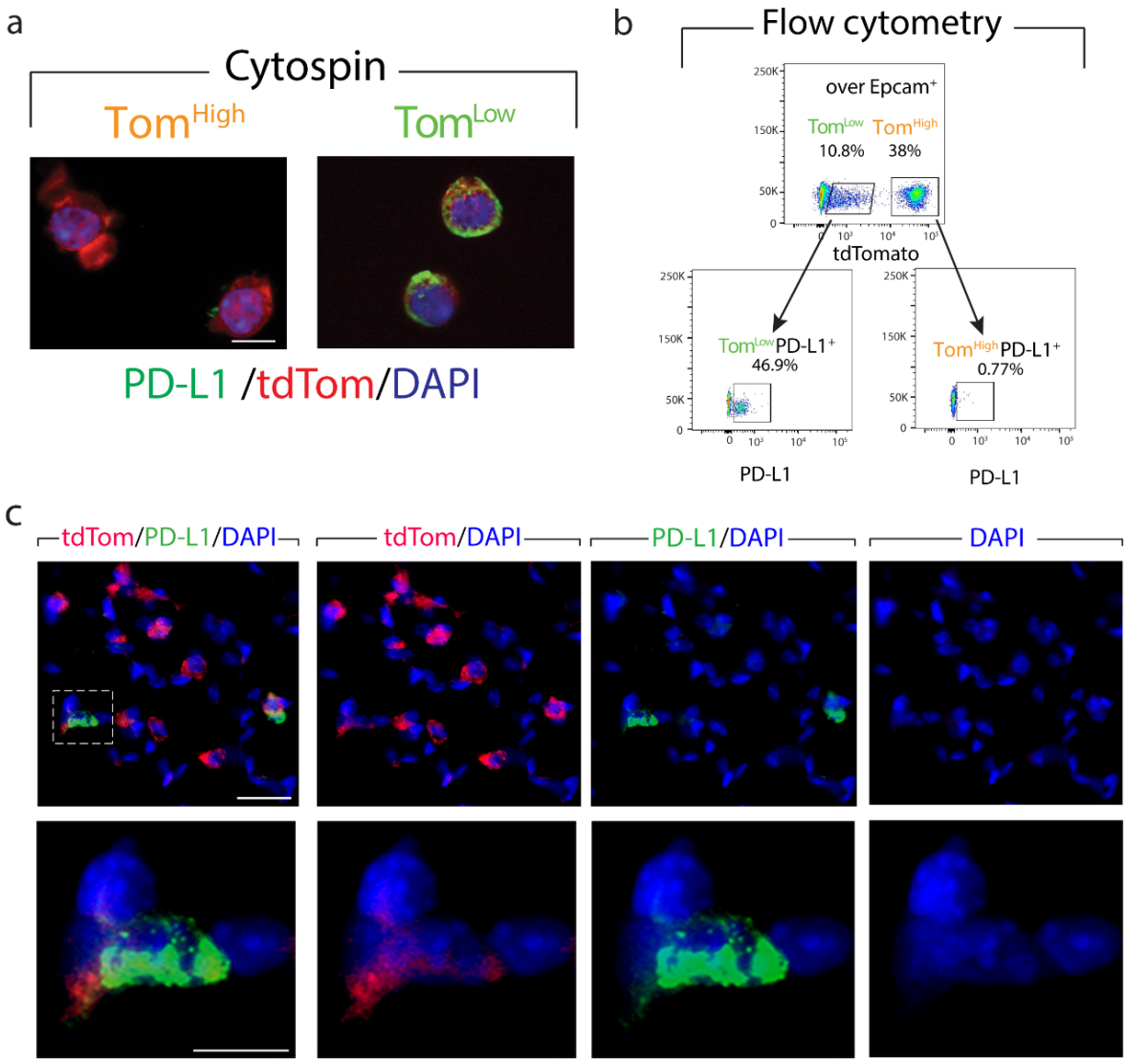

Figure 19: PD-L1 is enriched in Tom^{Low} cells. a) Representative PD-L1 Immunofluorescent staining on Tom^{Low} and Tom^{High} cytospin cells (Scale bar: 50µm). **b)** Representative flow cytometry analysis of PD-L1^{Pos} population in Tom^{Low} and Tom^{High}. **c)** Representative PD-L1 Immunofluorescent staining on the lung sections (scale bar: 10µm).

3.1.7 Identification of AT2 PD-L1^{+} Sftpc^{Low} in the wild type mice

To address whether PD-L1 could be used to isolate the equivalent of Tom^{Low} and Tom^{High} without the need for a lineage tracing approach, FACS-based analysis was performed on isolated C57BL/6 lungs. AT2 cells selection was done based on the gating of Epcam^{Pos}, Cd49f$^{Inter.}$, Podoplanin^{Neg} population, from which the percentage of PD-L1 positive and negative cells were analyzed (Figure 20a). In average, out of the AT2 population, 8.99% ± 0.51% (n=4) of AT2 cells are PD-L1^{Pos} and 90.23% ± 0.58%

(n=4) are PD-L1^{Neg} (Figure 20a). This ratio is consistent with the finding that most (80%) of the lineage-traced AT2 cells were composed of Tom^{High} (PD-L1^{Neg}) cells (Figure 20a). qPCR analysis on sorted PD-L1^{Pos} and PD-L1^{Neg} AT2 cells indicates a higher level of *Fgfr2b, Etv5*, and *Sftpc* in PD-L1^{Neg} compared to PD-L1^{Pos} cells (Figure 20b). This result is also in line with PD-L1^{Neg} cells correlating with Tom^{High} cells, while the expression profile of PD-L1^{High} fits with these cells being the equivalent of the Tom^{Low}.

Finally, flow cytometry analysis of alveolar epithelial cells (Epcam^{Pos}, Cd49f^{inter}) stained with Sftpc and PD-L1 identified a subpopulation of AT2 cells (6.8%) displaying low level of Sftpc and high level of PD-L1 (Figure 20c). This Sftpc^{Low} PD-L1^{High} likely contains the Tom^{Low} cells.

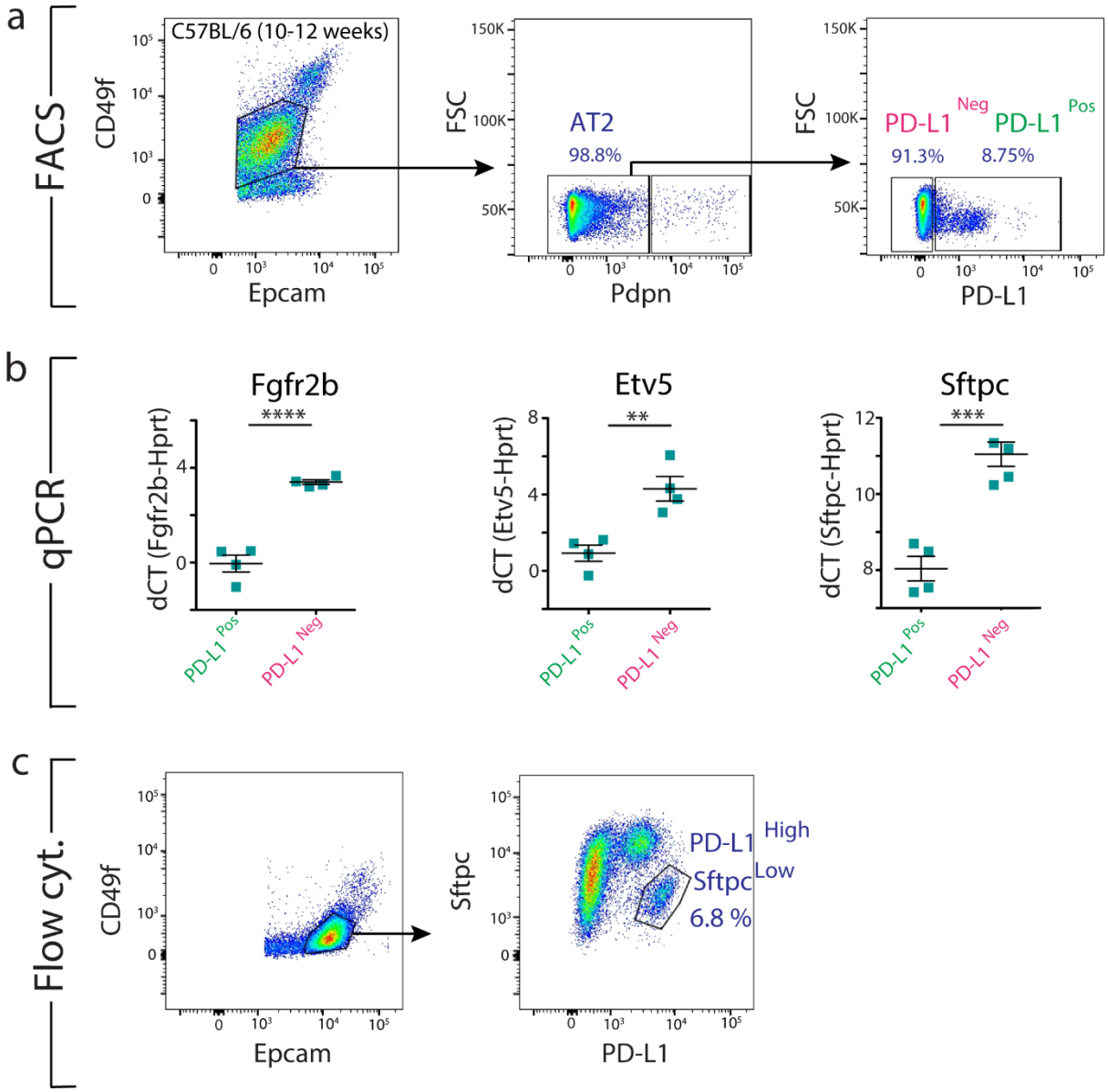

Figure 20: Identification of AT2 PD-L1^{+} Sftpc^{Low} in the wild type mice. a) Representative flow cytometry analysis of wild type mice lungs showing the gating strategy of Epcam^{+} CD49f^{Inter} population, followed by a negative selection of AT2 cells with the exclusion of AT1 Pdpn^{+} cells. Representative flow cytometry analysis of AT2 cells based on the PD-L1 marker. **b)** qPCR analysis of FACS-based sorted PD-L1^{Pos} and PD-L1^{Neg} for *Fgfr2b*, *Etv5*, and *Sftpc* expressions (n=4). Data are presented as mean values ± SEM. ∗p < 0.05, ∗∗p < 0.01, ∗∗∗p < 0.001. **c)** Representative flow cytometry analysis of Sftpc intracellular staining shows a distinct Sftpc^{Low} PD-L1^{High} population of AT2 cells.

3.1.8 Decrease of *bona fide* EPCAM^{Pos}HTII-280^{High} alveolar type 2 cells and amplification of EPCAM^{Pos}HTII-280$^{Low/Neg}$ PD-L1^{High} cells in human end-stage idiopathic lung fibrosis compared to donor lungs

Idiopathic pulmonary fibrosis (IPF) is a disease related to AT2 cell deficiency [135][136][137]. The flow cytometry was used to analyze the epithelial component of donor (n=5) and IPF (n=5) lungs (Figure 21a,b). From the live cells, first CD31^{Pos}CD45^{Pos} cells were excluded, and then EPCAM^{Pos} cells were selected for further analysis using the human AT2 cell marker HTII-280 and the surface marker PD-L1. These data indicate that HTII-280^{High} PD-L1^{Neg} (Q1), representing the *bona fide* differentiated AT2 cells, were drastically reduced in the context of IPF (25.21% ± 12.46 vs. 80.66% ± 3.49). More interestingly, the number of HTII-280$^{Low/Neg}$ PD-L1^{High} (Q3) was drastically increased (13.42% ± 4.92 vs. 1.13% ± 0.47) (Figure 21c), suggesting that HTII-280^{Low} PD-L1^{High} epithelial cells could represent a pool of progenitors linked to the deficient AT2 lineage.

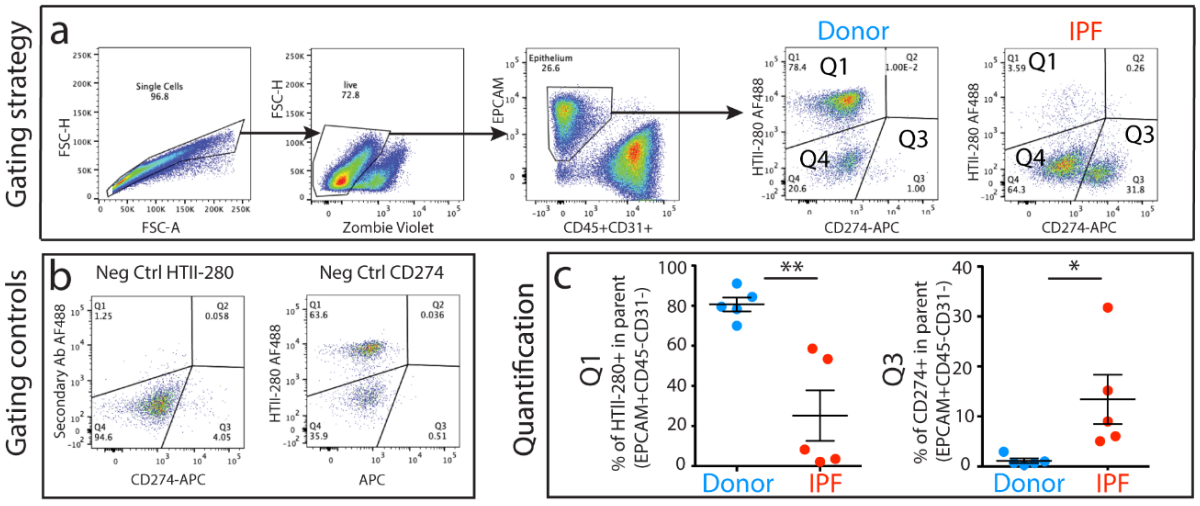

Figure 21: Decrease of bona fide EPCAM^{Pos}HTII-280^{High} alveolar type 2 cells and amplification of EPCAM^{Pos}HTII-280$^{Low/Neg}$ PD-L1^{High} cells in human end-stage idiopathic lung fibrosis compared to donor lungs. a) Representative flow cytometry of single cells and live cells gating, and EPCAM positive population selection and further analysis of HTII-280 and PD-L1 positive populations of IPF and donor lungs. **b)** The gating controls panel shows the negative control of HTII-280 and PD-L1 antibodies staining. **c)** Quantification of the number of HTII-280^{Pos} cells PD-L1^{Pos} cells in IPF versus donor (n=5). Data are presented as mean values ± SEM. $*p<0.05$, $**p< 0.01$, $***p < 0.001$.

The comparison of the expression of *SFTPC* and *SCGB1A1* for cells in Q1 (AT2 cells), Q3 (potential equivalent to Tom^{Low} cells) and Q4 (non-AT2 cells, mostly bronchial epithelial cells) in Donor and IPF lungs was carried out by qPCR (Figure 22a). Regardless of the IPF or Donor origin of these cells, qPCR results indicated that Q3 (potential equivalent to Tom^{Low} cells) express less *SFTPC* than Q1 (AT2 cells) confirming the flow cytometry data. In addition, Q4 (non-AT2 cells) express more *SCGB1A1* than Q3 (potential equivalent to Tom^{Low} cells) suggesting that Q3 cells do not represent bone fide bronchial cells. Interestingly, in IPF, the difference between *SCGB1A1* expression in Q3 (equivalent to Tom^{Low} cells) and Q1 (AT2 cells) is not statistically significant. Based on these results, it is proposed that these HTII-280^{Low}PD-L1^{High} (Q3) epithelial cells could represent the human equivalent of the Tom^{Low} cells characterized in mice (Figure 22a). Indeed, a similar approach carried out in mice with FACS-isolated Tom^{Neg} (mostly bronchial cells), Tom^{Low,} and Tom^{High} out of the Epcam+ cells indicated an almost identical expression profile for *Sftpc* and *Scgb1a1* as the one observed in human lungs (Figure 22b).

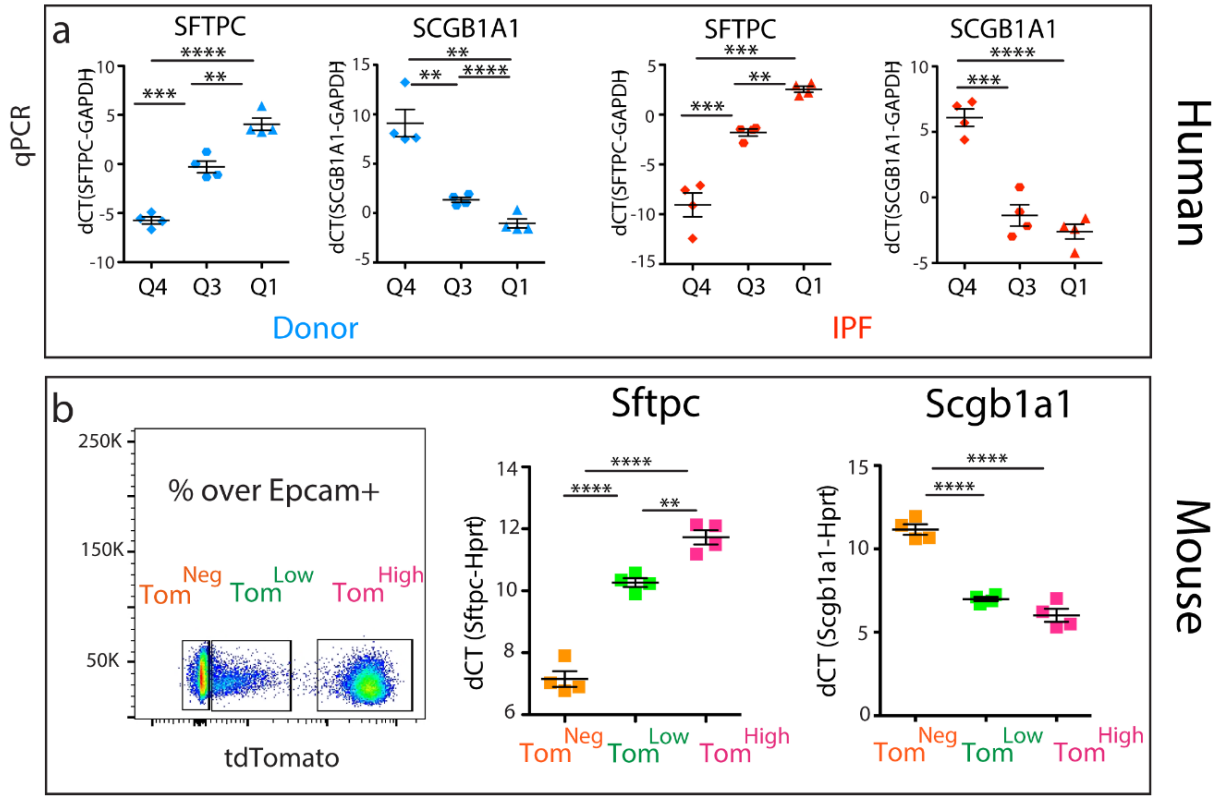

Figure 22: Differential *Sftpc* and *Scgb1a1* expressions in different isolated epithelial cells in the human and mice. a) qPCR analysis of FACS-based sorted HTII-280^{Neg}PD-L1^{Neg} (Q4) HTII-280$^{Low/Neg}$PD-L1^{High}(Q3) and HTII-280$^{Low/Neg}$PD-L1^{High}(Q1) cells for *SFTPC* and *SCGB1A1* expressions in donor and IPF lungs (n=4). Data are presented as mean values ± SEM. ∗p < 0.05, ∗∗p < 0.01, ∗∗∗p < 0.001. **b)** Representative flow cytometry analysis of Tom^{Neg},Tom^{Low} and Tom^{High} selection and qPCR analysis of FACS-based sorted Tom^{Neg} ,Tom^{Low,} and Tom^{High} cells for the expression of *Sftpc* and *Scgb1a1*. Data are presented as mean values ± SEM. ∗p < 0.05, ∗∗p < 0.01, ∗∗∗p < 0.001.

3.2 Evidence that *Fgfr2b* deletion in AT2 cells elicits a differential response in AT2 subpopulations

3.2.1 Tom^{Low} and Tom^{High} populations respond differently to *Fgfr2b* deletion

To test the hypothesis that Fgfr2b signaling is crucial in Tom^{High} population, and, more generally, to unravel the function of Fgfr2b signaling in AT2 cells, [*Sftpc*$^{CreERT2/+}$; *Fgfr2b*$^{flox/flox}$; *tdTom*$^{flox/flox}$] (*Fgfr2b*-cKO) mice, as experimental group, were treated with tamoxifen (Figure 23a). Flow cytometry analysis on harvested lungs underpinned the presence of Tom^{Low} and Tom^{High} populations. In average, the Tom^{Low} represented 27.05% (27.05% ± 1.83%, n=4) of the overall Epcam^{Pos} cells and the Tom^{High} represented 25.70 % (25.70% ± 2.45%, n=4) of the overall Epcam^{Pos} cells (Figure 23b). Comparison of the percentage of Tom^{High} cells between control (*Sftpc*$^{CreERT2/+}$; *tdTom*$^{flox/flox}$) and *Fgfr2b*-cKO demonstrate decreasing of the number of these cells upon *Fgfr2b* deletion (compare Figure 6b and Figure 23b, 25.70% vs. 42.75%) indicating the Fgfr2b pathway is critical for the maintenance of Tom^{High} cells. Interestingly, an increase in the percentage of Tom^{Low} cells in *Fgfr2b*-cKO versus control (compare Figure 6b and Figure 23b, 27.05% vs. 9.93) was observed. It suggests that Tom^{Low} cells, which were previously quiescent are becoming active and proliferative.

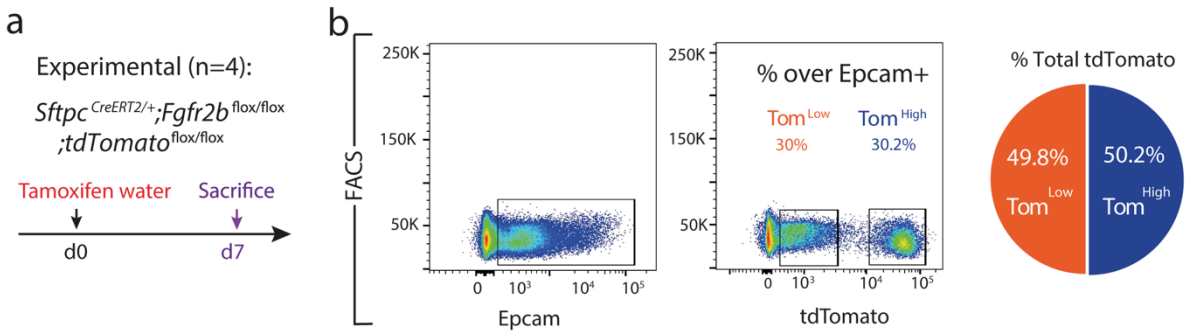

Figure 23: Tom^{Low} and Tom^{High} populations respond differently to *Fgfr2b* deletion. a) Timeline of tamoxifen treatment of Sftpc$^{CreERT2/+}$, Fgfr2b $^{flox/flox}$, *tdTomato*$^{flox/flox}$ mice (n=4). **b)** Representative flow cytometry analysis of Epcam positive population selection and the percentage of Tom^{Low} (30%) and Tom^{High} (30.2%) populations over Epcam+ cells. Pie chart shows the percentage of Tom^{Low} (49.8%) and Tom^{High} (50.2%) in total tdTomato.

Next, the distribution of fluorescence intensity of the tdTomato^{Pos} cells was analyzed on lung sections. The threshold was set at 48% based on the flow cytometry data and then the intensity of Sftpc immunofluorescence staining was quantified in each cell located on the left side (Tom^{Low}) and the right side (Tom^{High}) of the threshold. Interestingly, Sftpc quantification in Tom^{Low} and Tom^{High} cells indicates a switch towards the Sftpc^{High} status in both subpopulations (Figure 24a-c).

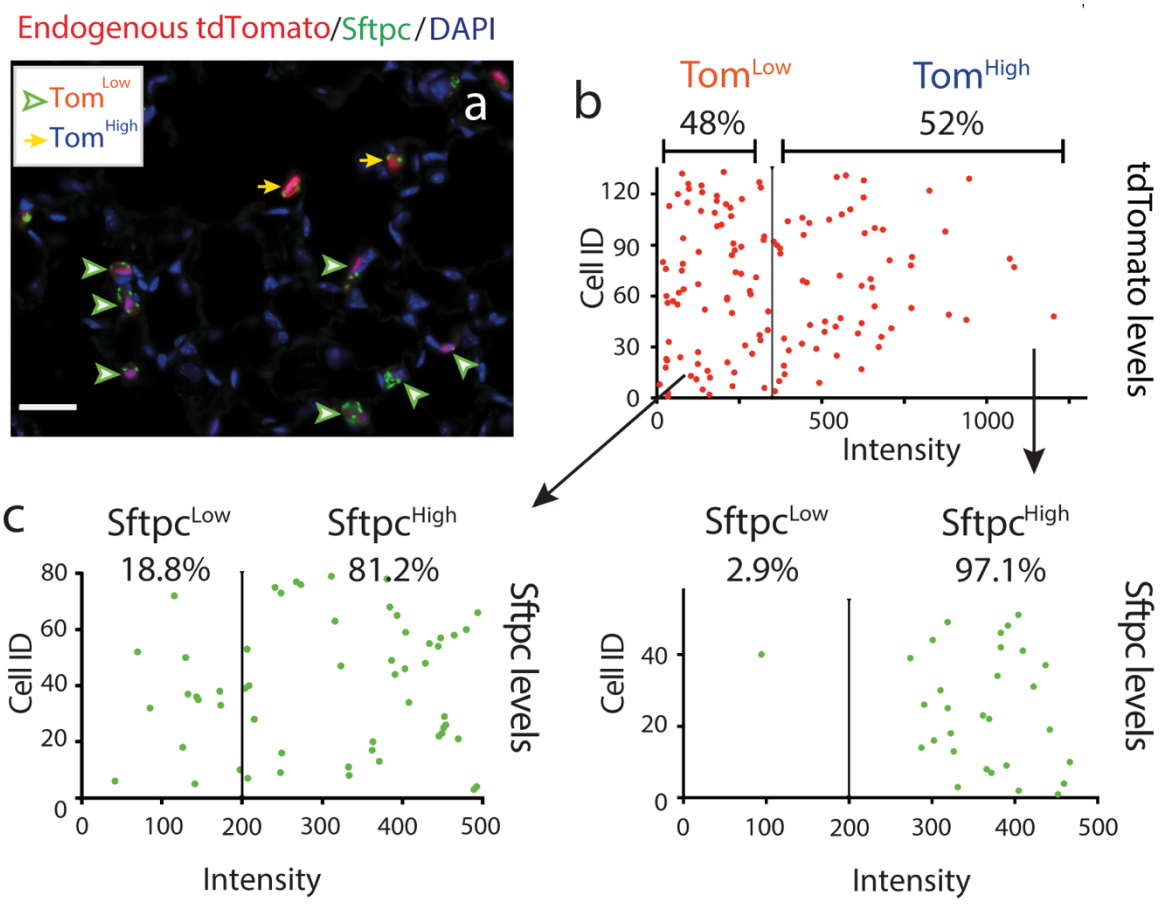

Figure 24: Quantification of tdTomato and Sftpc fluorescent intensity. a) Representative Sftpc immunofluorescence staining and localization of Tom^{Low} and Tom^{High} in alveoli (Scale bar: 50µm). **b)** Quantification of tdTomato fluorescent intensity. **c)** Quantification of Sftpc intensity of Tom^{Low} and Tom^{High} populations separately.

To investigate whether *Fgfr2b* was successfully deleted in both Tom^{Low} and Tom^{High}, RT-PCR was carried out to detect the wild type and mutant *Fgfr2b* transcripts (Figure 25a) [138]. The mutant *Fgfr2b* transcript (195 bp) was present in Tom^{Low} and Tom^{High} in *Fgfr2b*-cKO lungs, and as expected, was not detected in the corresponding cells from control lungs (Figure 25b).

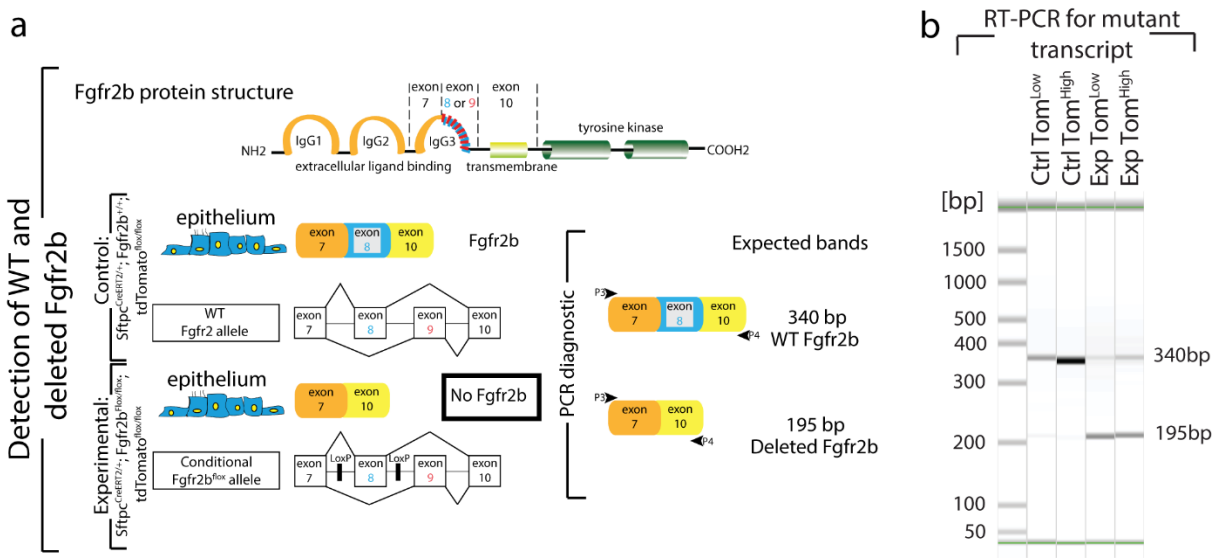

Figure 25: Detection of WT and mutant *Fgfr2b* transcripts. a) Schematic of Fgfr2b protein structure. Wild type Fgfr2b transcript consists of exon 7, exon 8 and exon 10 which is detected by band size of 340bp, whereas the exon 8 is deleted in mutant Fgfr2b form, resulting in shorter transcript which is detectable by the band size of 195bp. **b)** RT-PCR for the detection of *Fgfr2b* mutant form in FACS-based sorted Tom^{Low} and Tom^{High}. Wild type and mutant forms are detected by the size of 340bp and 195bp, respectively.

Next, qPCR was performed on FACS-isolated Tom^{Low} and Tom^{High} isolated cells from *Fgfr2b*-cKO lungs. The analysis shows that, in contrast to the control (Figure 11) *Fgfr2b* expression difference between Tom^{Low} and Tom^{High} is smaller (Figure 26). Moreover, *Etv5* expression is significantly downregulated in Tom^{High} versus Tom^{Low} and the expression levels of *Sftpc, Sftpb*, and *Sftpa1* are not substantially different between Tom^{Low} and Tom^{High} (Figure 26).

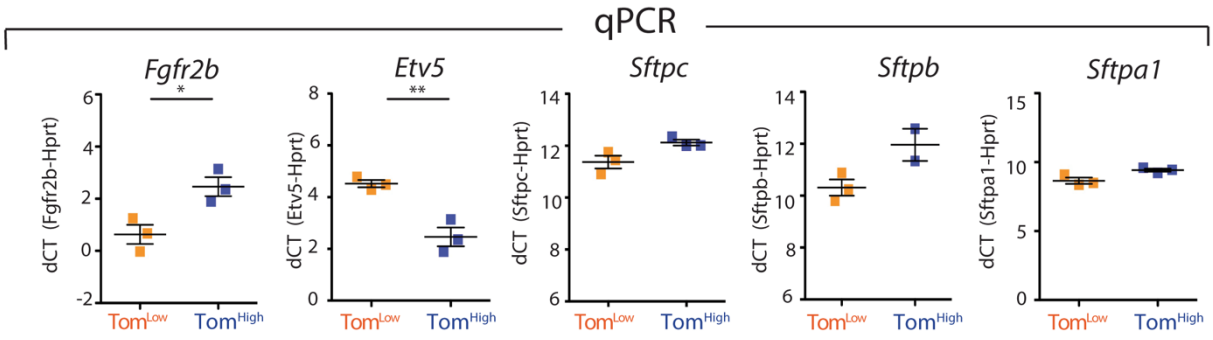

Figure 26: Gene expression analysis of isolated Tom^{Low} and Tom^{High} cells. qPCR analysis of FACS-based sorted Tom^{Low} and Tom^{High} cells for the expression of *Fgfr2b*, *Etv5*, *Sftpc*, *Sftpb,* and *Sftpa1*. Data are presented as mean values ± SEM. ∗p < 0.05, ∗∗p < 0.01, ∗∗∗p < 0.001.

3.2.2 Fgfr2b inactivation in the AT2 lineage leads to the loss of Fgfr2b signaling in Tom^{High} and activation of Fgfr2b signaling in Tom^{Low}

The Tom^{High} and Tom^{Low} cells were compared between *Fgfr2b*-cKO and control lungs using qPCR and immufluorescent staining on cytospins of sorted cells. QPCR analysis of Tom^{High} demonstrated significant decrease of *Fgfr2b* and *Etv5* expressions in *Fgfr2b*-cKO versus control lungs, corroborating the loss of the Fgfr2b signaling in these cells, however no changes in the expression of *Sftpc, Sftpb*, and *Sftpa1* was observed in these cells (Figure 27a). By contrast, in Tom^{Low}, significant upregulation of *Fgfr2b*, *Etv5, Sftpc and Sftpb* was identified (Figure 27b).

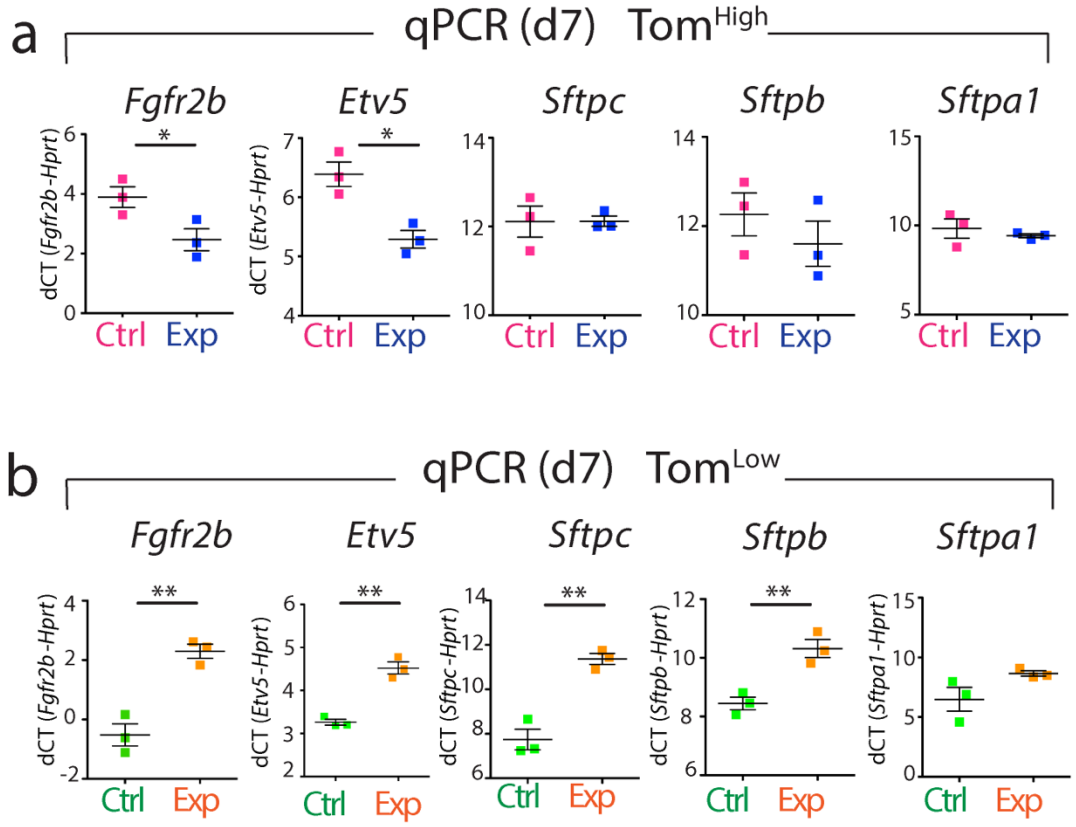

Figure 27: Fgfr2b inactivation in the AT2 lineage labeled cells leads to the loss of Fgfr2b signaling in Tom^{High} versus activation of Fgfr2b signaling in Tom^{Low}. a) qPCR analysis on FACS-based sorted Tom^{High} population for the expressions of *Fgfr2b*, *ETV5*, *Sftpc*, *Sftpb* and *Sftpa1* in the experimental compared to the control (n=4). Data are presented as mean values ± SEM. ∗p < 0.05, ∗∗p < 0.01, ∗∗∗p < 0.001. **b)** qPCR analysis on FACS-based sorted

Tom^{Low} population for the expressions of *Fgfr2b*, *ETV5*, *Sftpc*, *Sftpb* and *Sftpa1* in the experimental compared to the control (n=4). Data are presented as mean values ± SEM. ∗p < 0.05, ∗∗p <0.01, ∗∗∗p < 0.001.

These changes in *Fgfr2b* and *Sftpc* mRNA levels were validated at the protein level by cytospin of isolated Tom^{High} and Tom^{Low} from *Fgfr2b*-cKO and control lungs, followed by immunofluorescent staining (Figure 28a,b). This suggests losing Fgfr2b signaling in Tom^{High} and activation of Fgfr2b signaling in Tom^{Low} in *Fgfr2b*-cKO compared to control lungs.

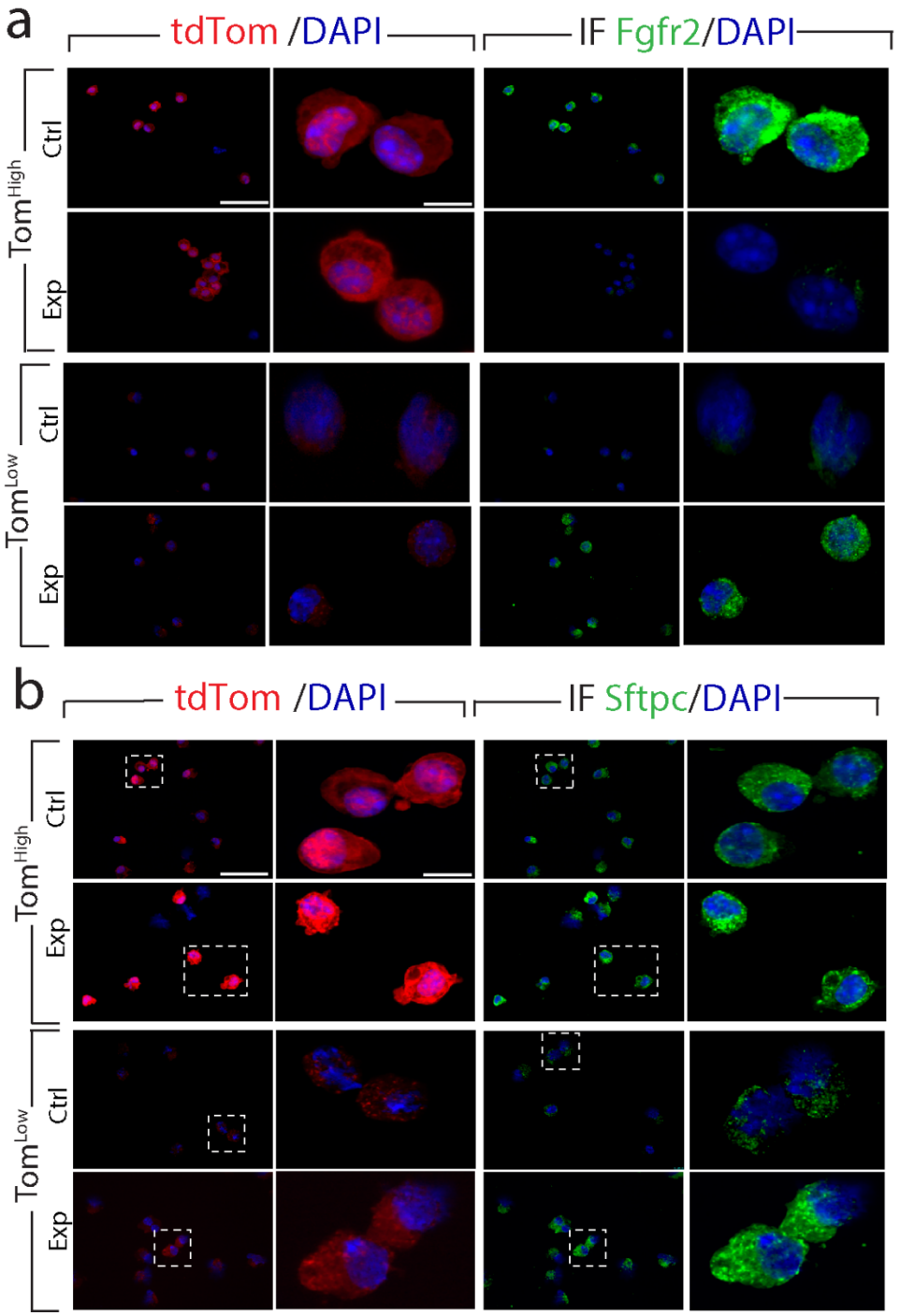

Figure 28: Loss of Fgfr2 in Tom^{High} and gain of Fgfr2 in Tom^{Low}. a) Representative Immunofluorescent staining against Fgfr2 on cytospins of Tom^{Low} and Tom^{High} in the experimental versus the control (n=4) (Scale bar: 50µm). **b)** Representative Sftpc Immunofluorescent staining on cytospins of Tom^{Low} and Tom^{High} between control and experimental (n=4) (Scale bar: 50µm).

3.2.3 Status of *Fgfr2b* wild type and muted transcripts in Tom^{Low} and Tom^{High} in different time points

Given the surprising result that Fgfr2b signaling was activated in Tom^{Low} despite the *Fgfr2b* deletion originally observed at day 7 after tamoxifen treatment (Figure 25 and 27b). The mice were treated for longer period with tamoxifen to ensure Fgfr2b deletion is completed. Next, the presence of the mutant and wild type *Fgfr2b* transcripts were analyzed by RT-PCR at day 14 after tamoxifen treatment (on continuous tamoxifen water treatment), as well as in animals treated for one week with tamoxifen water and then put on normal water for two weeks. The results surprisingly indicates that in Tom^{Low} from *Fgfr2b*-cKO lungs, the mutated *Fgfr2b* transcript was barely detectable, while the mutated transcript was still detected in *Fgfr2b*-cKO Tom^{High} at both time points (Figure 29a).

To detect the relative extent of the mutated and wild type *Fgfr2b* at day 7 and day 14, qPCR for the detection of exon 8 (the deleted exon) versus exon 7 (reflecting the intact *Fgfr2b* locus) was performed on the genomic DNA of Tom^{High} and Tom^{Low} from *Fgfr2b*-cKO and control lungs. The results show that at day 7, the relative presence of the mutated vs. wild type *Fgfr2b* in Tom^{Low} was 39% vs. 61%. However, at day 14 wild type *Fgfr2b* increased to 100%, indicating all Tom^{Low} cells contain wild type *Fgfr2b* (Figure 29b). In Tom^{High} cells, by contrast, there was an increase in the percentage of mutated *Fgfr2b* from day 7 to day 14 (from 61% to 79%) indicating that continuous deletion of the *Fgfr2b* allele in Tom^{High} cells occurs. It suggests, the amplification of Tom^{Low} cells containing wild type *Fgfr2b* and continuous deletion of *Fgfr2b* in Tom^{High}.

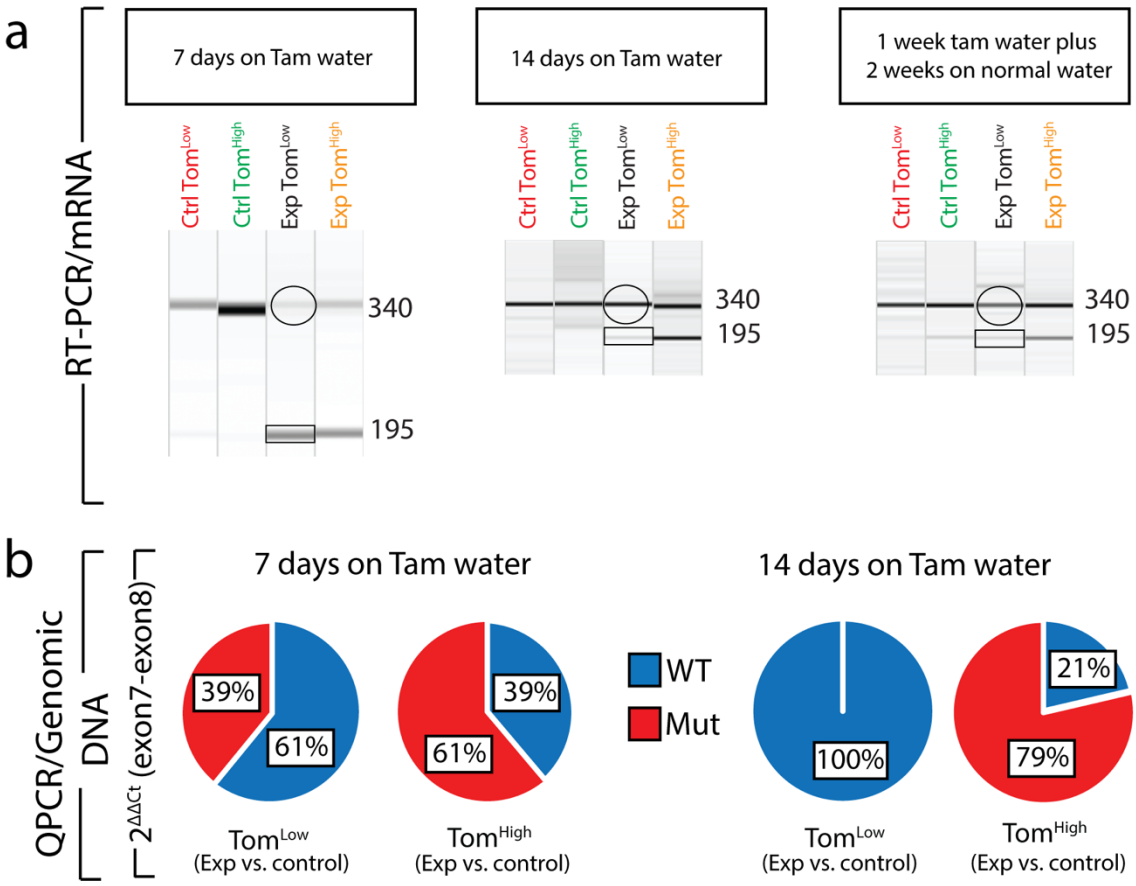

Figure 29: Status of WT and mutant *Fgfr2b* transcripts at different time points. a) RT-PCR results show the presence of WT *Fgfr2b* in Tom^{Low} and Tom^{High} in the control and the detection of *Fgfr2b* mutated *Fgfr2b* in Tom^{Low} and Tom^{High} in the experimental at day 7 on tamoxifen water. The results at day14 (on continuous tamoxifen water treatment), as well as in animals treated for one week with tamoxifen water and then put on normal water for two weeks indicate that in *Fgfr2b*-cKO Tom^{Low} the mutated *Fgfr2b* transcript was barely detectable while the mutated transcript was still detected in *Fgfr2b*-cKO Tom^{High}. **b)** Pie charts represent qPCR data on the detection of deleted exon 8 versus exon 7 (reflecting the intact *Fgfr2* locus) to detect the relative extent of the mutated and wild type *Fgfr2b* in two time points of 7 days and 14 days on the tamoxifen water.

3.2.4 Decrease of total tdTomato^{Pos} cells in *Fgfr2b*-cKO compared to control

FACs analysis of the percentage of Tdtomato^{+} Epcam^{+} in control and *Fgfr2b*-cKO represent the reduction of tdTomato labeled cells following *Fgfr2b* deletion at day 7, day 14 and day 28 (Figure 30a).

In addition, the number of Sftpc^{Pos} tdTom^{Pos} over total cells in *Fgfr2b*-cKO and control lungs was quantified, followed by Sftpc immunofluorescence staining. The results indicate the reduction of tdTom^{Pos} cells over total cells as well as the reduction of

Sftpc^{Pos} tdTom^{Pos} over total cells in *Fgfr2b*-cKO compared to control in three time points (Figure 30c,d).

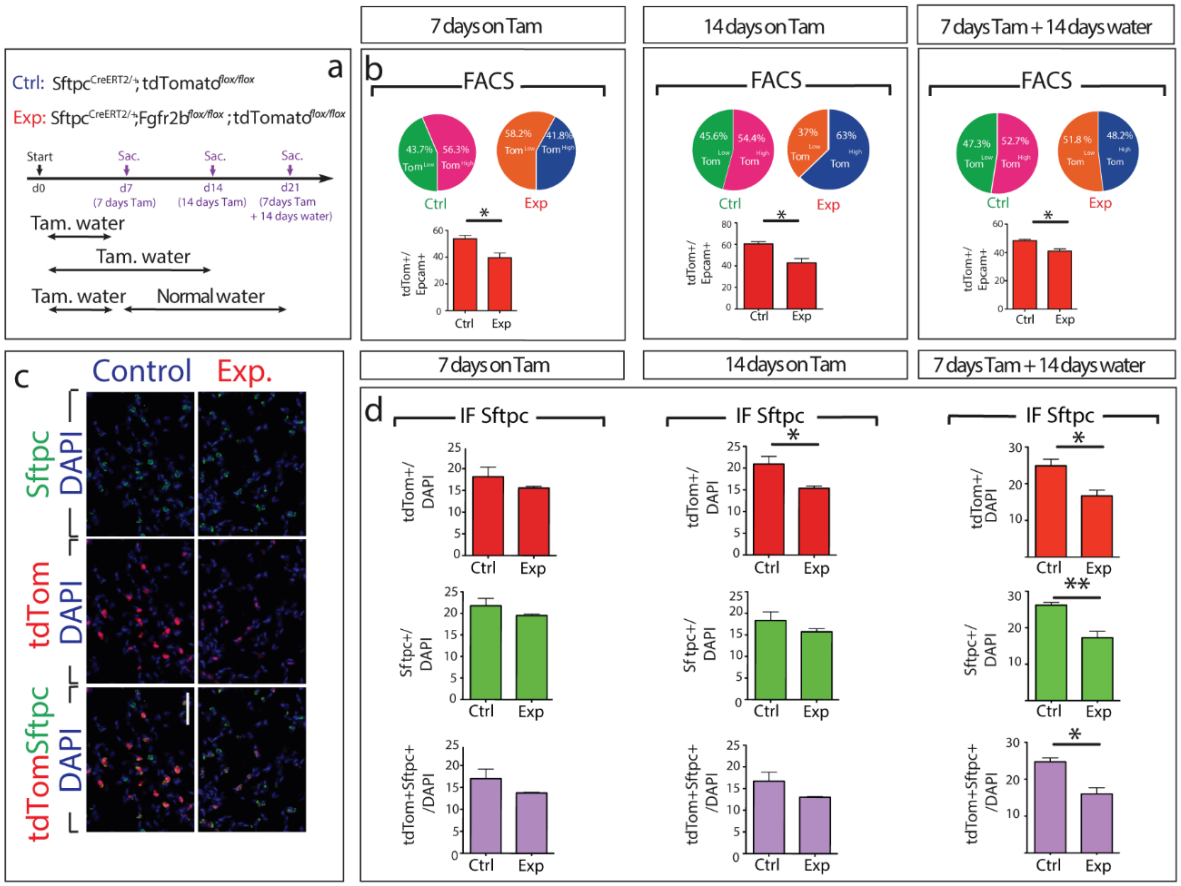

Figure 30: Quantification of tdTomato positive cells in control and *Fgfr2b*-cKO in different time points. a) Tamoxifen treatment timeline of Sftpc$^{CreERT2/+}$, *tdTomato*$^{flox/flox}$ and *Sftpc*$^{CreERT2/+}$*; Fgfr2b*$^{flox/flox}$*; tdTomato*$^{flox/flox}$ mice. **b)** Flowcytometry analysis of tdTomato positive cells in control and *Fgfr2b*-cKO in different time points.**c)** Representative Sftpc immunofluorescence staining (Scale bar: 50µm). **d)** Quantification of tdTomato+, Sftpc+, and tdTomato+ Sftpc+ cells in three different time points of day7, day 14 and day 21. (n=4).

3.2.5 Intact lung structure following *Fgfr2b* deletion

Losing bona fide AT2 cells in the lung result in the emerge of emphysema phenotype [139][140]. To investigate whether there is a change in the lung structure after *Fgfr2b* deletion, the lung morphometry analysis was performed at 7 days and 14 days after tamoxifen treatment. The analysis demonstrates no changes in alveolar space, septal wall thickness, and MLI in *Fgfr2b*-cKO compared to control at day 7 and day 14 (Figure 31a-e). It suggests that the lack of lung phenotype is because of the existence of a continuous compensatory mechanism that replenishes the lost mature AT2 cells with

newly generated AT2 cells. It appears that Tom^{Low} cells, as immature AT2 cells, are the cells that differentiate to mature Tom^{High} cells.

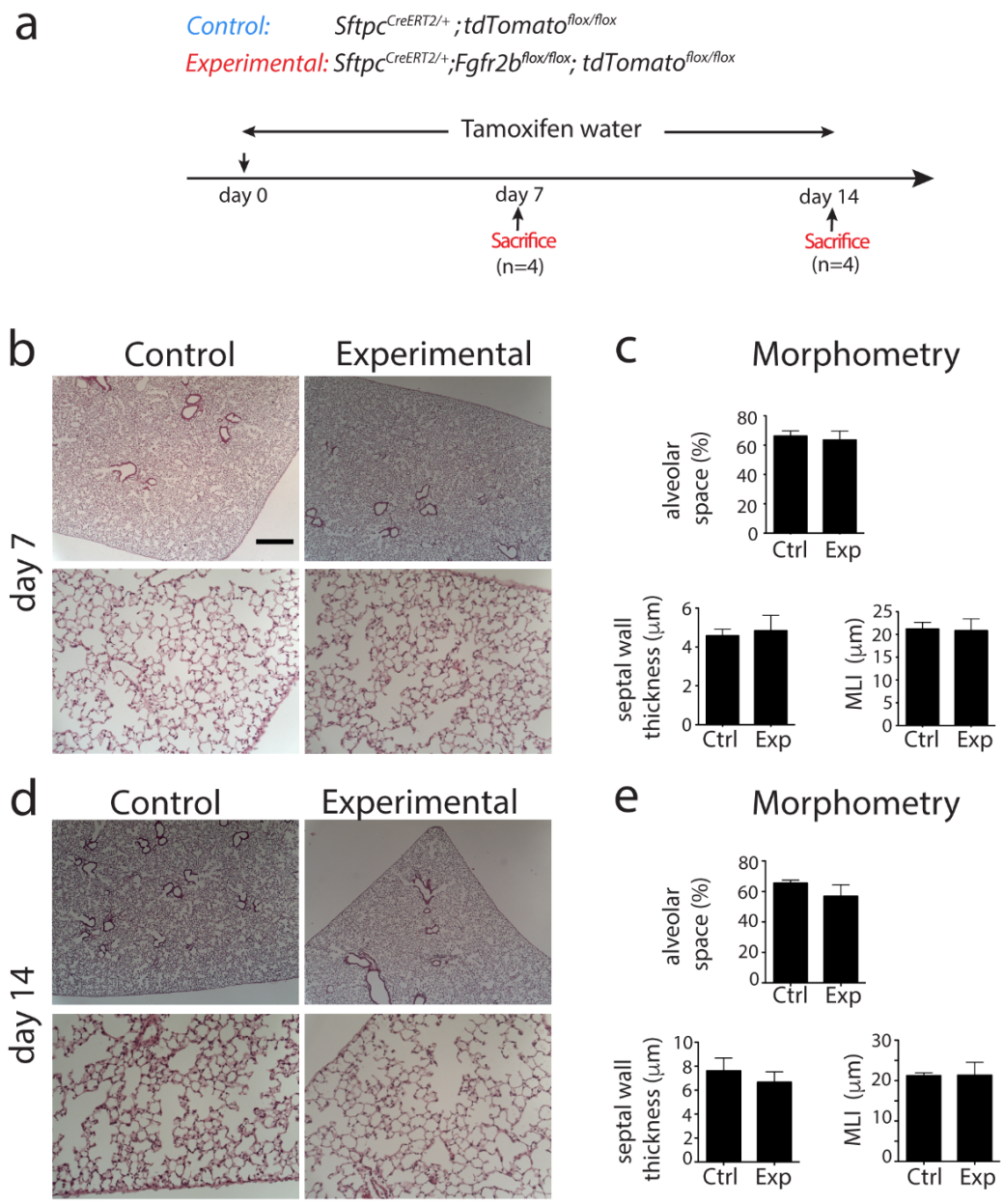

Figure 31: Morphometry analysis of *Fgfr2b*-cKO versus control lungs. a) Timeline of tamoxifen treatment of Sftpc$^{CreERT2/+}$, *tdTomato*$^{flox/flox}$ and *Sftpc*$^{CreERT2/+}$; *Fgfr2b*$^{flox/flox}$; *tdTomato*$^{flox/flox}$ mice. **b)** Hematoxylin and eosin staining of the control and the experimental lungs at 7 days on the tamoxifen water (scale bar 200 and 50 µm) **c)** Morphometry analysis (alveolar space, septal wall thickness, and MLI) of the control and the experimental lungs at 7 days on the tamoxifen water (n=4). **d)** Hematoxylin and eosin staining of the control and the experimental lungs at 14 days on the tamoxifen water (scale bar 200 and 50 µm). **e)** Morphometry analysis (alveolar space, septal wall thickness, and MLI) of the control and the experimental lungs at 14 days on the tamoxifen water (n=4). Data are presented as mean values ± SEM. $*p < 0.05$, $**p < 0.01$, $***p < 0.001$.

3.2.6 Proliferation and apoptosis of tdTomato^{Pos} AT2 cells

To examine whether cell death and cell amplification occur in tdTomato labeled AT2 cells, the proliferation and cell death of tdTom^{Pos} AT2 cells were analyzed by immunofluorescent staining on lung sections at day 7, day 14 and day 21. (Figure 32a-d). At day 7 and day 14, a significant increase in both proliferation and apoptosis in Tom^{Pos} cells was observed, whereas in animals treated for one week with tamoxifen water and then put on normal water for two weeks, a trend towards increased proliferation and apoptosis was detected. It suggests that different AT2 lineage labeled subpopulations undergo apoptosis and proliferation simultaneously in *Fgfr2b*-cKO condition.

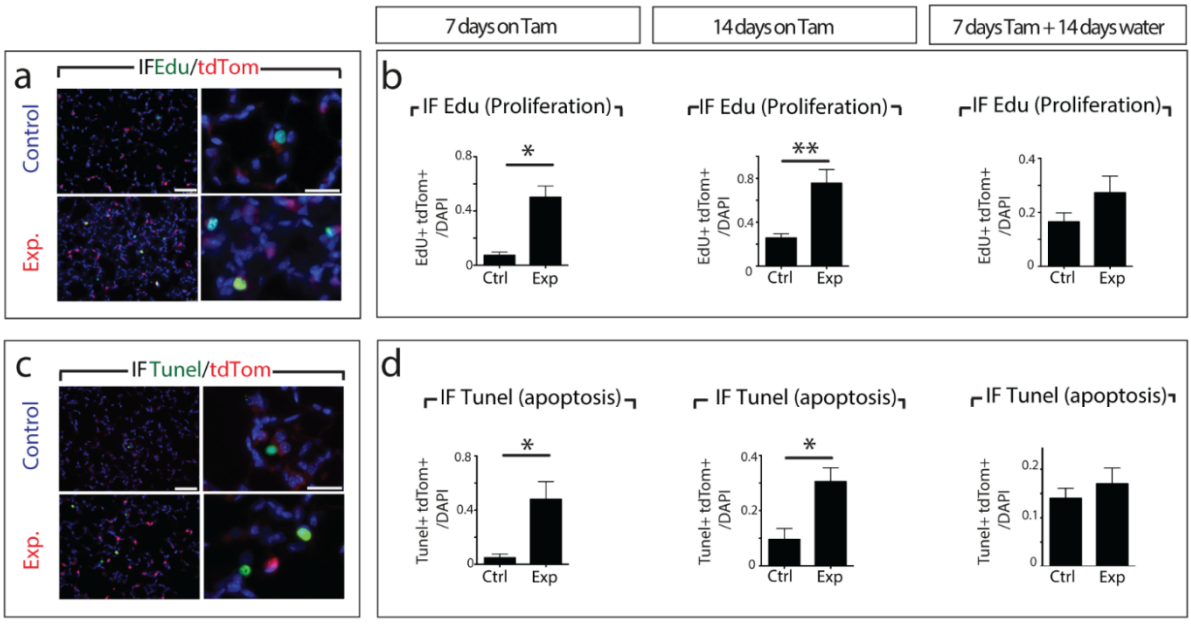

Figure 32: Proliferation and apoptosis of tdTomato^{Pos} AT2 cells at different time points. **a)** Representative EdU staining (Scale bar: 50µm). **b)** Quantification of tdTomato+ Edu+ cells in three different time points of 7 days,14 days, and one week with tamoxifen water and two weeks on normal water (n=4). **c)** Representative TUNEL staining, (n=4). **d)** Quantification of tdTomato+TUNEL+ cells in three different time points of day7, day 14 and day 21. Data are presented as mean values ± SEM. ∗p < 0.05, ∗∗p < 0.01, ∗∗∗p < 0.001.

3.2.7 Deletion of *Fgfr2b* in the AT2 lineage leads to loss of self-renewal capability in Tom^{High} and a gain of alveolosphere formation potential in Tom^{Low}

To compare the self-renewal capacity of Tom^{Low} and Tom^{High} in control and *Fgfr2b*-cKO lungs, FACS-based sorted cells were co-cultured with

$CD31^{Neg}CD45^{Neg}Epcam^{Neg}Sca1^{Pos}$ resident lung mesenchymal cells (Figure 14a). Tom^{High} from control lungs behaved as *bona fide* AT2 cells as they formed alveolospheres with the expected colony-forming efficiency (Figure 33a,c). By contrast, Tom^{High} from *Fgfr2b*-cKO lungs demonstrated a significant decrease in alveolosphere forming capabilities compared to the corresponding control, suggesting the loss of self-renewal capabilities upon *Fgfr2b* deletion (0.22% ± 0.13 vs.1.20% ± 0.36 n=3) (Figure 33a,c). Tom^{Low} from control lungs displayed very weak organoid forming capabilities, which is in line with their quiescent status. Interestingly, Tom^{Low} from *Fgfr2b*-cKO lungs showed a significant increase in alveolosphere formation, which is consistent with their transition towards the Tom^{High} status (0.02% ± 0.01 vs. 0.15% ± 0.05, n=3) (Figure 33a-c). Supporting this conclusion, we observed the differential viability of FACS-isolated Tom^{High} and Tom^{Low} from control and *Fgfr2b*-cKO lungs. Tom^{High} displayed decreased viability in experimental vs. control lungs (18,27% ± 1,64% vs. 72,33% ± 5,62%, n=3). By contrast, a sharp increase in viability was observed for Tom^{Low} in experimental vs. control lungs (72% ± 4% vs. 10,17% ± 0,98%, n=3) (Figure 34). These results suggest that Tom^{Low} in *Fgfr2b*-cKO lungs display progenitor behavior characteristics similar to Tom^{High} in the control lungs.

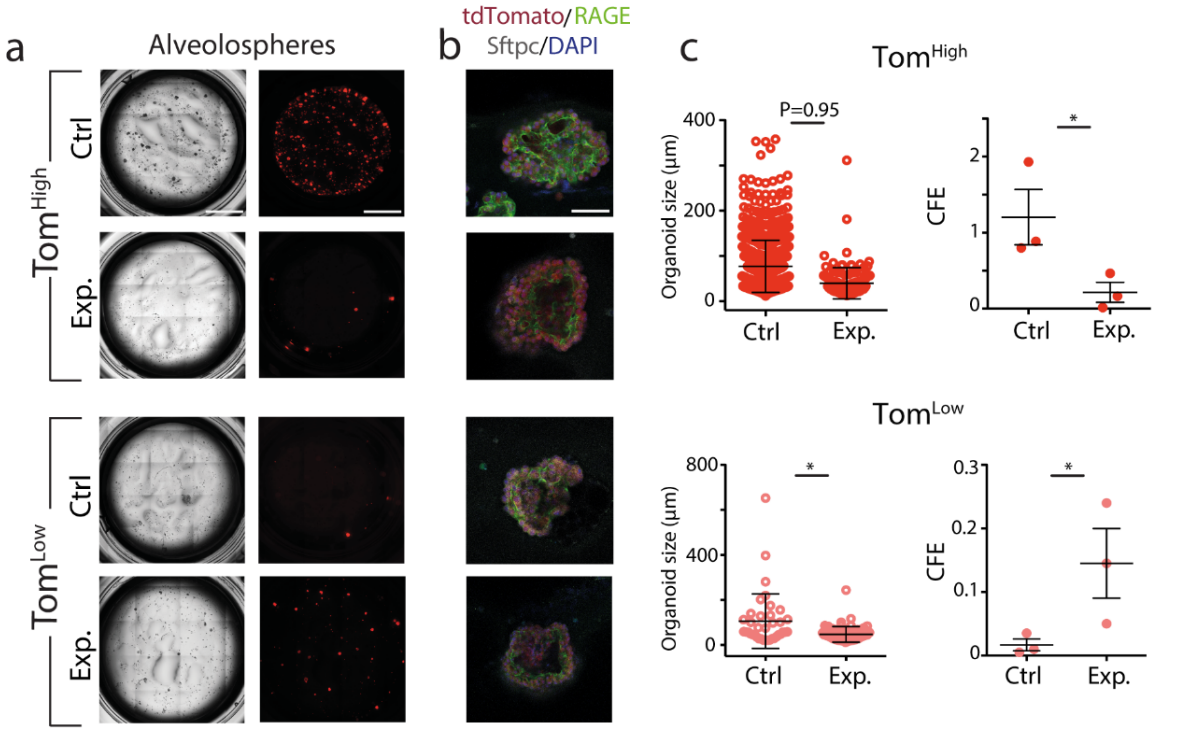

Figure 33: Deletion of *Fgfr2b* in the AT2 lineage labeled cells leads to the loss of self-renewal in Tom^{High} and the gain of alveolosphere formation in Tom^{Low}. (a) Representative of alveospheres from Tom^{High} and Tom^{Low} in the control and in the experimental conditions (n=3), Scale bar: 100µm **(c)** Representative of Sftpc and RAGE Immunofluorescent staining of alveospheres after 14 days in culture, Scale bar: 50µm. **(d)** Quantification of alveospheres size and Colony-forming unit (CFU) in Tom^{High} and Tom^{Low} in the control and experimental conditions (n=3).

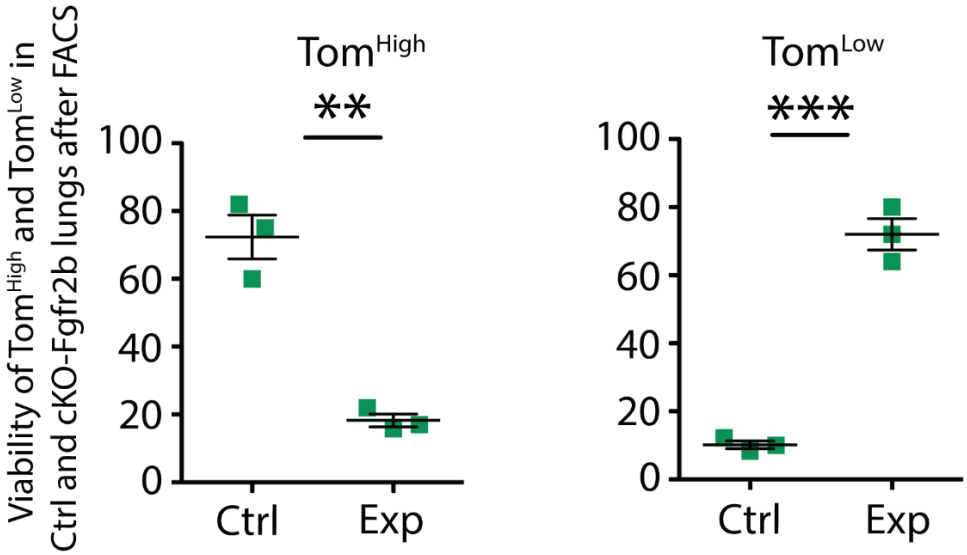

Figure 34: Viability of Tom^{Low} and Tom^{High} in the control and experimental following FACS. Quantification of live and dead cells of Tom^{Low} and Tom^{High} by NucleoCounter, following FACS in the experimental compared to the control (n=4). Data are presented as mean values ± SEM. ∗p < 0.05, ∗∗p < 0.01, ∗∗∗p < 0.001.

3.2.8 The Transition of Tom^{Low} to Tom^{High}

The tdTomato intensity in the Tom^{Low} cells, obtained by flow cytometry, in *Fgfr2b*-cKO and control lungs, was quantified (Figure 35a). The results indicated that there was an expansion of the Tom^{Low} cells in *Fgfr2b*-cKO vs. control lungs towards higher tdTomato intensity. The quantification of the mean fluorescence intensity in Tom^{Low} in *Fgfr2b*-cKO vs. control lungs confirmed this increase (Figure 35b). Next, the level of expression of *Tomato* mRNA in FACS-isolated Tom^{Low} in *Fgfr2b*-cKO vs. control lungs was quantified by qPCR, and a substantial upregulation of *Tomato* expression upon *Fgfr2b* deletion was observed (Figure 35c), suggesting that in the *Fgfr2b*-cKO lungs, Tom^{Low} is transitioning towards a Tom^{High} status. This is also in line with the qPCR

analysis of AT2 cell differentiation markers (Figure 27), representing the upregulation of these genes in Tom^{Low} in *Fgfr2b*-cKO compared to control.

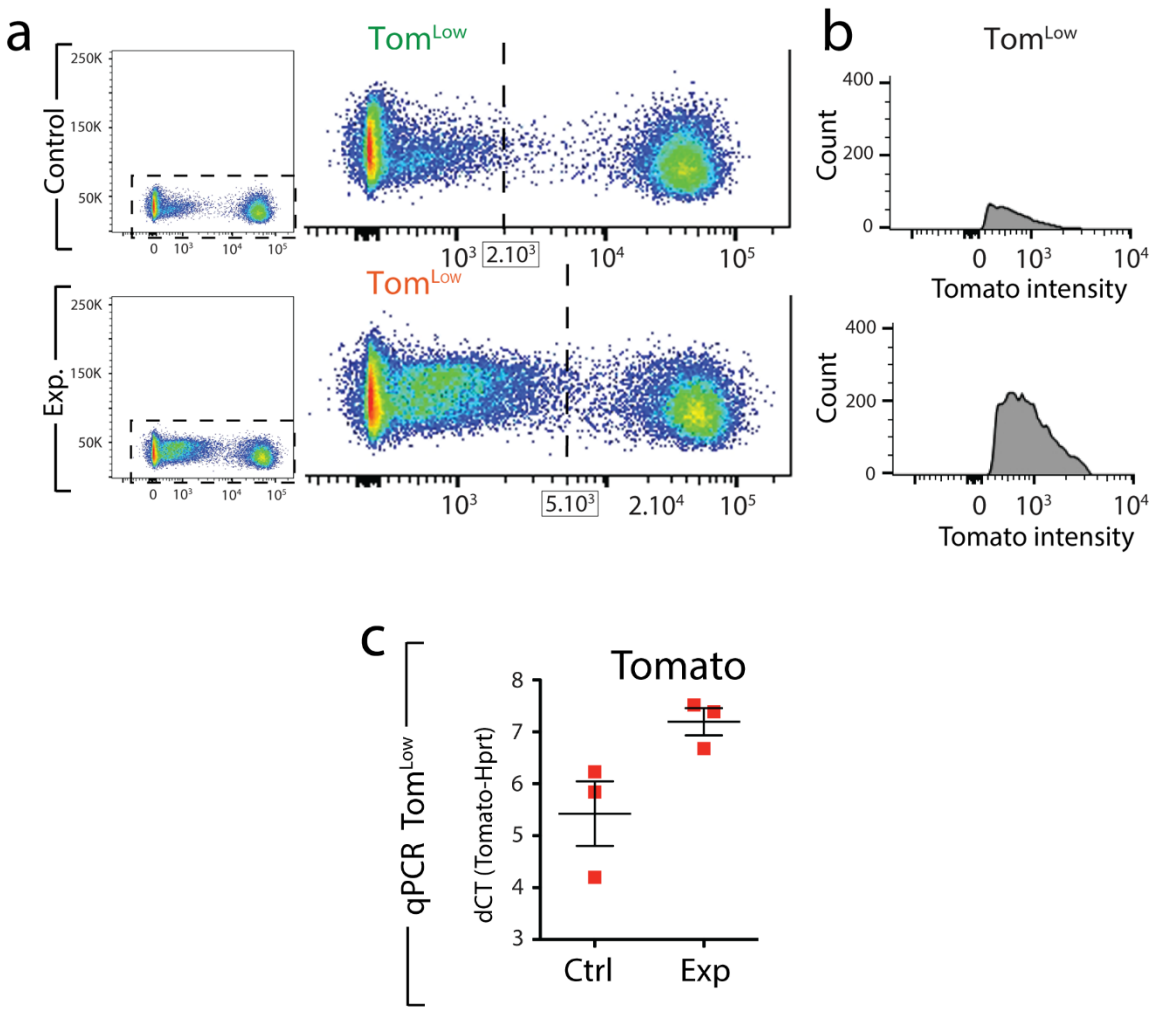

Figure 35: Quantification of Rfp intensity of Tom^{Low} in control and *Fgfr2b*-cKO lungs. a) Representative flow cytometry analysis of Tom^{Low} cells shows the expansion of Tom^{Low} cells towards higher Rfp intensity in experimental vs. control lungs. **b)** Rfp intensity quantification of Tom^{Low} in control and *Fgfr2b*-cKO lungs. **c)** qPCR on FACS-based sorted Tom^{Low} cells displays the upregulation of Rfp expression in the experimental compared to the control. Data are presented as mean values ± SEM. $*p < 0.05$, $**p < 0.01$, $***p < 0.001$.

4 Discussion

4.1 Heterogeneity in AT2 cell population

AT2 cells as alveolar stem cells play a significant role in the maintenance of alveolar epithelium during homeostasis. These cells protect the gas exchange surface area by repopulating the lost AT1 cells after injury. Although AT2 subpopulations have been identified based on the expression of different markers, there are still unanswered questions about privileged AT2 subsets with higher progenitor activity and the existence of unmatured, quiescent AT2 cells activating at the time of regeneration/repair.

The present study introduces a new subset of AT2 cells which is distinct from already identified AT2 subpopulation. These cells (Tom^{Low}) are immature AT2 cells expressing lower levels of AT2 differentiation markers (Sftpc, *Sftpb*, and *Sftpa1*), *Fgfr2b,* and *Etv5* compared to *bona fide* AT2 cells (Tom^{High}) (Figure11). Tom^{Low} subsets are transcriptionally less active and contain less open chromatin compared to Tom^{High} cells (Figure13). Upon pneumonectomy, Tom^{Low} but not Tom^{High} cells display progenitor behavior. These cells proliferate and upregulate the expression of *Fgfr2b*, *Etv5*, *Sftpc*, *Ccnd1* and *Ccnd2* compared to sham (Figure16). Tom^{Low} cells overexpress PD-L1, an immune inhibitory membrane receptor ligand, which is used by flow cytometry to differentially isolate this subpopulation (Figure 18 and19).

Previously, two independent studies characterized Axin2 positive cells as alveolar progenitor cells. The number of these cells ranges from 1% to 20% of AT2s at steady state [62][63]. Nabhan et.al identified rare alveolar stem cells (1%) with active Wnt signaling which are mostly located near Wnt- expressing fibroblasts. These cells express all AT2 cell markers and are physiologically active. It appears that Axin2+ cells with these characteristics refer to a subset of mature AT2 cells (Tom^{High}) in the present study. *β-catenin* deletion, as a transducer of canonical Wnt pathway activity, in these cells results in substantially increasing the number of AT1 cells. However, there is no evidence of cell death in these cells after the inhibition of Wnt signaling, suggesting Wnt signaling is required for keeping the identity of AT2 cells but it is not necessary for their survival. On the other side, keeping constant Wnt signaling in these cells by stabilized *β-catenin* (*β-catenin*^{Ex3}) maintain AT2 cell identity, with no change in the

number of AT2 cells and prevent their reprogramming to AT1 cells. This suggests that Wnt signaling does not play a role in AT2 cell proliferation [62].

Based on our study, Fgfr2b signaling is the critical pathway in the AT2 cell maintenance and survival, as a significant reduction in the number of *bona fide* mature AT2 cells was observed after the deletion of *Fgfr2b* in these cells. Furthermore, the upregulation of Fgfr2b signaling in proliferating Tom^{Low} cells following pneumonectomy and in Ffgr2b-Ko displays the significance of Fgfr2b signaling in AT2 cell proliferation (Figure 16 and 27).

Alveolar epithelial progenitors (AEPs) are another identified Axin2 positive subpopulations expressing the same level of AT2 specific genes as other mature AT2 cells. ATAC-seq analysis shows differential open chromatin between the genome of AEPs and AT2 cells. AEPs show enriched gene expression profiles of lung developmental genes and tube development genes including *Fgfr2*, *Nkx2.1*, *Id2*, *Etv4*, *Etv5*, and *Foxa1*, which is comparable with the high level of *Fgfr2* and *Etv5* in Tom^{High} population in our study (Figure11). It suggests AEPs could be a subpopulation of Tom^{High} with higher progenitor activity. Moreover, these genes are expressed at a lower level in Tom^{Low} versus Tom^{High}, which separates them from Tom^{Low}. The equivalent of AEPs was identified in human by using antibody against $TM4SF1^{+}$, which is enriched in these cells. AEPs act as functional alveolar progenitors in 3D organoids culture. Both mouse and human AEPs form more and larger organoids containing AT1 and AT2 cells and demonstrate increased responsiveness to Wnt modulation compared to other AT2 cells. Wnt activation leads to an increase in AT2 differentiation whereas Wnt inhibition results in an increase in AT1 differentiation. Moreover, these cells respond to Fgfr2b ligands, Fgf7 and Fgf10, with an increase in colony size and colony-forming efficiency. Comparison of colony-forming efficiency of AEPs with Tom^{Low} and Tom^{High} shows that, in contrast to AEPs, Tom^{Low} as quiescent cells with very weak organoid forming capacity (Figure14). Moreover, part of cultured Tom^{High} elicits greater progenitor activity with the formation of alveolosphere which could be AEPs in this cell pool [63].

Sca1+ AT2 cells are another AT2 subpopulations existing in limited number in the steady-state. These cells display higher progenitor behaviour compare to Sca1 negative AT2 cells in response to *Pseudomonas aeruginosa* infection [141]. Wnt pathway genes are upregulated in these cells during repair [141]; however, it is not clear how these cells are different from Axin2 positive and AEPs subpopulations.

Interestingly, a proportion of AT2 cells express low levels of Scgb1a1 locating in the alveoli. These cells are identified with lineage tracing of Scga1b1 positive cells and no particular function has not been attributed to them yet [16].

In this regard, integrin α6β4 positive population was characterized as alveolar progenitor cells locating in both bronchoalveolar junction and within alveoli. These cells express differentiation markers of neither club cells nor AT2 cells, but they can regenerate AT2 Sftpc+ cells in the alveoli after severe injury. A limitation of Chapman et.al study was the lack of a method to separate integrin α6β4 positive cells in the bronchoalveolar junction from those in alveoli. Therefore, it is not clear which population shows higher progenitor activity. Since this population are negative for *Sftpc*, therefore cannot be lineage traced by the *Sftpc*^{CreERT2} driver line. These cells are termed lineage negative epithelial stem/progenitor (LNEP) cells and they are CD200+, CD14+, and are known as the major source of ΔNp63+ (a p63 splice variant) and cytokeratin 5+ cells [61][64].The newly identified Tom^{Low} cells are different from integrin α6β4 positive population because of displaying different gene expression profiles.

One recent study by Han et al using single-cell transcriptomic analysis introduced alveolar bipotent-like cells co-expressing AT1 cell markers (*Ager* and *Aqp5*) and AT2 cell markers (*Sftpd* and *Sftpa1)*. These cells are very different from AT1 and AT2 cells because of the high expression of the epithelial markers of *Krt8* and *Krt18* [142]. Another study supported this finding by immunohistochemistry staining of a small subpopulation (less than 1%) of AT2s co-expressing Sftpc and Ager. The proportion of these dual-positive cells increases to 20% by 7 days after PNX, suggesting differentiation of this population into AT1 cells during compensatory lung growth mechanism. In addition, cultured isolated AT2 cells in 3D organoid culture transiently become dual positive for Sftpc and Ager. This indicates the inversion of mature AT2 cells to a more plastic, bipotential status. Further experiments are required to study how this subpopulation is different from others, and whether these cells are privileged to differentiate to AT1 cells during lung regeneration [143].

4.2 AT2 cell progenitor activity after lung injury

The repair mechanism of alveolar epithelium response to various types of injury, depends on the pathogenicity and the extent of the injury. Therefore, to reveal the

repair mechanism and contribution of AT2 population/subpopulations progenitor cells, a comparison of alveolar repair in diverse injury models would be essential.

To trigger different alveolar injury in rodents, mainly three types of agents have been applied as follows:

First, gas inhalation, for instance, toxic nitrogen dioxide (NO2) or high oxygen (O2) concentration (80%-100%). NO2 produces nitrating oxidants, leading to inflammatory responses [144][81][145]. In response to NO2, AT2 cells proliferate and transdifferentiate into AT1 cells within 2 days after injury induction [144][81].

The Hyperoxia model is a commonly used alveolar injury model. In this injury model, releasing reactive oxygen species or free radicals from O2 results in apoptosis or necrosis of alveolar epithelial cells [146]. Hyperoxia also activates NF-κB signaling and inflammatory responses, thereby increasing alveolar damage [147][146][148]. AT2 cell proliferation, expansion, and conversion into AT1 cells are observed after exposure of neonatal and adult mice to hyperoxia [80][147][29][149]. In a study in rats, highly proliferative AT2 cells arise in response to hyperoxia injury. These cells express a lower level of E-cadherin and compose around 50% of AT2 cells. Telomerase activity is induced in these cells following oxygen exposure. This indicates the heterogeneity of AT2 cells in response to the damage. In this regard E-cadherin expression has a revers correlation with the expression of β-catenin. Nevertheless, the molecular mechanism in these cells that is activated after injury is not well characterized or analyzed [60]. Moreover, exposing *Axin2*$^{creERT2\text{-}tdT;}$ *R26*^{eYFP} adult mice to hyperoxic injury results in autocrine activation of the canonical Wnt pathway in AT2 Axin2+ cells.

In addition, according to different studies, there is no correlation between high Sftpc mRNA and low Sftpc protein levels after hyperoxia [150][79]. This might be explained by increasing the level of mRNA in Tom^{Low} cells in the process of repair (Figure16a) while the level of Sftpc protein is still low because of damaged AT2 cells.

Second, the administration of chemicals or antibiotics. For example, the HCL aspiration model causes alveolar cell death, acute inflammatory responses, and elevated alveolar barrier permeability [148]. Bleomycin is the most commonly used antibiotic, forming a complex with oxygen and metals like Fe, after administration into the lung, resulting in the generation of oxygen radicals that trigger inflammatory responses in the injured lungs and alveolar cells death [151][148][152]. Bleomycin induces acute lung injury in the earlier phase which leads to fibrosis in the later phase of injury. AT2 cell

proliferation and accelerated AT2 into AT1 conversion has been shown using lineage tracing of these cells [28][30].

Damaged AT2 cells are mostly replaced by Scgb1a1 positive cells locating in the bronchiolar epithelium after bleomycin-induced injury. Moreover, some of the damaged AT2 cells are replenished by Scgb1a1 negative, Sftpc negative/low cells. Decreased Sftpc expression is reported in the lineage labeled isolated AT2 cells, 14- and 21-days post-bleomycin injury compared to saline treated controls. This could be associated with the loss of Tom^{High} which express high level of Sftpc (Figure 11) and resistance of Tom^{Low} with low level of Sftpc to the injury. Moreover, BrdU proliferation assay displays 10 times enhanced amplification of AT2 lineage-labeled cells, using *SftpcCreER;ROSA-Tomato* mice,14 days after bleomycin administration [30]. Low level of Sftpc expression and high rate of AT2 proliferation might be explained by the amplification of Tom^{Low} cells expressing low level of Sftpc. Moreover, the expression of Pdpn was increased in the lineage-labeled population 21 days post bleomycin, representing increase rate of AT2 to AT1 turnover. Further studies are required to investigate whether Tom^{Low} are capable of giving rise to AT1 in the context of injury or Tom^{High} are the cells repopulate lost AT1 cells. This requires the generation of mice that allow the differential labeling of Tom^{Low} and Tom^{High} based on two markers (Sftpc and PD-L1) using the Dre and Cre technology and a tomato/GFP dual Dre/Cre reporter [153]. Using this approach, it is possible to label only Sftpc+ (Tomato), PDL1+ (GFP) or double Sftpc+PDL1 (Yellow) positive cells.

Moreover, it has been shown that Scgb1a1 lineage-labeled cells give rise to large numbers of AT1 and AT2 cells in the alveoli after bleomycin treatment, however their origin is still controversial. These progenitor cells may initially reside in the terminal bronchioles or the alveoli and may correspond to the proposed integrin α6β4-positive progenitors. Integrin α6β4 positive cells are another candidate for the maintenance of AT2 cells during the repair. The number of these cells is increased 7-10 days following bleomycin-induced injury. α6β4 positive cells which expand into alveolar space during the fibrogenic phase of bleomycin injury are either Scgb1a1+ or Spc+, but it is not clear what is the proportion of each of these two populations in the alveolar repair. Applying in vivo lineage tracing using tamoxifen-inducible Cre recombinase driven by Spc locus showed that these cells are not traceable, indicating very low level of Sftpc in these cells.

Third, administration of pathogens such as *Pseudomonas aeruginosa* or H1N1 influenza virus. *Pseudomonas aeruginosa* infection mimics pneumonia with the production of toxins which penetrate cell membrane leading to cell death [154]. Studying the progenitor behaviour of AT2 cells following *Pseudomonas aeruginosa* (PA) injury, shows the emerge of Sca1+ AT2 cells 24 hours after PA infection. Sca1+ AT2, which are few in normal lung, increasing to 60% in injured lungs. These cells are more proliferative compared to Sca1^{neg} AT2 cells and they mostly contribute to AT1 cell replacement through the involvement of the Wnt signalling pathway. These cells also show a higher potential of transdifferentiation into AT1 cells *in vitro* [141][155]. Moreover, *FoxM1*, a member of the forkhead box family (FOX) of transcription factors, is upregulated in Sca1+ AT2 cells after injury. It plays a key role in the cell cycle progression at S and G2/M phases and mediates cell differentiation during lung development [156][157][158]. FACS analysis of lineage-labeled Sca1+ cells demonstrate that they are mostly derived from Sftpc-expressing cells. Interestingly, *FoxM1* knock-out mice display delayed alveolar barrier restoration after PA-induced lung injury because of inhibition of AT2 cell proliferation and their transdifferentiation into AT1 cells [141].

The H1N1 influenza virus also causes cell death and inflammatory responses in infected lungs [70][159]. To study the progenitor activity of Axin2+ AT2 cells, the H1N1 influenza virus was applied to injure the lungs of *Axin2$^{creERT2\text{-}tdT}$; R26^{eYFP}* adult mice. Four different regions of injury were defined base on the severity of the injury. In zone 1, no morphological changes in the lung were observed and AEPs and their progeny were present at the homeostatic levels in this zone one month after injury. In zone 2, mild injury accompanied by mild interstitial thickening and in zone 3 substantial injury occurred. In these two zones, the number of AT2 cells significantly increased, with an elevated percentage of lineage labeled AT1 and AT2 cells. In zone 4 with total alveolar destruction, Sox2-derived Krt5 positive cells were detectable. This suggests that AEPs self-renew to maintain AEP lineage in mild injured regains of lung and generate new lineage labeled alveolar epithelial cells. Interestingly, few non-AEP AT2 cells acquire the AEP phenotype even after severe lung injury [63]. However, the percentage of these cells is not quantified, and this subset of cells could be undifferentiated Tom^{Low} cells in our study that gain mature AT2 cell profile after injury.

Another model of AT2 cell injury is using *Sftpc-CreER; Rosa-DTA*/*Rosa-Tm* knock-in mice in which the expression of diphtheria toxin is induced in these cells after induction of Cre recombinase with tamoxifen.

In Barkauskas study, an AT2 cell-specific injury using *Sftpc-CreER; Rosa-DTA*/*Rosa-Tm* triple heterozygous mice were applied to investigate AT2 stem cell behaviour. Interestingly, the induction of the catalytic subunit of diphtheria toxin expression in AT2 cells results in cell death in some, but not all AT2 cells. Although the number of lost AT2 cells are not quantified, it is estimated that half of the AT2 cells undergo apoptosis, which is not led to change in the overall histology of the lung. Survivor AT2 cells begin clonal proliferation after targeted injury and they are capable of repopulating lost AT2 cells within 21 days [28]. The identity of these AT2 survivor cells is unknown, however, they might be Tom^{Low} cells which are transcriptionally less active compared to mature AT2 cells (Figure13), leading to the lower level of Diphtheria toxin receptor (DTR) in these cells and being more resistant to Diphtheria toxin injury. To elucidate this, more experiments still need to be performed. Further analysis of clonal proliferation using *Sftpc-CreER;Rosa-DTA/Rosa-Confetti* and *SftpcCreER;Rosa-Confetti* (as control) demonstrate the random distribution of distinct clones of single colours throughout the lung in DTA-Confetti mice. This indicates that at least a subset of AT2 cells proliferates clonally in response to alveolar epithelium injury and clones are mostly located throughout the alveoli. Moreover, AT2 to AT1 transdifferentiation also occurs during DTA-induced repair, however, the rate of turnover is substantially lower compared to repair after bleomycin-induced lung injury [28].

In Nabhan et.al study, to investigate the progenitor activity of AT2 cells, especially rare Axin2+ cells, a genetic system was applied to ablate alveolar epithelial cells. *Shh-Cre* adult mice were employed to induce the expression of Diphtheria toxin receptor throughout the lung epithelium. Following injury, around 85% of surviving AT2 cells proliferate at the highest rate on day 5, which returns to baseline after restoring the epithelium integrity. Although the expansion of rare Axin2+ AT2 is not reported after injury, canonical Wnt signaling is induced in the most (73%) of proliferating ancillary AT2 stem cells. Therefore, it appears that rare AT2 Axin2+ cells are insufficient to repair alveolar epithelium, and bulk AT2 cells are recruited to function as stem cells with induction of autocrine Wnt signaling. Therefore, Wnt signaling plays a role in AT2 cells' stemness features in two ways. First, it maintains AT2 identity by preventing reprogramming to AT1 cells. Second, it contributes to AT2s ability to proliferate

extensively [62]. However, it is not clear how Wnt signaling activates AT2 cell stem cells. This might be in parallel interaction with EGFR/KRAS signaling or Fgf10-Fgfr2b pathway. In Nabhan et.al study 'bulk'AT2 cells are considered as AT2 Axin2 negative cells, but it is not clear whether all cells which are grouped as 'bulk'AT2 are arising from the mature AT2 cells or originating from undifferentiated progenitor cells which are differentiated to mature AT2 cells following the injury. In contrast to rare Axin2+ AT2 cells, which are not expanded during repair, AEPs self-renew, expand and transdifferentiate to AT1 cells after epithelium injury. Rare Axin2+ AT2 cells might be either subpopulation of AEPs with different behavior after injury or distinct small AT2 subsets.

Altogether, according to studies on different injury models, AT2 subpopulations are activated in response to lung damage. Intriguingly, evidence was also provided on the existence of AT2 cells with low levels of Sftpc after hyperoxia and bleomycin lung injury [79][150]. These cells could refer to newly identified Tom^{Low} cells expressing low Sftpc levels in our study. Furthermore, PD-L1 is known to be upregulated in adenocarcinoma and appears to be correlated with elevated tumour proliferation and aggressiveness [133][134][160][161][162]. Here high expression of PD-L1 was detected in Tom^{Low} (Figure 19). This let us suggest further investigations to elucidate PD-L1 function in Tom^{Low} and its potential interaction with the immune system as well as their contribution to cancer. In the future, it will be worth investigating to design dual lineage tracing strategies based on the expression of Sftpc and PD-L1 to specifically label the Tom^{Low} cells.

The equivalent of this population also was identified in human lung. Further characterization of these cells in homeostatic and repair/regeneration conditions will allow identifying the signaling pathways activated in these cells with the ultimate goal to enhance repair after injury.

4.3 The significance of Fgf10-Fgfr2b signaling in lung homeostasis and repair

Fgf10 is expressed in the lung mesenchyme during embryonic development and postnatal playing critical role in lineage commitment and epithelial proliferation. During embryogenesis, Fgf10 is expressed by mesenchymal progenitor cells, and in the adult lung is expressed in mesenchymal stromal niches. The mesenchymal stromal niches

are located in proximity basal cells in the upper conducting airways between cartilage rings, and in the lipofibroblasts adjacent to AT2 cells. Fgf10 derives lung epithelial regeneration after different types of lung injuries. Fgf10 signaling dysregulation is contributed to the pathogenesis of different human lung diseases such as bronchopulmonary dysplasia (BPD), chronic obstructive pulmonary disease (COPD), and idiopathic pulmonary fibrosis (IPF).

During alveologenesis, Fgfr2b ligands play a critical role in the differentiation of AT2 cells in the neonatal mice. The ratio of AT2 cells is decreased in the lungs of *Fgf10*$^{+/-}$ (heterozygous) compared to *Fg10*$^{+/+}$ (WT) demonstrating that Fgf10 is essential for the formation of the AT2 lineage [84].

During homeostasis, basal stem cells (BSCs) in cartilaginous airways activate Hippo signaling pathway by controlling Fgf10-Fgfr2b to maintain their stemness. In these cells increased nuclear Yap as a result of Hippo signaling inactivation, leads to *Fgf10* expression in stromal niche [112]. By contrast, in non-cartilaginous airways, differentiated airway epithelial cells inhibit Fgf10 expression in airway smooth muscle cells (ASMCs) to keep these cells quiescent through Hippo signaling activation. However, after injury *Fgf10* expression is induced in ASMCs following downregulation of the Hippo pathway, resulting in BSC niche extension and amplification of the stem cell population through Fgf10-Fgfr2b signaling.

Moreover, Fgfr2b signaling controls the expression of Sox2 as a key transcription factor for basal cell self-renewal and differentiation. Intriguingly, the deletion of one copy of *Fgfr2* in BSCs cells leads to a reduction in their self-renewal capacity and they become senescent. Treatment of cultured BSCs with Fgf7 and Fgf10 promotes their colony expansion and increases the size of colonies [113].

Balasooriya et al showed that, conditional deletion of *Fgfr1* in tracheal BSCs leads to their amplification and elevated ERK/AKT signaling. This suggests Fgfr2b signaling is activated in these cells because of the lack of Spry2 activation by Fgfr1. Interestingly, the overexpression of Fgf10 in the trachea generates similar phenotypes. It suggests Fgf10/Fgfr2b/ERK/AKT signaling, being essential for keeping BSCs quiescent, might be antagonized by the Fgfr1-SPRY2 signaling axis [163].

Fgf10-Fgfr2b signaling derives lung epithelial amplification and restoration after different injuries. For instance, the renewal capacity of epithelial stem/progenitor cells (EpiSPC) in influenza virus infected lungs is impaired because of the blockage of β-catenin-dependent Fgfr2b signaling. Interestingly, the epithelial proliferative potential

is improved by intratracheal administration of exogenous recombinant Fgf10 by the involvement of non-infected EpiSPC in lung regeneration. Moreover, self-renewal capability and differentiation of EpiSPC *in vitro* are associated with Fgf10 [115].

Furthermore, following bleomycin injury to the lungs, losing Fgf10-Fgfr2b signaling in bronchial epithelial cells leads to impairment of neo basal, AT1 and AT2 cells generation. Added to this, Fgf10 overexpression in bronchial epithelial cells results in their differentiation to AT2 cells rather than basal cells after injury. This promotes fibrosis resolution by the reduction of honeycomb cysts development [114].

Intriguingly, the induction of *Fgf10* expression in alveolar epithelium using Sftpc-rtTA;Tet Fgf10 mice in bleomycin-induced injury model demonstrates the protective and regenerative function of Fgf10 in inflammation and fibrosis. *Fgf10* overexpression, results in increased *Sftpc* expression, decreased number of apoptotic AT2 cells and elevated survival rate of isolated and cultured AT2 cells *in vitro* [47]. This indicates that Fgf10 has a protective as well as a regenerative effect on epithelial progenitor cells [47]. Fgf10 also attenuates H_2O_2-induced alveolar epithelial DNA damage through the Grb2-SOS/Ras/Raf-1/MAPK pathway, suggesting the possible role of Fgf10 in preventing oxidant-induced lung injury [164].

Moreover, Fgf10 attenuates acute lung injury induced by Lipopolysaccharide (LPS) exposure. Treatment of injured lungs with Fgf10 leads to increased AT2 cell proliferation accompanied by elevated levels of Sftpa and Sftpc [119].

In the present study, the function of Fgfr2b signaling in AT2 cells during homeostasis was investigated by conditional deletion of *Fgfr2b* in AT2 cells by lineage tracing using *Sftpc*$^{CreERT2/+}$*; Fgfr2b*$^{flox/flox}$*; tdTom*$^{flox/flox}$ (*Fgfr2b*-cKO) mice. Intriguingly, our data revealed two AT2 subpopulations (Tom^{Low} and Tom^{High}) respond differently to *Fgfr2b* deletion.

Tom^{High} as bona fide AT2 cells express high levels of *Fgfr2b* in steady-state. *Fgfr2b* deletion induced apoptosis in these cells and consequently a significant reduction of their numbers, suggesting the significance of Fgfr2b signaling in their maintenance (Figure 36). In addition, isolated and cultured Tom^{High} cells from *Fgfr2b-cKO* lungs displayed substantially reduced self-renewal capability compared to isolated cells from control lungs (Figure 33). By contrast, Tom^{Low} cells express low levels of *Fgfr2b* in steady-state. Interestingly, we found upregulation of Fgfr2b signaling in these cells following *Fgfr2b* deletion (Figure 27). Tom^{Low} cells as quiescent and undifferentiated cells displaying very weak alveolospheres formation capacity. Interestingly, after

Fgfr2b activation in these cells, their ability to form organoids was enhanced. This denotes the essential of Fgfr2b signaling in AT2 cell self-renewal (Figure 33). Overall, subsets of Tom^{Low} cells elicited resistance to *Fgfr2b* deletion as they upregulated *Fgfr2b* and were expanded to compensate lost Tom^{High} cells in *Fgfr2b*-cKO lungs (Figure 36).

To study the contribution of Fgf10-Fgfr2b pathway in AT2 cells upon lung epithelial regeneration, the left lung pneumonectomy model was employed in which compensatory lung growth is triggered in the remaining lung lobes. Notably, Fgfr2b signaling is upregulated in Tom^{Low} cells in pneumonectomised lungs compared to sham which is in line with higher proliferation in these cells (Figure 16). This implies Fgfr2b signaling activation in lung regeneration following pneumonectomy. To further elucidate the mechanism and function of Fgfr2b signaling in AT2 cells during lung regeneration after PNX, inhibition of Fgfr2b signaling in these cells using transgenic mice expressing conditionally soluble Fgfrb2 would be required.

Altogether, Fgf10-Fgfr2b signaling appears to be essential for the repair and regeneration of alveolar epithelium and our data provided new insights into Fgfr2b activation in proliferating AT2 cells during lung regeneration; however the molecular mechanism controlling the proliferation and transdifferentiation of AT2 to AT1 cells in lung regeneration and their interaction with mesenchymal niches expressing Fgfs need to be further investigated.

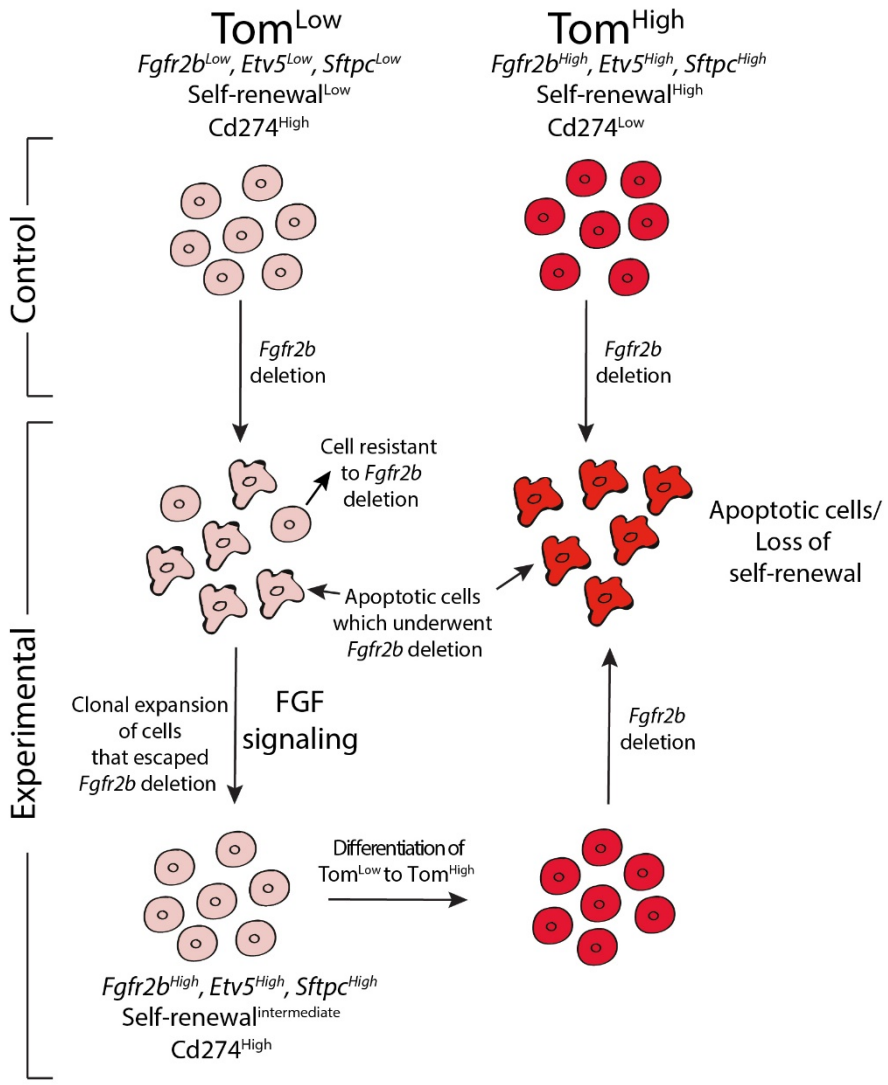

Figure 36: Schematic representation of characteristics and behavior of Tom^{Low} and Tom^{High} in control and experimental lungs. Tom^{Low} cells are immature and quiescent cells expressing low levels of *Sftpc, Fgfr2b* and *Etv5* and high level of *PDL1*. These cells display weak self-renewal capability in culture. Tom^{Low} contains resistant cells to *Fgfr2b* deletion, cable of bypassing the deletion, expanding and differentiating to Tom^{High} cells. Tom^{High} as mature AT2 cells express high levels of *Sftpc, Fgfr2b* and *Etv5. Fgfr2b* deletion in induce apoptosis in these cells.

5 Summary

Alveolar type 2 (AT2) cells are a heterogeneous population; where specialized AT2 subpopulations within this lineage exhibit stem cell properties. However, the existence of quiescent, immature cells within the AT2 lineage, which become activated during lung regeneration, is unknown.

In this study *Sftpc*$^{CreERT2/+}$*; tdTomato*$^{flox/flox}$ mice were used for the labelling of AT2 cells, and two distinct AT2 subpopulations were detected with low tdTomato level (Tom^{Low}) and high tdTomato level (Tom^{High}). Tom^{Low} express lower levels of AT2 differentiation markers, *Fgfr2b* and *Etv5*, while Tom^{High}, as *bona fide* mature AT2 cells, showed higher levels of *Sftpc*, *Sftpb*, *Sftpa1*, *Fgfr2b*, and *Etv5*. ATAC-seq analysis indicated that Tom^{Low} and Tom^{High} constitute two distinct cell populations with specific silencing of *Sftpc*, *Rosa26* and cell cycle gene loci in Tom^{Low}. Upon pneumonectomy, Tom^{Low} but not Tom^{High} cells proliferated and upregulated the expression of *Fgfr2b*, *Etv5*, *Sftpc*, *Ccnd1* and *Ccnd2* compared to sham. This study revealed that, Tom^{Low} cells overexpress PD-L1, an immune inhibitory membrane receptor ligand, which was used by flow cytometry to differentially isolate these two AT2 sub-populations. In support, in the human lung, PD-L1 and HTII-280 antibodies by flow cytometry were employed to differentially sort mature AT2 (HTII-280-high, PD-L1-low) as well as an additional subpopulation of epithelial cells characterized by HTII-280-low and PD-L1-high. Altogether, in the first part of this study, a novel population of AT2 quiescent immature progenitor cells was identified in mouse that proliferates upon pneumonectomy and provided evidence for the existence of such cells in human.

In the second part of this study, the function of Fgfr2b signaling in AT2 subpopulations was investigated using *Sftpc*$^{CreERT2/+}$*; Fgfr2b*$^{flox/flox}$*; tdTom*$^{flox/flox}$ (*Fgfr2b*-cKO) mice. Intriguingly, Tom^{Low} and Tom^{High} responded differently to *Fgfr2b* deletion. Losing Fgfr2b expectedly resulted in Fgfr2b downregulation and consequently decrease in Tom^{High} cell percentage, whereas in Tom^{Low} cells led to *Fgfr2b* upregulation and their expansion. As a consequence of Tom^{Low} to Tom^{High} transition and replenishment of the lost Tom^{High}, no lung phenotype was observed. Interestingly, Tom^{High} cells isolated from *Fgfr2b-cKO* lungs lost the self-renewal capability *in vitro*. By contrast, Tom^{Low} cells as quiescent and undifferentiated cells displayed weak alveolospheres formation capacity during steady state, while their ability to form organoids was enhanced after Fgfr2b

activation. This shed light on the significance of Fgfr2b signaling in AT2 cell self-renewal. Overall, in the second part of this study , our data demonstrated the existence of subsets of Tom^{Low} cells which are resistant to *Fgfrb2* deletion and they are able to bypass the deletion, expand and replace the lost Tom^{High} cells.

6 Zusammenfassung

Alveoläre Typ-2-Zellen (AT2) bilden eine heterogene Population, wobei spezialisierte AT2-Subpopulationen innerhalb dieser Linie Stammzelleigenschaften aufweisen. Die Existenz von inaktiven, unreifen Zellen innerhalb der AT2-Linie, die während der Lungenregeneration aktiviert werden, ist jedoch unbekannt.

In der vorliegenden Studie wurden *Sftpc$^{CreERT2/+}$; tdTomato$^{flox/flox}$* -Mäuse für die Markierung von AT2-Zellen verwendet, und es wurden zwei verschiedene AT2-Subpopulationen mit niedrigem tdTomato-Level (Tom^{Low}) und hohem tdTomato-Level (Tom^{High}) nachgewiesen. Tom^{Low} exprimieren niedrigere Level der AT2-Differenzierungsmarker Fgfr2b und Etv5, während Tom^{High} - als bona fide reife AT2-Zellen - höhere Level von *Sftpc, Sftpb, Sftpa1, Fgfr2b und Etv5* aufweisen. Die ATAC-seq-Analyse deutet darauf hin, dass Tom^{Low} und Tom^{High} zwei verschiedene Zellpopulationen mit spezifischer Stilllegung von Sftpc, Rosa26 und Zellzyklus-Genloci in Tom^{Low} darstellen. Nach einer Pneumonektomie proliferieren zwar Tom^{Low}-, nicht aber Tom^{High}-Zellen und regulieren die Expression von *Fgfr2b*, *Etv5*, *Sftpc*, *Ccnd1* und *Ccnd2* im Vergleich zu den Kontrollzellen hoch. Tom^{Low}-Zellen überexprimieren PD-L1, einen immuninhibitorischen Membranrezeptor-Liganden, der mittels Durchflusszytometrie zur differentiellen Isolierung dieser beiden Subpopulationen verwendet wird. In der menschlichen Lunge werden PD-L1- und HTII-280-Antikörper mittels Durchflusszytometrie verwendet, um reife AT2 (HTII-280-hoch, PD-L1-niedrig) sowie eine zusätzliche Subpopulation von Epithelzellen, die durch HTII-280-niedrig und PD-L1-hoch charakterisiert sind, differentiell zu sortieren. Insgesamt wurde im ersten Teil dieser Studie eine neue Population von AT2- inaktiven, unreifen Vorläuferzellen in der Maus identifiziert, deren Anzahl sich nach einer Pneumonektomie erhöht; ebenfalls wurde der Nachweis für die Existenz solcher Zellen beim Menschen erbracht.

Im zweiten Teil dieser Studie wurden *Sftpc$^{CreERT2/+}$; Fgfr2b$^{flox/flox}$; tdTom$^{flox/flox}$* (*Fgfr2b*-cKO) Mäuse verwendet, um die Funktion der Fgfr2b-Signalisierung in AT2-Subpopulationen zu untersuchen. Interessanterweise reagieren Tom^{Low} und Tom^{High} unterschiedlich auf die Deletion von *Fgfr2b*. Der Verlust von Fgfr2b führt erwartungsgemäß zu einer Fgfr2b-Abwärtsregulation und folglich zu einer Abnahme des Tom^{High}-Zellprozentsatzes, wohingegen Tom^{Low}-Zellen zu einer Fgfr2b-

Hochregulation und der Ausbreitung dieser Zellen führen. Nach der Umwandelung von Tom^{Low} in Tom^{High} und des Ausgleichs von verlorenem Tom^{High} konnte kein spezieller Lungenphänotyp beobachtet werden. Interessanterweise verlieren aus Fgfr2b-cKO-Lungen isolierte Tom^{High}-Zellen die Fähigkeit zur Selbsterneuerung in vitro. Im Gegensatz dazu weisen Tom^{Low}-Zellen als inaktive, undifferenzierte Zellen im Gleichgewichtszustand eine sehr schwache Fähigkeit zur Bildung von Alveolosphären auf, wobei ihre Fähigkeit zur Bildung von Organoiden nach Aktivierung von Fgfr2b verstärkt ist. Hier wird die Bedeutung des Fgfr2b-Signals für die Selbstregeneration von AT2-Zellen deutlich. Untergruppen von Tom^{Low}-Zellen sind resistent gegen die *Fgfrb2*-Deletion und sind in der Lage, die Deletion zu umgehen, zu expandieren und die verlorenen Tom^{High}-Zellen zu ersetzen.

7 References

[1] P. Rao Tata and J. Rajagopal, “Plasticity in the lung: Making and breaking cell identity,” *Development (Cambridge)*. 2017, doi: 10.1242/dev.143784.

[2] J. R. Rock *et al.*, “Basal cells as stem cells of the mouse trachea and human airway epithelium,” *Proc. Natl. Acad. Sci. U. S. A.*, 2009, doi: 10.1073/pnas.0906850106.

[3] Jing Yao Liu, P. Nettesheim, and S. H. Randell, “Growth and differentiation of tracheal epithelial progenitor cells,” *Am. J. Physiol. - Lung Cell. Mol. Physiol.*, 1994, doi: 10.1152/ajplung.1994.266.3.l296.

[4] J. K. Watson *et al.*, “Clonal Dynamics Reveal Two Distinct Populations of Basal Cells in Slow-Turnover Airway Epithelium,” *Cell Rep.*, 2015, doi: 10.1016/j.celrep.2015.06.011.

[5] A. Pardo-Saganta *et al.*, “Injury induces direct lineage segregation of functionally distinct airway basal stem/progenitor cell subpopulations,” *Cell Stem Cell*, 2015, doi: 10.1016/j.stem.2015.01.002.

[6] E. L. Rawlins and B. L. M. Hogan, “Epithelial stem cells of the lung: Privileged few or opportunities for many?,” *Development*. 2006, doi: 10.1242/dev.02407.

[7] K. U. Hong, S. D. Reynolds, S. Watkins, E. Fuchs, and B. R. Stripp, “Basal Cells Are a Multipotent Progenitor Capable of Renewing the Bronchial Epithelium,” *Am. J. Pathol.*, 2004, doi: 10.1016/S0002-9440(10)63147-1.

[8] K. U. Hong, S. D. Reynolds, S. Watkins, E. Fuchs, and B. R. Stripp, “In vivo differentiation potential of tracheal basal cells: Evidence for multipotent and unipotent subpopulations,” *Am. J. Physiol. - Lung Cell. Mol. Physiol.*, 2004, doi: 10.1152/ajplung.00155.2003.

[9] J. R. Rock and B. L. M. Hogan, “Epithelial Progenitor Cells in Lung Development, Maintenance, Repair, and Disease,” *Annu. Rev. Cell Dev. Biol.*, 2011, doi: 10.1146/annurev-cellbio-100109-104040.

[10] V. H. Teixeira *et al.*, “Stochastic homeostasis in human airway epithelium is achieved by neutral competition of basal cell progenitors,” *Elife*, 2013, doi: 10.7554/eLife.00966.

[11] T.-L. Hackett *et al.*, “Characterization of Side Population Cells from Human Airway Epithelium,” *Stem Cells*, 2008, doi: 10.1634/stemcells.2008-0171.

[12] P. R. Tata *et al.*, “Dedifferentiation of committed epithelial cells into stem cells in vivo,” *Nature*, 2013, doi: 10.1038/nature12777.

[13] K. U. Hong, S. D. Reynolds, A. Giangreco, C. M. Hurley, and B. R. Stripp, “Clara cell secretory protein-expressing cells of the airway neuroepithelial body microenvironment include a label-retaining subset and are critical for epithelial renewal after progenitor cell depletion,” *Am. J. Respir. Cell Mol. Biol.*, 2001, doi: 10.1165/ajrcmb.24.6.4498.

[14] A. Guha *et al.*, “Neuroepithelial body microenvironment is a niche for a distinct subset of Clara-like precursors in the developing airways,” *Proc. Natl. Acad. Sci. U. S. A.*, 2012, doi: 10.1073/pnas.1204710109.

[15] S. D. Reynolds, P. R. Reynolds, G. S. Pryhuber, J. D. Finder, and B. R. Stripp, “Secretoglobins SCGB3A1 and SCGB3A2 define secretory cell subsets in mouse and human airways,” *Am. J. Respir. Crit. Care Med.*, 2002, doi: 10.1164/rccm.200204-285OC.

[16] E. L. Rawlins *et al.*, “The Role of Scgb1a1+ Clara Cells in the Long-Term Maintenance and Repair of Lung Airway, but Not Alveolar, Epithelium,” *Cell Stem Cell*, 2009, doi: 10.1016/j.stem.2009.04.002.

[17] M. J. Evans, S. G. Shami, L. J. Cabral-Anderson, and N. P. Dekker, “Role of nonciliated cells in renewal of the bronchial epithelium of rats exposed to NO2,” *Am. J. Pathol.*, 1986.

[18] E. L. Rawlins, L. E. Ostrowski, S. H. Randell, and B. L. M. Hogan, “Lung development and repair: Contribution of the ciliated lineage,” *Proc. Natl. Acad. Sci. U. S. A.*, 2007, doi: 10.1073/pnas.0610770104.

[19] H. Song, E. Yao, C. Lin, R. Gacayan, M. H. Chen, and P. T. Chuang, “Functional characterization of pulmonary neuroendocrine cells in lung development, injury,and tumorigenesis,” *Proc. Natl. Acad. Sci. U. S. A.*, 2012, doi: 10.1073/pnas.1207238109.

[20] C. F. Bender Kim *et al.*, “Identification of bronchioalveolar stem cells in normal lung and lung cancer,” *Cell*, 2005, doi: 10.1016/j.cell.2005.03.032.

[21] J. H. Lee *et al.*, “Lung stem cell differentiation in mice directed by endothelial cells via a BMP4-NFATc1-thrombospondin-1 axis,” *Cell*, 2014, doi: 10.1016/j.cell.2013.12.039.

[22] Q. Liu *et al.*, “Lung regeneration by multipotent stem cells residing at the

bronchioalveolar-duct junction," *Nat. Genet.*, 2019, doi: 10.1038/s41588-019-0346-6.

[23] J. L. McQualter, K. Yuen, B. Williams, and I. Bertoncello, "Evidence of an epithelial stem/progenitor cell hierarchy in the adult mouse lung," *Proc. Natl. Acad. Sci. U. S. A.*, 2010, doi: 10.1073/pnas.0909207107.

[24] B. L. M. Hogan *et al.*, "Repair and regeneration of the respiratory system: Complexity, plasticity, and mechanisms of lung stem cell function," *Cell Stem Cell*. 2014, doi: 10.1016/j.stem.2014.07.012.

[25] D. N. Kotton and E. E. Morrisey, "Lung regeneration: Mechanisms, applications and emerging stem cell populations," *Nature Medicine*. 2014, doi: 10.1038/nm.3642.

[26] H. Fehrenbach, "Alveolar epithelial type II cell: Defender of the alveolus revisited," *Respiratory Research*. 2001, doi: 10.1186/rr36.

[27] J. A. Whitsett and T. Alenghat, "Respiratory epithelial cells orchestrate pulmonary innate immunity," *Nature Immunology*. 2015, doi: 10.1038/ni.3045.

[28] C. Barkauskas *et al.*, "Type 2 alveolar cells are stem cells in adult lung," *J. Clin. Invest.*, vol. 123, no. 7, pp. 3025–3036, 2013, doi: 10.1172/JCI68782DS1.

[29] T. J. Desai, D. G. Brownfield, and M. A. Krasnow, "Alveolar progenitor and stem cells in lung development, renewal and cancer," *Nature*, 2014, doi: 10.1038/nature12930.

[30] J. R. Rock *et al.*, "Multiple stromal populations contribute to pulmonary fibrosis without evidence for epithelial to mesenchymal transition," *Proc. Natl. Acad. Sci. U. S. A.*, 2011, doi: 10.1073/pnas.1117988108.

[31] R. J. Mason, "Biology of alveolar type II cells," in *Respirology*, 2006, doi: 10.1111/j.1440-1843.2006.00800.x.

[32] H. C. Folkesson and M. A. Matthay, "Alveolar epithelial ion and fluid transport: Recent progress," *American Journal of Respiratory Cell and Molecular Biology*. 2006, doi: 10.1165/rcmb.2006-0080SF.

[33] J. L. Alcorn, "Pulmonary Surfactant Trafficking and Homeostasis," in *Lung Epithelial Biology in the Pathogenesis of Pulmonary Disease*, 2017.

[34] Z. Chroneos, Z. Sever-Chroneos, and V. Shepherd, "Pulmonary surfactant: An immunological perspective," *Cellular Physiology and Biochemistry*. 2010, doi: 10.1159/000272047.

[35] V. Goss, A. N. Hunt, and A. D. Postle, “Regulation of lung surfactant phospholipid synthesis and metabolism,” *Biochimica et Biophysica Acta - Molecular and Cell Biology of Lipids*. 2013, doi: 10.1016/j.bbalip.2012.11.009.

[36] M. F. Beers and Y. Moodley, “When Is an alveolar type 2 cell an alveolar type 2 cell?: A conundrum for lung stem cell biology and regenerative medicine,” *American Journal of Respiratory Cell and Molecular Biology*. 2017, doi: 10.1165/rcmb.2016-0426PS.

[37] J. Pérez-Gil, “Structure of pulmonary surfactant membranes and films: The role of proteins and lipid-protein interactions,” *Biochimica et Biophysica Acta - Biomembranes*. 2008, doi: 10.1016/j.bbamem.2008.05.003.

[38] S. Mulugeta and M. F. Beers, “Surfactant protein C: Its unique properties and emerging immunomodulatory role in the lung,” *Microbes and Infection*. 2006, doi: 10.1016/j.micinf.2006.04.009.

[39] E. Davis, “Disorders of the Respiratory System,” in *Equine Internal Medicine: Fourth Edition*, 2018.

[40] S. Kannan *et al.*, “Alveolar epithelial type II cells activate alveolar macrophages and mitigate P. aeruginosa infection,” *PLoS One*, 2009, doi: 10.1371/journal.pone.0004891.

[41] K. Sato, H. Tomioka, T. Shimizu, T. Gonda, F. Ota, and C. Sano, “Type II Alveolar Cells Play Roles in Macrophage-Mediated Host Innate Resistance to Pulmonary Mycobacterial Infections by Producing Proinflammatory Cytokines,” *J. Infect. Dis.*, 2002, doi: 10.1086/340040.

[42] E. Fuchs, T. Tumbar, and G. Guasch, “Socializing with the neighbors: Stem cells and their niche,” *Cell*. 2004, doi: 10.1016/S0092-8674(04)00255-7.

[43] T. Volckaert and S. De Langhe, “Lung epithelial stem cells and their niches: Fgf10 takes center stage,” *Fibrogenesis and Tissue Repair*. 2014, doi: 10.1186/1755-1536-7-8.

[44] M. F. Beers and E. E. Morrisey, “The three R’s of lung health and disease: Repair, remodeling, and regeneration,” *Journal of Clinical Investigation*. 2011, doi: 10.1172/JCI45961.

[45] D. W. Borthwick, M. Shahbazian, Q. T. Krantz, J. R. Dorin, and S. H. Randell, “Evidence for stem-cell niches in the tracheal epithelium,” *Am. J. Respir. Cell Mol. Biol.*, 2001, doi: 10.1165/ajrcmb.24.6.4217.

[46] X. Liu and J. F. Engelhardt, “The glandular stem/progenitor cell niche in airway development and repair,” in *Proceedings of the American Thoracic Society*, 2008, doi: 10.1513/pats.200801-003AW.

[47] V. V. Gupte *et al.*, “Overexpression of fibroblast growth factor-10 during both inflammatory and fibrotic phases attenuates bleomycin-induced pulmonary fibrosis in mice,” *Am. J. Respir. Crit. Care Med.*, 2009, doi: 10.1164/rccm.200811-1794OC.

[48] Y. C. Hsu, H. A. Pasolli, and E. Fuchs, “Dynamics between stem cells, niche, and progeny in the hair follicle,” *Cell*, 2011, doi: 10.1016/j.cell.2010.11.049.

[49] T. Volckaert *et al.*, “Parabronchial smooth muscle constitutes an airway epithelial stem cell niche in the mouse lung after injury,” *J. Clin. Invest.*, 2011, doi: 10.1172/JCI58097.

[50] S. E. McGowan and J. S. Torday, “THE PULMONARY LIPOFIBROBLAST (LIPID INTERSTITIAL CELL) AND ITS CONTRIBUTIONS TO ALVEOLAR DEVELOPMENT,” *Annu. Rev. Physiol.*, 1997, doi: 10.1146/annurev.physiol.59.1.43.

[51] V. K. Rehan *et al.*, “Evidence for the presence of lipofibroblasts in human lung,” *Exp. Lung Res.*, 2006, doi: 10.1080/01902140600880257.

[52] N. B. Kaplan, M. M. Grant, and J. S. Brody, “The lipid interstitial cell of the pulmonary alveolus. Age and species differences,” *Am. Rev. Respir. Dis.*, 1985, doi: 10.1164/arrd.1985.132.6.1307.

[53] E. El Agha *et al.*, “Fgf10-positive cells represent a progenitor cell population during lung development and postnatally,” *Dev.*, 2014, doi: 10.1242/dev.099747.

[54] T. Volckaert, A. Campbell, E. Dill, C. Li, P. Minoo, and S. De Langhe, “Localized Fgf10 expression is not required for lung branching morphogenesis but prevents differentiation of epithelial progenitors,” *Dev.*, 2013, doi: 10.1242/dev.096560.

[55] J. C. Clark *et al.*, “FGF-10 disrupts lung morphogenesis and causes pulmonary adenomas in vivo,” *Am. J. Physiol. - Lung Cell. Mol. Physiol.*, 2001, doi: 10.1152/ajplung.2001.280.4.l705.

[56] B. A. Hyatt, X. Shangguan, and J. M. Shannon, “FGF-10 induces SP-C and Bmp4 and regulates proximal-distal patterning in embryonic tracheal epithelium,” *Am. J. Physiol. - Lung Cell. Mol. Physiol.*, 2004, doi: 10.1152/ajplung.00033.2004.

[57] J. Klar *et al.*, “Fibroblast growth factor 10 haploinsufficiency causes chronic obstructive pulmonary disease,” *J. Med. Genet.*, 2011, doi: 10.1136/jmedgenet-2011-100166.

[58] M. Selman, A. Pardo, and N. Kaminski, “Idiopathic pulmonary fibrosis: Aberrant recapitulation of developmental programs?,” *PLoS Medicine*. 2008, doi: 10.1371/journal.pmed.0050062.

[59] T. E. King, A. Pardo, and M. Selman, “Idiopathic pulmonary fibrosis,” in *The Lancet*, 2011, doi: 10.1016/S0140-6736(11)60052-4.

[60] R. Reddy *et al.*, “Isolation of a putative progenitor subpopulation of alveolar epithelial type 2 cells,” *Am. J. Physiol. - Lung Cell. Mol. Physiol.*, 2004, doi: 10.1152/ajplung.00159.2003.

[61] H. A. Chapman *et al.*, “Integrin α6β4 identifies an adult distal lung epithelial population with regenerative potential in mice,” *J. Clin. Invest.*, 2011, doi: 10.1172/JCI57673.

[62] A. N. Nabhan, D. G. Brownfield, P. B. Harbury, M. A. Krasnow, and T. J. Desai, “Single-cell Wnt signaling niches maintain stemness of alveolar type 2 cells,” *Science (80-.).*, 2018, doi: 10.1126/science.aam6603.

[63] W. J. Zacharias *et al.*, “Regeneration of the lung alveolus by an evolutionarily conserved epithelial progenitor,” *Nature*, 2018, doi: 10.1038/nature25786.

[64] A. E. Vaughan *et al.*, “Lineage-negative progenitors mobilize to regenerate lung epithelium after major injury,” *Nature*, 2015, doi: 10.1038/nature14112.

[65] D. B. Frank *et al.*, “Emergence of a wave of Wnt signaling that regulates lung alveologenesis through controlling epithelial self-renewal and differentiation HHS Public Access,” *Cell Rep*, vol. 17, no. 9, pp. 2312–2325, 2016, doi: 10.1016/j.celrep.2016.11.001.

[66] A. L. Degryse and W. E. Lawson, “Progress toward improving animal models for idiopathic pulmonary fibrosis,” in *American Journal of the Medical Sciences*, 2011, doi: 10.1097/MAJ.0b013e31821aa000.

[67] Y. Aso, K. Yoneda, and Y. Kikkawa, “Morphologic and biochemical study of pulmonary changes induced by bleomycin in mice,” *Lab. Investig.*, 1976.

[68] D. Zheng *et al.*, “Regeneration of Alveolar Type I and II Cells from Scgb1a1-Expressing Cells following Severe Pulmonary Damage Induced by Bleomycin and Influenza,” *PLoS One*, 2012, doi: 10.1371/journal.pone.0048451.

[69] T. Narasaraju, H. H. Ng, M. C. Phoon, and V. T. K. Chow, “MCP-1 antibody treatment enhances damage and impedes repair of the alveolar epithelium in influenza pneumonitis,” *Am. J. Respir. Cell Mol. Biol.*, 2010, doi: 10.1165/rcmb.2008-0423OC.

[70] P. A. Kumar *et al.*, “Distal airway stem cells yield alveoli in vitro and during lung regeneration following H1N1 influenza infection,” *Cell*, 2011, doi: 10.1016/j.cell.2011.10.001.

[71] P. Nettesheim and A. K. Szakal, “Morphogenesis of alveolar bronchiolization.,” *Lab. Investig.*, 1972.

[72] K. M. Akram, N. J. Lomas, M. A. Spiteri, and N. R. Forsyth, “Club cells inhibit alveolar epithelial wound repair via TRAIL-dependent apoptosis,” *Eur. Respir. J.*, 2013, doi: 10.1183/09031936.00213411.

[73] T. Betsuyaku, Y. Fukuda, W. C. Parks, J. M. Shipley, and R. M. Senior, “Gelatinase B is required for alveolar bronchiolization after intratracheal bleomycin,” *Am. J. Pathol.*, 2000, doi: 10.1016/S0002-9440(10)64563-4.

[74] B. D. Adamson IY, “Origin of ciliated alveolar epithelial cells in bleomycin-induced lung injury,” *Am J Pathol*, 1977.

[75] D. Zheng *et al.*, “A Cellular Pathway Involved in Clara Cell to Alveolar Type II Cell Differentiation after Severe Lung Injury,” *PLoS One*, 2013, doi: 10.1371/journal.pone.0071028.

[76] D. Zheng, L. Yin, and J. Chen, “Evidence for Scgβ1a1+ cells in the generation of p63 + cells in the damaged lung parenchyma,” *Am. J. Respir. Cell Mol. Biol.*, 2014, doi: 10.1165/rcmb.2013-0327OC.

[77] J. D. Crapo, “Morphologic Changes in Pulmonary Oxygen Toxicity,” *Annu. Rev. Physiol.*, 1986, doi: 10.1146/annurev.ph.48.030186.003445.

[78] A. F. Tryka, H. Witschi, D. G. Gosslee, A. H. McArthur, and N. K. Clapp, “Patterns of cell proliferation during recovery from oxygen injury. Species differences,” *Am. Rev. Respir. Dis.*, 1986, doi: 10.1164/arrd.1986.133.6.1055.

[79] M. Yee, B. W. Buczynski, and M. A. O’Reilly, “Neonatal hyperoxia stimulates the expansion of alveolar epithelial type II cells,” *Am. J. Respir. Cell Mol. Biol.*, 2014, doi: 10.1165/rcmb.2013-0207OC.

[80] J. Lee, R. Reddy, L. Barsky, K. Weinberg, and B. Driscoll, “Contribution of proliferation and DNA damage repair to alveolar epithelial type 2 cell recovery

from hyperoxia," *Am. J. Physiol. - Lung Cell. Mol. Physiol.*, 2006, doi: 10.1152/ajplung.00020.2005.

[81] M. J. Evans, L. J. Cabral, R. J. Stephens, and G. Freeman, "Transformation of alveolar Type 2 cells to Type 1 cells following exposure to NO2," *Exp. Mol. Pathol.*, 1975, doi: 10.1016/0014-4800(75)90059-3.

[82] X. Zhang, X. Chu, B. Weng, X. Gong, and C. Cai, "An Innovative Model of Bronchopulmonary Dysplasia in Premature Infants," *Front. Pediatr.*, 2020, doi: 10.3389/fped.2020.00271.

[83] M. Yee *et al.*, "Type II epithelial cells are critical target for hyperoxia-mediated impairment of postnatal lung development," *Am. J. Physiol. - Lung Cell. Mol. Physiol.*, 2006, doi: 10.1152/ajplung.00126.2006.

[84] C. M. Chao *et al.*, "Fgf10 deficiency is causative for lethality in a mouse model of bronchopulmonary dysplasia," *J. Pathol.*, 2017, doi: 10.1002/path.4834.

[85] M. Saito *et al.*, "Diphtheria toxin receptor-mediated conditional and targeted cell ablation in transgenic mice," *Nat. Biotechnol.*, 2001, doi: 10.1038/90795.

[86] T. Mitamura, S. Higashiyama, N. Taniguchi, M. Klagsbrun, and E. Mekada, "Diphtheria toxin binds to the epidermal growth factor (EGF)-like domain of human heparin-binding EGF-like growth factor/diphtheria toxin receptor and inhibits specifically its mitogenic activity," *J. Biol. Chem.*, 1995, doi: 10.1074/jbc.270.3.1015.

[87] "Mechanisms and limits of induced postnatal lung growth," in *American Journal of Respiratory and Critical Care Medicine*, 2004, doi: 10.1164/rccm.200209-1062st.

[88] H. Wada *et al.*, "Transplantation of alveolar type II cells stimulates lung regeneration during compensatory lung growth in adult rats," *J. Thorac. Cardiovasc. Surg.*, 2012, doi: 10.1016/j.jtcvs.2011.09.024.

[89] B. D. Uhal, S. R. Rannels, and D. E. Rannels, "Flow cytometric identification and isolation of hypertrophic type II pneumocytes after partial pneumonectomy," *Am. J. Physiol. - Cell Physiol.*, 1989, doi: 10.1152/ajpcell.1989.257.3.c528.

[90] B. D. Uhal and M. D. Etter, "Type II pneumocyte hypertrophy without activation of surfactant biosynthesis after partial pneumonectomy," *Am. J. Physiol. - Lung Cell. Mol. Physiol.*, 1993, doi: 10.1152/ajplung.1993.264.2.l153.

[91] B. D. Uhal, G. D. Hess, and D. E. Rannels, "Density-independent isolation of

type II pneumocytes after partial pneumonectomy," *Am. J. Physiol. - Cell Physiol.*, 1989, doi: 10.1152/ajpcell.1989.256.3.c515.

[92] J. S. Brody, R. Burki, and N. Kaplan, "Deoxyribonucleic acid synthesis in lung cells during compensatory lung growth after pneumonectomy," *Am. Rev. Respir. Dis.*, 1978, doi: 10.1164/arrd.1978.117.2.307.

[93] K. Chamoto *et al.*, "Alveolar Epithelial Dynamics in Postpneumonectomy Lung Growth," *Anat. Rec.*, 2013, doi: 10.1002/ar.22659.

[94] R. D. Nolen-Walston *et al.*, "Cellular kinetics and modeling of bronchioalveolar stem cell response during lung regeneration," *Am. J. Physiol. - Lung Cell. Mol. Physiol.*, 2008, doi: 10.1152/ajplung.00298.2007.

[95] R. Jain *et al.*, "Plasticity of Hopx+ type I alveolar cells to regenerate type II cells in the lung," *Nat. Commun.*, 2015, doi: 10.1038/ncomms7727.

[96] J. A. Whitsett, S. E. Wert, and T. E. Weaver, "Alveolar Surfactant Homeostasis and the Pathogenesis of Pulmonary Disease," *Annu. Rev. Med.*, 2010, doi: 10.1146/annurev.med.60.041807.123500.

[97] J. F. Lewis and R. Veldhuizen, "The Role of Exogenous Surfactant in the Treatment of Acute Lung Injury," *Annu. Rev. Physiol.*, 2003, doi: 10.1146/annurev.physiol.65.092101.142434.

[98] D. A. Todd *et al.*, "Surfactant phospholipids, surfactant proteins, and inflammatory markers during acute lung injury in children," *Pediatr. Crit. Care Med.*, 2010, doi: 10.1097/PCC.0b013e3181ae5a4c.

[99] A. Günther *et al.*, "Surfactant abnormalities in idiopathic pulmonary fibrosis, hypersensitivity pneumonitis and sarcoidosis," *Eur. Respir. J.*, 1999, doi: 10.1034/j.1399-3003.1999.14c14.x.

[100] S. E. Wert *et al.*, "Increased metalloproteinase activity, oxidant production, and emphysema in surfactant protein D gene-inactivated mice," *Proc. Natl. Acad. Sci. U. S. A.*, 2000, doi: 10.1073/pnas.100448997.

[101] C. Botas *et al.*, "Altered surfactant homeostasis and alveolar type II cell morphology in mice lacking surfactant protein D," *Proc. Natl. Acad. Sci. U. S. A.*, 1998, doi: 10.1073/pnas.95.20.11869.

[102] M. Griese *et al.*, "Pulmonary surfactant, lung function, and endobronchial inflammation in cystic fibrosis," *Am. J. Respir. Crit. Care Med.*, 2004, doi: 10.1164/rccm.200405-575OC.

[103] M. G. Foreman *et al.*, “Polymorphic variation in surfactant protein B is associated with COPD exacerbations,” *Eur. Respir. J.*, 2008, doi: 10.1183/09031936.00040208.

[104] H. L. Halliday, “Surfactants: Past, present and future,” in *Journal of Perinatology*, 2008, doi: 10.1038/jp.2008.50.

[105] S. Shulenin, L. M. Nogee, T. Annilo, S. E. Wert, J. A. Whitsett, and M. Dean, “ABCA3 Gene Mutations in Newborns with Fatal Surfactant Deficiency,” *N. Engl. J. Med.*, 2004, doi: 10.1056/NEJMoa032178.

[106] T. Tsuji, K. Aoshiba, and A. Nagai, “Alveolar cell senescence in patients with pulmonary emphysema,” *Am. J. Respir. Crit. Care Med.*, 2006, doi: 10.1164/rccm.200509-1374OC.

[107] K. Aoshiba and A. Nagai, “Senescence hypothesis for the pathogenetic mechanism of chronic obstructive pulmonary disease,” in *Proceedings of the American Thoracic Society*, 2009, doi: 10.1513/pats.200904-017RM.

[108] M. P. Steele and D. A. Schwartz, “Molecular Mechanisms in Progressive Idiopathic Pulmonary Fibrosis,” *Annu. Rev. Med.*, 2013, doi: 10.1146/annurev-med-042711-142004.

[109] D. M. Ornitz *et al.*, “Receptor specificity of the fibroblast growth factor family,” *J. Biol. Chem.*, 1996, doi: 10.1074/jbc.271.25.15292.

[110] C. J. Powers, S. W. McLeskey, and A. Wellstein, “Fibroblast growth factors, their receptors and signaling,” *Endocrine-Related Cancer*. 2000, doi: 10.1677/erc.0.0070165.

[111] D. M. Ornitz and N. Itoh, “Fibroblast growth factors,” *Genome Biology*. 2001, doi: 10.2165/00128415-200711520-00032.

[112] T. Volckaert *et al.*, “Fgf10-Hippo Epithelial-Mesenchymal Crosstalk Maintains and Recruits Lung Basal Stem Cells,” *Dev. Cell*, 2017, doi: 10.1016/j.devcel.2017.09.003.

[113] G. I. Balasooriya, M. Goschorska, E. Piddini, and E. L. Rawlins, “FGFR2 is required for airway basal cell self-renewal and terminal differentiation,” *Dev.*, 2017, doi: 10.1242/dev.135681.

[114] T. Yuan *et al.*, “FGF10-FGFR2B Signaling Generates Basal Cells and Drives Alveolar Epithelial Regeneration by Bronchial Epithelial Stem Cells after Lung Injury,” *Stem Cell Reports*, 2019, doi: 10.1016/j.stemcr.2019.04.003.

[115] J. Quantius *et al.*, “Influenza Virus Infects Epithelial Stem/Progenitor Cells of the Distal Lung: Impact on Fgfr2b-Driven Epithelial Repair,” *PLoS Pathog.*, 2016, doi: 10.1371/journal.ppat.1005544.

[116] J. T. Benjamin, R. J. Smith, B. A. Halloran, T. J. Day, D. R. Kelly, and L. S. Prince, “FGF-10 is decreased in bronchopulmonary dysplasia and suppressed by Toll-like receptor activation,” *Am. J. Physiol. - Lung Cell. Mol. Physiol.*, 2007, doi: 10.1152/ajplung.00329.2006.

[117] D. Chanda *et al.*, “Developmental Reprogramming in Mesenchymal Stromal Cells of Human Subjects with Idiopathic Pulmonary Fibrosis,” *Sci. Rep.*, 2016, doi: 10.1038/srep37445.

[118] I. Hokuto, A. K. T. Perl, and J. A. Whitsett, “FGF signaling is required for pulmonary homeostasis following hyperoxia,” *Am. J. Physiol. - Lung Cell. Mol. Physiol.*, 2004, doi: 10.1152/ajplung.00278.2003.

[119] L. Tong *et al.*, “Keratinocyte growth factor-2 is protective in lipopolysaccharide-induced acute lung injury in rats,” *Respir. Physiol. Neurobiol.*, 2014, doi: 10.1016/j.resp.2014.06.011.

[120] L. Tong *et al.*, “Fibroblast Growth Factor-10 (FGF-10) Mobilizes Lung-resident Mesenchymal Stem Cells and Protects Against Acute Lung Injury,” *Sci. Rep.*, 2016, doi: 10.1038/srep21642.

[121] L. Madisen *et al.*, “A robust and high-throughput Cre reporting and characterization system for the whole mouse brain,” *Nat. Neurosci.*, 2010, doi: 10.1038/nn.2467.

[122] R Core Team, “R Core Team (2014). R: A language and environment for statistical computing.,” *R Found. Stat. Comput. Vienna, Austria. URL http//www.R-project.org/.*, 2014.

[123] G. K. Smyth, “limma: Linear Models for Microarray Data,” in *Bioinformatics and Computational Biology Solutions Using R and Bioconductor*, 2005.

[124] R. C. Gentleman *et al.*, “Bioconductor: open software development for computational biology and bioinformatics.,” *Genome Biol.*, 2004, doi: 10.1186/gb-2004-5-10-r80.

[125] G. K. Smyth and T. Speed, “Normalization of cDNA microarray data,” *Methods*, 2003, doi: 10.1016/S1046-2023(03)00155-5.

[126] G. K. Smyth, “Linear models and empirical bayes methods for assessing

differential expression in microarray experiments," *Stat. Appl. Genet. Mol. Biol.*, 2004, doi: 10.2202/1544-6115.1027.

[127] J. D. Buenrostro, P. G. Giresi, L. C. Zaba, H. Y. Chang, and W. J. Greenleaf, "Transposition of native chromatin for fast and sensitive epigenomic profiling of open chromatin, DNA-binding proteins and nucleosome position," *Nat. Methods*, 2013, doi: 10.1038/nmeth.2688.

[128] A. M. Bolger, M. Lohse, and B. Usadel, "Trimmomatic: A flexible trimmer for Illumina sequence data," *Bioinformatics*, 2014, doi: 10.1093/bioinformatics/btu170.

[129] A. Dobin *et al.*, "STAR: Ultrafast universal RNA-seq aligner," *Bioinformatics*, 2013, doi: 10.1093/bioinformatics/bts635.

[130] Y. Zhang *et al.*, "Model-based analysis of ChIP-Seq (MACS)," *Genome Biol.*, 2008, doi: 10.1186/gb-2008-9-9-r137.

[131] S. Anders and W. Huber, "Differential expression analysis for sequence count data," *Genome Biol.*, 2010, doi: 10.1186/gb-2010-11-10-r106.

[132] A. J. Lechner *et al.*, "Recruited Monocytes and Type 2 Immunity Promote Lung Regeneration following Pneumonectomy," *Cell Stem Cell*, 2017, doi: 10.1016/j.stem.2017.03.024.

[133] K. Pawelczyk *et al.*, "Role of PD-L1 expression in non-small cell lung cancer and their prognostic significance according to clinicopathological factors and diagnostic markers," *Int. J. Mol. Sci.*, 2019, doi: 10.3390/ijms20040824.

[134] T. Miyazawa *et al.*, "PD-L1 expression in non-small-cell lung cancer including various adenocarcinoma subtypes," *Ann. Thorac. Cardiovasc. Surg.*, 2019, doi: 10.5761/atcs.oa.18-00163.

[135] T. Parimon, C. Yao, B. R. Stripp, P. W. Noble, and P. Chen, "Alveolar epithelial type II cells as drivers of lung fibrosis in idiopathic pulmonary fibrosis," *Int. J. Mol. Sci.*, vol. 21, no. 7, 2020, doi: 10.3390/ijms21072269.

[136] D. F. Zoz, W. E. Lawson, and T. S. Blackwell, "Idiopathic pulmonary fibrosis: A disorder of epithelial cell dysfunction," in *American Journal of the Medical Sciences*, 2011, doi: 10.1097/MAJ.0b013e31821a9d8e.

[137] T. H. Sisson *et al.*, "Targeted injury of type II alveolar epithelial cells induces pulmonary fibrosis," *Am. J. Respir. Crit. Care Med.*, 2010, doi: 10.1164/rccm.200810-1615OC.

[138] L. De Moerlooze, B. Spencer-Dene, J. M. Revest, M. Hajihosseini, I. Rosewell, and C. Dickson, “An important role for the IIIb isoform of fibroblast growth factor receptor 2 (FGFR2) in mesenchymal-epithelial signalling during mouse organogenesis,” *Development*, 2000, doi: 10.1042/cs099005p.

[139] N. Yokohori, K. Aoshiba, A. Nagai, and T. Kuriyama, “Increased Levels of Cell Death and Proliferation in Alveolar Wall Cells in Patients with Pulmonary Emphysema,” *Chest*, 2004, doi: 10.1378/chest.125.2.626.

[140] Y. Kasahara, R. M. Tuder, C. D. Cool, D. A. Lynch, S. C. Flores, and N. F. Voelkel, “Endothelial cell death and decreased expression of vascular endothelial growth factor and vascular endothelial growth factor receptor 2 in emphysema,” *Am. J. Respir. Crit. Care Med.*, 2001, doi: 10.1164/ajrccm.163.3.2002117.

[141] Y. Liu *et al.*, “FoxM1 mediates the progenitor function of type II epithelial cells in repairing alveolar injury induced by Pseudomonas aeruginosa,” *J. Exp. Med.*, 2011, doi: 10.1084/jem.20102041.

[142] X. Han *et al.*, “Mapping the Mouse Cell Atlas by Microwell-Seq,” *Cell*, 2018, doi: 10.1016/j.cell.2018.02.001.

[143] M. I. Chung, M. Bujnis, C. E. Barkauskas, Y. Kobayashi, and B. L. M. Hogan, “Niche-mediated BMP/SMAD signaling regulates lung alveolar stem cell proliferation and differentiation,” *Dev.*, 2018, doi: 10.1242/dev.163014.

[144] M. J. Evans, L. J. Cabral, R. J. Stephens, and G. Freeman, “Renewal of alveolar epithelium in the rat following exposure to NO2,” *Clinical Research*. 1973.

[145] R. L. Persinger, W. M. Blay, N. H. Heintz, D. R. Hemenway, and Y. M. W. Janssen-Heininger, “Nitrogen dioxide induces death in lung epithelial cells in a density-dependent manner,” *Am. J. Respir. Cell Mol. Biol.*, 2001, doi: 10.1165/ajrcmb.24.5.4340.

[146] A. Pagano and C. Barazzone-Argiroffo, “Alveolar Cell Death in Hyperoxia-Induced Lung Injury,” in *Annals of the New York Academy of Sciences*, 2003, doi: 10.1196/annals.1299.074.

[147] M. S. Pogach, Y. Cao, G. Millien, M. I. Ramirez, and M. C. Williams, “Key developmental regulators change during hyperoxia-induced injury and recovery in adult mouse lung,” *J. Cell. Biochem.*, 2007, doi: 10.1002/jcb.21142.

[148] G. Matute-Bello, C. W. Frevert, and T. R. Martin, “Animal models of acute lung

injury," *American Journal of Physiology - Lung Cellular and Molecular Physiology*. 2008, doi: 10.1152/ajplung.00010.2008.

[149] A. Hou *et al.*, "Hyperoxia stimulates the transdifferentiation of type II alveolar epithelial cells in newborn rats," *Am. J. Physiol. - Lung Cell. Mol. Physiol.*, 2015, doi: 10.1152/ajplung.00099.2014.

[150] C. W. White, K. E. Greene, C. B. Allen, and J. M. Shannon, "Elevated expression of surfactant proteins in newborn rats during adaptation to hyperoxia," *Am. J. Respir. Cell Mol. Biol.*, 2001, doi: 10.1165/ajrcmb.25.1.4296.

[151] A. S. Flozak *et al.*, "β-Catenin/T-cell factor signaling is activated during lung injury and promotes the survival and migration of alveolar epithelial cells," *J. Biol. Chem.*, 2010, doi: 10.1074/jbc.M109.070326.

[152] C. Wansleeben, C. E. Barkauskas, J. R. Rock, and B. L. M. Hogan, "Stem cells of the adult lung: Their development and role in homeostasis, regeneration, and disease," *Wiley Interdiscip. Rev. Dev. Biol.*, 2013, doi: 10.1002/wdev.58.

[153] L. He *et al.*, "Enhancing the precision of genetic lineage tracing using dual recombinases," *Nat. Med.*, 2017, doi: 10.1038/nm.4437.

[154] R. T. Sadikot, T. S. Blackwell, J. W. Christman, and A. S. Prince, "Pathogen-host interactions in pseudomonas aeruginosa pneumonia," *American Journal of Respiratory and Critical Care Medicine*. 2005, doi: 10.1164/rccm.200408-1044SO.

[155] Y. Liu, V. S. Kumar, W. Zhang, J. Rehman, and A. B. Malik, "Activation of type II cells into regenerative stem cell antigen-1+ cells during alveolar repair," *Am. J. Respir. Cell Mol. Biol.*, 2015, doi: 10.1165/rcmb.2013-0497OC.

[156] I. M. Kim, S. Ramakrishna, G. A. Gusarova, H. M. Yoder, R. H. Costa, and V. V. Kalinichenko, "The Forkhead Box m1 transcription factor is essential for embryonic development of pulmonary vasculature," *J. Biol. Chem.*, 2005, doi: 10.1074/jbc.M500936200.

[157] T. V. Kalin *et al.*, "Forkhead Box m1 transcription factor is required for perinatal lung function," *Proc. Natl. Acad. Sci. U. S. A.*, 2008, doi: 10.1073/pnas.0806748105.

[158] R. H. Costa, V. V. Kalinichenko, M. L. Major, and P. Raychaudhuri, "New and unexpected: Forkhead meets ARF," *Current Opinion in Genetics and Development*. 2005, doi: 10.1016/j.gde.2004.12.007.

[159] C. M. Hendrickson and M. A. Matthay, “Viral pathogens and acute lung injury: Investigations inspired by the SARS epidemic and the 2009 H1N1 influenza pandemic,” *Semin. Respir. Crit. Care Med.*, 2013, doi: 10.1055/s-0033-1351122.

[160] W. A. Cooper *et al.*, “PD-L1 expression is a favorable prognostic factor in early stage non-small cell carcinoma,” *Lung Cancer*, 2015, doi: 10.1016/j.lungcan.2015.05.007.

[161] K. J. Lastwika *et al.*, “Control of PD-L1 expression by oncogenic activation of the AKT-mTOR pathway in non-small cell lung cancer,” *Cancer Res.*, 2016, doi: 10.1158/0008-5472.CAN-14-3362.

[162] H. Yu, T. A. Boyle, C. Zhou, D. L. Rimm, and F. R. Hirsch, “PD-L1 expression in lung cancer,” *Journal of Thoracic Oncology*. 2016, doi: 10.1016/j.jtho.2016.04.014.

[163] G. I. Balasooriya, J. A. Johnson, M. A. Basson, and E. L. Rawlins, “An FGFR1-SPRY2 Signaling Axis Limits Basal Cell Proliferation in the Steady-State Airway Epithelium,” *Dev. Cell*, 2016, doi: 10.1016/j.devcel.2016.03.001.

[164] D. Upadhyay, M. Bundesmann, V. Panduri, E. Correa-Meyer, and D. W. Kamp, “Fibroblast growth factor-10 attenuates H2O2-induced alveolar epithelial cell DNA damage: Role of MAPK activation and DNA repair,” *Am. J. Respir. Cell Mol. Biol.*, 2004, doi: 10.1165/rcmb.2003-0064OC.

8 Supplementary material

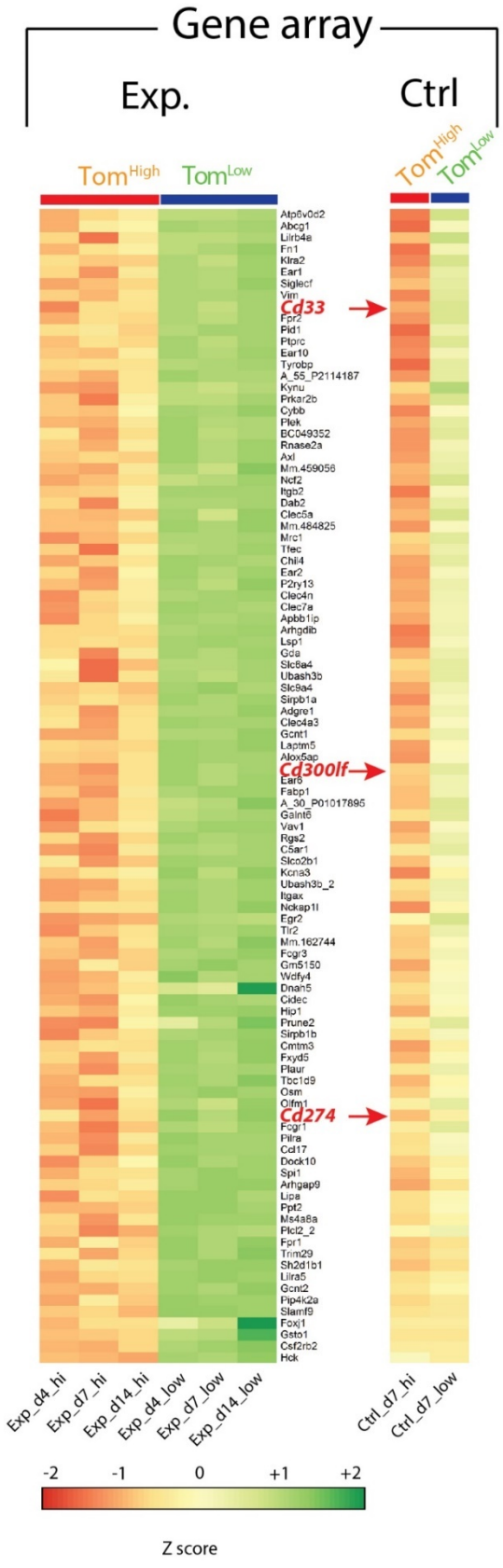

Figure S1: Gene array-based/Heat map analysis of sorted Tom^{Low} and Tom^{High} cells from the experimental and the control groups. The data in three different time points (d4, d7 and d14) of experimental group displaying 100 top regulated genes between Tom^{Low} and Tom^{High}. Plugging the upregulated genes in to the control also shows the higher expression of three cell surface markers in Tom^{Low} compared to Tom^{High} in the control.

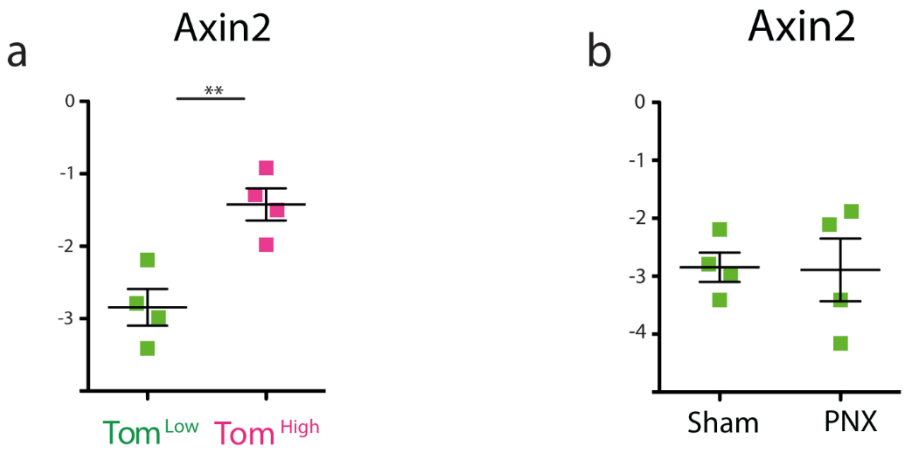

Figure S2: *Axin2* expression analysis. a) qPCR analysis of FACS-based sorted Tom^{Low} and Tom^{High} cells for the expression of *Axin2*. **b)** qPCR analysis of FACS-based sorted Tom^{Low} cells for the expression of *Axin2* from sham and PNX groups. Data are presented as mean values ± SEM. $*p < 0.05$, $**p < 0.01$, $***p < 0.001$.

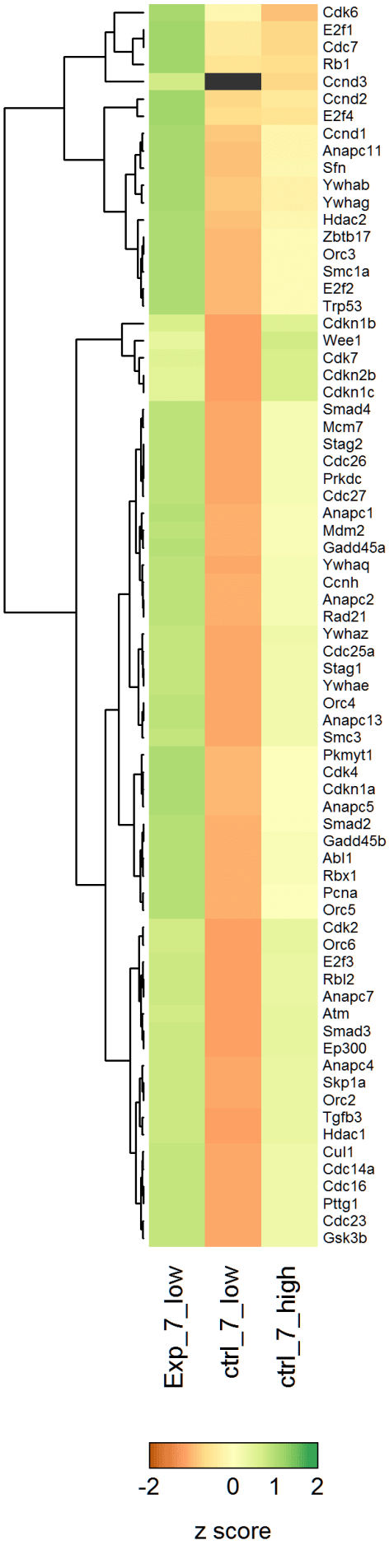
Cdk6
E2f1
Cdc7
Rb1
Ccnd3
Ccnd2
E2f4
Ccnd1
Anapc11
Sfn
Ywhab
Ywhag
Hdac2
Zbtb17
Orc3
Smc1a
E2f2
Trp53
Cdkn1b
Wee1
Cdk7
Cdkn2b
Cdkn1c
Smad4
Mcm7
Stag2
Cdc26
Prkdc
Cdc27
Anapc1
Mdm2
Gadd45a
Ywhaq
Ccnh
Anapc2
Rad21
Ywhaz
Cdc25a
Stag1
Ywhae
Orc4
Anapc13
Smc3
Pkmyt1
Cdk4
Cdkn1a
Anapc5
Smad2
Gadd45b
Abl1
Rbx1
Pcna
Orc5
Cdk2
Orc6
E2f3
Rbl2
Anapc7
Atm
Smad3
Ep300
Anapc4
Skp1a
Orc2
Tgfb3
Hdac1
Cul1
Cdc14a
Cdc16
Pttg1
Cdc23
Gsk3b
Exp_7_low
ctrl_7_low
ctrl_7_high
-2
0
1
2
z score

Figure S3: Gene array-based/Heat map analysis of cell cycle genes from sorted Tom^{Low} and Tom^{High} cells from the experimental and the control groups. The data at day 7 displays upregulation of cell cycle related genes in Tom^{Low} in the experimental condition compared to Tom^{Low} in the control.

9 Acknowledgments

I would like to express my gratitude and appreciation to people who helped me in this research project.

Foremost, I would like to express my sincere gratitude to Prof. Dr. Saverio Bellusci whose guidance, support and encouragement have been invaluable throughout this study. Thanks to him for being an understanding, inspiring and encouraging supervisor. I have learned from him how to interpret data, construct manuscripts, and develop scientific discussions. His positive attitude, passion and energy were very motivating in conducting this research project. I am extremely grateful for the friendly work atmosphere that he provided in the lab.

I want to especially thank Kerstin Goth who has been very supportive and kind to me. She helped in the mice breeding and genotyping. I also thank another lab technician, Jana for her friendship and technical support. I would like to thanks Heike Habermann for all her administrative help and for being friendly in the translation of German documents. I would like to express my appreciation to Dr. Thomas Sontag whose help and efforts in writing, translating animal proposals and communication with animal welfare officers was crucial in the approval of two animal proposals to conduct this research.

I would like to thank all Bellusci lab members for their friendly and supportive attitudes during the last years and fun times that we spend together. I want to thank Mattew Jones who was my peer in the PhD program, we had great discussion on scientific topics and statistics. I would like also to express my appreciation to Dr. Stefano Rivetti who joined the Bellusci lab at the beginning of 2019 and during this time we had constructive discussions on this research project.

I would like to appreciate the help and support of Dr. Ana Ivonne Vazquez-Armendariz and Dr. Monika Heiner for their collaboration in FACS measurements and cell sorting. I want to express my deep gratitude to Dr. Roxana Wasnick who taught me FACS principle and always was welcoming to answer my questions. She also contributed in providing isolated human cells from Donor and IPF patients.

I want to appreciate Dr. Jochen Wilhelm for his contribution and help to run the gene array and providing heat maps. I would like to thank Dr. Stefan Gunther for all his support and help in running ATAT-seq and its analysis.

I would like to express my gratitude to Alberto Rodríguez Castillo who taught me how to perform pneumonectomy in mice, he was very generous to teach me the tips that he learned with experience.

I would also like to acknowledge Prof. Dr. Eveline Baumgart-Vogt and Dr. Lorna Lück, the organizers of the GGL program with seminars and events which helped me to socialize with scientists from different research groups. I much appreciate Justus-Liebig-University of Giessen for provision of educational facilities. I would like to thank Deutsche Zentrum für Lungenforschung (DZL) to financially support and fund this research project. I would like to express my gratitude and love to my parents who always have encouraged me and believing in me. I am thankful to my kind and supportive brothers (Payam and Pouya) who encourage and motive me in tough times. My greatest gratitude and appreciation with love go to my husband and best friend Dr. Farhad Khosravi who has been standing on my side in every step of the path and gave me strength and purpose. He supported me in this research project spiritually and scientifically. He also provided thoughtful comments and recommendations for this dissertation.

The Faculties of Veterinary Medicine and Medicine
of the Justus Liebig University Giessen

hereby award to

Negah Ahmadvand
born June 3rd, 1982 in Toyserkan, Iran

the degree of

Doctor of Philosophy
(Ph.D.)

after fulfilment of the doctoral requirements laid down in the "Ph.D.-Ordnung der Fachbereiche Veterinärmedizin und Medizin der Justus-Liebig-Universität Giessen" issued on December 11th and 16th, 2002.

On the basis of her proven academic ability in the form of a dissertation entitled

„Identification of a novel subset of alveoloar type 2 cells expanding following pneumonectomy, responding differently to Fgfr2b deletion and enriched in PD-L1"

awarded the category "summa cum laude",
as well as by oral examination, the candidate has been awarded
the final grade of "summa cum laude"

Giessen, December 7th, 2020